

AALTO UNIVERSITY
School of Science and Technology
Faculty of Engineering and Architecture
Department of Applied Mechanics

Blé Bernard Wongui

Morphing Unmanned Aerial Vehicles

Thesis submitted in partial fulfilment of the requirements for the degree of Master
of Science in Technology

30 May 2010

Supervisor: Professor Olli Saarela
Instructor: Professor Olli Saarela

Author:	Blé Bernard WONGUI	
Title:	Morphing Unmanned Aerial Vehicles	
Date:	30 May 2010	Pages: 96 + 7
Faculty:	Faculty of Engineering and Architecture	
Department:	Department of Applied Mechanics	
Professorship:	Kul-34 Aeronautical Engineering	
Supervisor:	Professor Olli Saarela	
Instructor:	Professor Olli Saarela	
<p>The performance and dynamic efficiency of an aircraft are significantly influenced by the aircraft shape and configuration. Therefore, the wing which is an important element in the aircraft load response in terms of drag and lift has been given increasing attention through morphing technology. Several governmental programs and academic research projects on morphing aircraft have investigated methods of efficiently changing the wing geometric characteristics in-flight.</p> <p>The present thesis reviews the current knowledge on wing morphing concepts and investigates the type of methods that can be used to model morphing structures.</p> <p>This review includes the principles of the morphing concept, realization of a morphing structure, aspects of morphing structure design, current methods to model morphing structures, challenges, and the perspectives of the morphing UAVs.</p> <p>It concludes that the wing cover skins must possess a high degree of deformability; but they must be able to maintain their shape and structural integrity under the compression, tension, shear and bending characteristics of aerodynamic and flight loads including the effects of added masses. In order to meet these requirements, thermoplastic elastomers and shape memory polymers are suggested as good candidate materials for smart skins. Nevertheless, an excessively flexible skin is exposed to the hazard of sagging under pressure loads.</p> <p>It is suggested that bio-inspired micro air vehicles based on bat wing structure will gain intensive attention since such a structure possesses a high flexibility with anisotropy and non-linear elasticity.</p>		
Keywords:	Morphing, UAV, Actuators, Sensors, Lagrange, Rayleigh-Ritz, FSDT.	

PREFACE

The great rise of Unmanned Aerial Vehicles dates from the "Cold War" between the USA and the former USSR after the Second World War. During that period, UAVs were confidentially developed by the US army as a means of strategic superiority to allow surveillance and military intervention in the enemy fields without incurring the death risk that human could not stand the view.

This superiority has been gained through technological innovations in the field of Automation and Transmission systems. Later on, the Morphing Aircraft Structure program aimed to design and build active variable geometry wing structures with the ability to morph in-flight to optimize the flight.

The first aircraft capable of changing the sweep of its wing in-flight was the Bell X-5 produced by the USA in 1951. Since then, the increasing interest in morphing structure is the result of their significant advantages over conventional Unmanned Aerial Vehicles.

This thesis leading to the award of a Master's of Science degree in Technology to Mr. Blé Bernard WONGUI, holder of a BSc. in Mechanical Engineering, provides an appropriate documentation to address the modeling of morphing structures. His work provides current information on the state of the art in UAVs.

Jovin GREYE.

Acknowledgments

The author is grateful to Professors Olli SAARELA and Erkki SOINNE for motivating the funding the present Master's thesis. The assistance and the succinct advices of Professor SAARELA; but also the support of Professor SOINNE for aerodynamic modeling were extremely valuable in completing this work.

The author would like to express his gratitude particularly to the professionals with whom he has exchanged on the topic and who have shared the result of their investigations. The first of them is Professor Michael I. FRISWELL¹, School of Engineering Swansea University. Professor Friswell made significant contributions by providing the author with materials including his publications and lecture notes. Dr Fabrizio SCARPA, Reader in Smart Structures, Department of Aerospace Engineering, Bristol University, and Dr Zhong YOU, Lecturer (Structures), Department of Engineering Science, Oxford University provided the author with their publications or lecture notes.

The author addresses a grateful regard to the friends and course mates who have assisted him in several respects including proof-reading and bringing forth constructive comments on the linguistic level; but also for the technical assistance in software issues. Thanks to Dr YALAHO, J. GREYE, J. CHOO, B. ZOKO, and M. WEGELIUS.

Finally, the author would like to embrace his daughters Julina Nagnon WONGUI, Lilja Wahzi WONGUI and Michelle Nadrey WONGUI for their patience, and thank his companion Dace KALNINA for her support.

Espoo, 30 May 2010,

Blé Bernard WONGUI.

¹Email correspondence included at the end of the present work.

Contents

Abbreviations	3
1 Introduction	5
1.1 Morphing Aircraft	5
1.2 Background Of Unmanned Aerial Vehicles	5
1.3 Research Problem And Approach	6
1.4 Thesis Overview	7
2 Unmanned Aerial Vehicles	8
2.1 Classification Of UAVs	12
2.2 Mission Aspects of UAVs	14
3 Morphing Concepts	15
3.1 Morphing Shape Alternatives	18
3.2 Wing Planform Alternations	19
3.2.1 Wing Span Morphing	20
3.2.2 Inflatable Wing Concept	21
3.2.3 Sweep Angle Variation	22
3.3 Out-Of-Plane Transformations	24
3.3.1 Camber And Chord Control	25
3.3.2 Wing Twist Control	26
3.4 Airfoil Profile Adjustments	28
3.5 Morphing UAVs	30
4 Actuators And Sensors	33
4.1 Fiber Optic Sensors	33
4.2 Smart Materials	34
4.3 Shape Memory Alloys	37
4.4 Piezo-Electric Materials	38
4.4.1 Active Fiber Composites	38
4.4.2 Macro Fiber Composite	38
5 Structure Solutions	39
5.1 Design Aspects of Morphing Structures	39
5.2 Multi-Stable Composite Materials	41
5.3 Adaptive Aero-Elastic Structures	44
5.3.1 Variable Geometry Truss	45
5.3.2 Variable Stiffness Spar	46
5.3.3 Bend-Twist Coupled Beams	47
5.3.4 Preloaded Internal Spine Structures	49

5.3.5	Kagome Lattice Structures	50
5.3.6	Auxetic Materials	52
5.3.7	Belt Rib Concept	53
5.3.8	Finger Concept	54
5.4	NextGen's Wing Mechanism	55
5.5	Lockheed's Wing Mechanisms	56
5.6	Scaling Limitations	57
5.7	Control Issues Of Morphing UAVs	58
6	Modeling Principles of Morphing Structures	59
6.1	Basic Static And FE Formulations	59
6.2	Force-Displacements Relationship	61
6.2.1	Differential Method	61
6.2.2	Rayleigh-Ritz Energy Method	63
6.3	Span Morphing Wing Model	64
6.3.1	Aero-Elastic Model	64
6.3.2	Aerodynamic Model	65
6.4	Camber Morphing Model	66
6.4.1	Structural Model	66
6.4.2	Theodorsen's Model	69
6.5	Continuously Morphing Wing Model	71
6.5.1	Structural Model	71
6.5.2	Piezo And Thermo Actuator Model	78
6.6	Snap-Through Model	80
7	Conclusion	86
7.1	Challenges	86
7.2	Perspectives	87
	Bibliography	87

List of Figures

2.1	Black Hornet [9].	11
3.1	Ader’s Eole [33].	16
3.2	Eagle in various wing configurations [109].	16
3.3	Classification for shape morphing of wing [111].	19
3.4	In-flight deployment of I2000 inflatable Wing [46].	22
3.5	Aerodynamic coefficients of an inflatable wing [12].	22
3.6	F-14 wing sweep mechanism [23].	23
3.7	Chord-wise bending achieved by the heating of SMA strips in an antagonistic design. (a) Un-morphed and (b) morphed [133].	26
3.8	Twisting of a wing section achieved by antagonistic SMA actuation. (a) The left rib is flexed downward and right rib upward. (b) The left rib is actuated upward and the right one downward [133].	27
3.9	Nominal wing (left) and morphed wing (right) [116].	27
3.10	Airfoil profile control [117].	28
3.11	Position of the wing skins [118].	29
3.12	NextGen’s morphing wing planform configurations [62].	31
3.13	Lockheed’s folding wing concept [62].	32
4.1	Basic fiber optic smart structure system [40].	34
5.1	Morphing smart design concept [98].	40
5.2	One dimensional morphing concept [78].	42
5.3	Bi-stable composite materials [88].	43
5.4	Wing with two VGTs as spars [95].	45
5.5	Double octahedral VGT unit [95]	45
5.6	Wing box with movable central spar [92].	46
5.7	Wing box with rotating leading and trailing edge spars [92].	46
5.8	a) Layup for bend-twist coupling and b) layup for extension-twist coupling [93].	48
5.9	a) Single box layup, b) double box layup and c) patch layup [93].	49
5.10	A beam column with eccentric load [52].	50
5.11	A planar Kagome lattice [38].	51
5.12	Chiral airfoil structure [130].	53
5.13	The belt rib concept [103].	53
5.14	Finger concept [102].	54
5.15	NextGen’s bat wing mechanism [89].	55
5.16	Lockheed’s morphing wing joint design [62].	56

6.1	Member with actuator force [71].	61
6.2	Forces and displacements for a post-buckled member [71].	62
6.3	Trailing edge framework for morphing wing [71].	63
6.4	Camber line with PBP [83].	66
6.5	Wing morphing part model [83].	67
6.6	Stress and moment resultants for a laminate element [84].	68
6.7	Generic trapezoidal wing (left) and wing- box (right)[127].	72
6.8	Geometry of laminate-actuator combination [120].	81

List of Tables

2.1	UAV programs of the US military [14].	9
2.2	Extremum records of UAVs [8].	10
2.3	USAF classification of UAVs [10].	12
2.4	UAV classification by altitude and endurance [8]	13
2.5	UAV classification by weight.	13
3.1	Effects of the change type on the aerodynamic characteristics in the scale 1-5 [34].	18
3.2	Morphing concepts, actuation and skin types.	29
4.1	Most common smart materials [54].	36

ADVENT	Adaptive Versatile Engine Technology
AFC	Active Fiber Composites or Antagonistic Flexural unit Cell
AFRL	Air Force Research Labs
CPT	Classical Plate Theory
DARPA	Defense Advanced Research Projects Agency
DC	Direct current
DHM	Doublet-Hybrid Method
DLR	Deutsches Zentrum für Luft-und Raumfahrt e.V
DoD	Department of Defense
EAP	Electro-Active Polymers
EO	Electro Optical
FE	Finite Element
FEA	Finite Element Analysis
FEM	Finite Element Method
FLIR	Forward Looking InfraRed
FMC	Flexible Matrix Composite
FPASS	Force Protection Aerial Surveillance System
FSDT	First-order Shear Deformation Theory
HAE	High Altitude Endurance
HALE	High Altitude Long Endurance
HSDT	Higher-order Shear Deformation Theory
IR	Infra Red
ISR	Intelligence, Surveillance, Reconnaissance
ISTAR	Intelligence, Surveillance, Target Acquisition and Reconnaissance
LO-HAE	Low Observable High Altitude Endurance
MAE	Medium Altitude Endurance
MAS	Morphing Aircraft Structure
MAW	Mission Adaptive Wing
MUAV	Micro UAV
NASA	National Aeronautics and Space Administration
NSMV	Near Space Maneuvering Vehicle
PBP	Post-Buckled Precompressed
PVDF	Polyvinylidene Fluoride
PZN-PT	Lead Zinc Niobate-Lead Titanate
PZT	Lead Zirconate Titanate
SAR	Synthetic Aperture Radar
SMA	Shape Memory Alloys
SMP	Shape Memory Polymers
STOL	Short Take-Off and Landing
SUAV	Small UAV
UAV	Unmanned Aerial Vehicle
UCAV	Unmanned Combat Air Vehicle
USA	United States of America
USAF	United States Air Force
VGT	Variable Geometry Truss
VLM	Vortex Lattice Method
VSS	Variable Stiffness Spar
VTOL	Vertical Take-Off and Landing

Chapter 1

Introduction

1.1 Morphing Aircraft

Morphing aircraft are flight vehicles that are capable of altering their shape to meet changing mission requirements of the aircraft and to perform flight control without the use of conventional control surfaces. Therefore, the shape characteristics of such an aircraft change in-flight to optimize performance. This morphing is realized by monitoring the wing geometric parameters. These parameters include the wing span, planform, aspect ratio, thickness, chord, camber, and consequently the wing area.

Aircraft morphing research is generally conducted for benefits including the improvement of the versatility of a given airframe by improving the performance for multiple flight regimes, the replacement of conventional control mechanisms, the increase of cruise efficiencies and the reduction of structural vibration.

1.2 Background Of Unmanned Aerial Vehicles

Unmanned Aerial Vehicles (UAVs) have been under development since the beginning of powered flight. Prior to the first manned airplane flight in 1903, rudimentary UAV technology was applied to combat and surveillance [16]. However, World War I is referred to as the effective introduction period of UAVs by US army [14]. Nevertheless, those UAVs flew inaccurately; they were imperfect and unreliable. Despite the lack of success of those vehicles, the UAV concept survived due to the tenacity of a small group of persons influencing politics for funding [4].

Thus, research on morphing unmanned aerial vehicles has experienced over recent decades increasing investigations in both military and civilian domains for applications including surveillance, attack, fire detection, and traffic monitoring. Subsequently, the NASA morphing project [1] focused on developing novel applications for smart materials and inventing methods for applying those materials to aircraft. Additionally, the Morphing Aircraft Structure (MAS) program [2] aimed to design and build active, variable geometry wing structures with the ability to morph in-flight. Furthermore, the US Air Force's Adaptive Versatile Engine Technology (ADVENT) program [3] supplied inlet, engine and exhaust technologies to optimize propulsion system performance.

This increasing interest in morphing structures is the result of their significant advantages over conventional UAV structures. These advantages comprise the increase in the capability and versatility of the aircraft. According to [2], such an aircraft is a multi role platform that firstly, changes its state substantially to adapt to changing mission requirements. Secondly, it provides a superior system capability in term of an optimal performance into a single system with a low turning radius, long endurance, increased payload, and high speed. This is not possible without the wing reconfiguration. Finally, it uses a design that integrates innovative combinations of advanced materials, actuators, flow controllers and mechanisms to achieve the state change.

1.3 Research Problem And Approach

The performance and dynamic efficiency of an aircraft are significantly influenced by the aircraft shape and configuration. Thus, the wing which is an important element in the aircraft load response has been given particular attention through morphing technology. Therefore, several governmental programs [2, 3], and academic research projects [15, 17] on morphing aircraft have investigated methods of efficiently changing the wing geometric characteristics in-flight.

The present master's thesis commissioned by the Department of Applied Mechanics of Aalto University reviews the current knowledge on wing morphing concepts and investigates the type of methods that can be used to model morphing structures. This review includes:

1. Description of morphing concepts,
2. Principles of the morphing concept,
3. Realization of a morphing structure,
4. Design aspects of morphing structures,
5. Modeling principles of morphing structures,
6. Challenges and perspectives of the morphing UAVs.

1.4 Thesis Overview

The remaining Chapters of this thesis are organized as follows:

Chapter 2 reviews existing projects of UAV and gives their common classifications. Chapter 3 describes morphing concepts, following the introduction of the morphing shape alternatives. Section 3.5 is dedicated to the two most successful morphing UAV programs launched by NextGen Aeronautics and Martin Lockheed.

Chapter 4 presents sensors and actuators. Additionally, it reviews the common smart materials.

Chapter 5 introduces the factors that need to be considered when designing a morphing structure. Additionally, it reviews the structural solutions to achieve the morphing of a planform. The two last sections of this Chapter discuss the limitations set by the square-cube law on the use of materials in term of scalability and address the control issues of morphing vehicles.

Chapter 6 presents the basis of finite element formulation of a morphing structure. Additionally, this Chapter includes the methods that may be used to model a camber and span morphing wing. It establishes the relationship between the actuation force and the structural displacement using the differential and energy methods. Furthermore, it reviews the modeling of a continuously morphing flying wing and the snap-through of unsymmetric composite laminates. Finally, this Chapter presents the Theodorsen's function as a means to express the pressure distribution over a morphing wing.

Chapter 7 concludes this review by assessing the challenges of the morphing technology and giving a potential perspective.

Chapter 2

Unmanned Aerial Vehicles

This Chapter reviews existing projects of UAV and gives their common classifications.

Generally, an aircraft refers to any flying vehicle with configurations including fixed-wing, rotary-wing, helicopters, vertical take-off and landing (VTOL), and short take-off and landing (STOL) vehicles. According to [5], an aircraft may be either heavier or lighter than air, with balloons and airships belonging to the latter category. Moreover, the term unmanned aerial vehicle refers to a pilotless (no human crew on board) aircraft. However, ballistic vehicles, cruise missiles, and artillery projectiles are not considered as UAVs. As described, UAVs are not limited by human performance factors nor by his physiological and psychological characteristics to accomplish missions that may be perishing for a human. Therefore, unmanned aerial vehicles can operate in environments contaminated by chemical, biological, or radioactive agents. They can carry cameras, sensors, communications equipment or other payloads including weapons.

Worth mentioning is the fact that UAVs are generally used for military applications. Nevertheless, vertical take-off and landing applications extend to civilian domains. The VTOL unmanned aerial vehicle military applications include surveillance and reconnaissance, combat, and testing for new weapon systems. QH-50 Gyrodyne Torpedo delivery drone [58] is an example of VTOL UAV. Additionally, civilian applications include pipelines and power lines inspection and surveillance, oil and natural gas search, and fire prevention. As the UAV field matures, the tendency shifts to smaller, more flexible and versatile UAVs. New composite materials and improved propulsion systems result in lighter, smaller, and more stealthy airframes, with the resulting fuel efficiency leading to levels of endurance that exceed human tolerance.

As mentioned above, most of UAVs are used for military missions. Nonetheless, civilian applications gain momentum; but the consensus is that much more cost effective UAVs need to be utilized. Thus, well documented UAVs are those used by the military around the world with the United States of America (USA) leading the market and investments in research and development programs [4].

Table 2.1 depicts characteristics of current UAV programs implemented by the Department of Defense (DoD) of the USA.

Table 2.1: UAV programs of the US military [14].

UAV Model	Producer	Radius (nm)	Max. Alt. (ft)	Endurance (hours)	Payload (lbs)	Wt. (lbs)	Est. Unit Cost per vehicle (\$)
Pioneer	AAI	100	15,000	5	75	452	1M
Hunter	Northrop Grumman	144	15,000	11.6	200	1,600	1.2M
Shadow	AAI	27	15,000	4	60	327	350,000
Predator	General Atomics	400	25,000	24+	450	2,250	4.5M
Global Hawk	Northrop Grumman	5,400	65,000	32	1,950	26,750	57 M

UAV advantages over manned aircraft in terms of endurance due to pilot fatigue and expendability have been demonstrated and proven in conflicts. For instance, a model of Pioneer [7] (a short range UAV) was used as a source of intelligence at the tactical level during the Operation Desert Storm in Iraq. Additionally, a model of Predator [82] performed surveillance missions such as monitoring area roads for weapon movements and conducting battle damage assessment in the Balkan conflicts [4].

UAVs range in size from 15 grams (Black hornet) capable of carrying role equipment to meet their specific mission, to a full size aircraft (Global Hawk).

Table 2.2 presents the extremum records of UAVs.

Table 2.2: Extremum records of UAVs [8].

	Flying Today
Fastest	RQ-4/Global Hawk (390 mph)
Highest	Pathfinder plus (80,400 ft)
Biggest (size)	Centurion (206 foot wing span)
Biggest (weight)	RQ-4/Global Hawk (25,600 lbs)
Smallest	Spot MAV made by Kun Kuk University , South Korea (15 cm)
Longest Flight Hour	HERON UAV made IAI (52hrs)
Longest Flight Distance	RQ-4/Global Hawk (13,840 km) Cross the Pacific Ocean

Currently, the smallest prototyped UAV called Black Hornet¹ [9] is a 15 grams spy nanocopter developed by Prox Dynamics for military use. It is expected to provide soldiers with their own immediate intelligence, surveillance and reconnaissance capability for operations indoors and outdoors, in confined areas; looking behind, between, and below obstacles with a bird's eye view² of areas of interest.

¹Black Hornet is expected operational in 2011.

²A view of an object from above, as though the observer were a bird.

Figure 2.1 illustrates the Black Hornet.

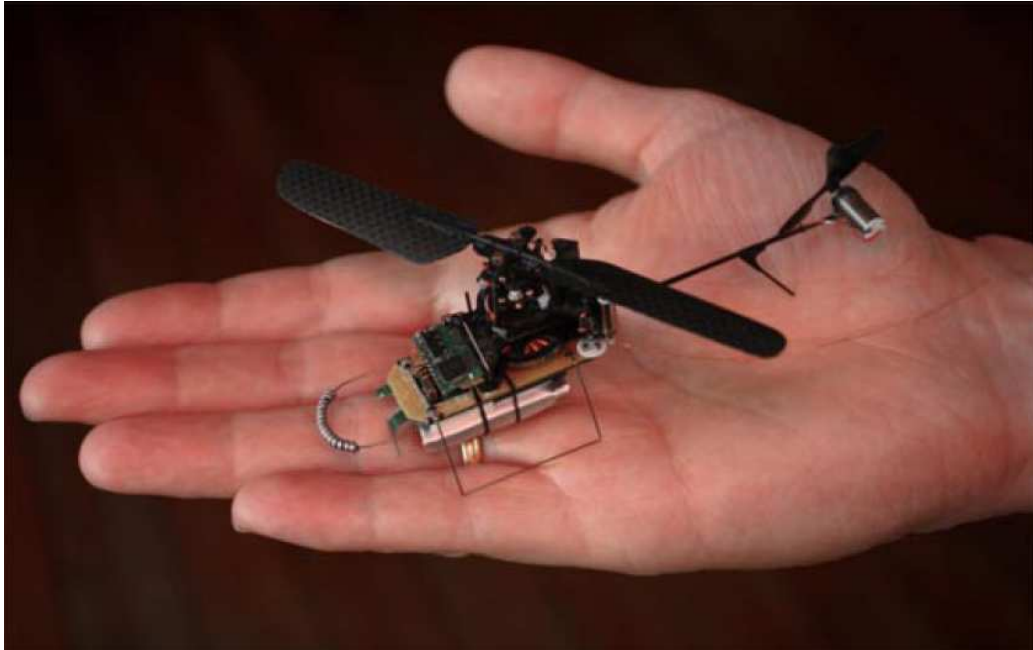


Figure 2.1: Black Hornet [9].

The modern concept of U.S. military is to have the various aircraft systems working together in support of personnel on the ground. The integration scheme is described in terms of a "Tier" system. It is used by military planners to designate the various individual aircraft elements in an overall usage plan for integrated operations. The Tiers do not refer to specific models of aircraft; but to roles for which various models and their manufacturers competed [13].

Table 2.3 presents the classification of UAVs according to the United States Airforce (USAF) standard.

Table 2.3: USAF classification of UAVs [10].

Category	Designation	Max Alt	Radius	Speed	Endurance	Example
Tier I (Tactical)	Interim-Medium Altitude, Endurance	Up to 15,000 ft	Up to 250km	60- 100kts	5-24hrs	Pioneer, Searcher
Tier II (Operative)	Medium Altitude, Endurance	3,000ft to 25,000ft	900km	70kts cruise	More than 24hrs	Predator
Tier II Plus (Strategic HAE)	High Altitude, Endurance	65,000ft max	Up to 5,000km	350kts cruise	Up to 24hrs	Global Hawk
Tier III Minus (Strategic LO-HAE)	Low Observable, High Altitude, Endurance	45,000ft to 65,000ft	800km	300kts cruise	Up to 12hrs	Darkstar

2.1 Classification Of UAVs

UAVs can be classified based on number of characteristics including performance and mission. The performance characteristics consist of:

1. Weight,
2. Range,
3. Altitude and endurance,
4. Wing loading,
5. Engine type,
6. Power/Thrust Loading.

Table 2.4 and Table 2.5 show UAV classifications by altitude and endurance, and by weight respectively.

Table 2.4: UAV classification by altitude and endurance [8]

CLASS	ALTITUDE	PAYLOAD	UAVs
Low Altitude UAV	Lower than 20,000 ft	EO Camera, IR, FLIR Sensors, etc.	Hunter, Aerosonde, Outrider, Shadow
Medium Altitude UAV	Lower than 45,000 ft Fly in the troposphere.	EO Camera, SAR, Etc.	
Medium Altitude Endurance (MAE)	Lower than 45,000 ft Fly in the troposphere. Flight hour more about than 24 hours.	EO Camera, SAR, Etc.	Gnat750, Model000, Predator, Heron
High Altitude UAV	Higher than 45,000 ft Fly in the stratosphere.	SAR, Etc.	Dark Star
High Altitude Endurance (HAE)	Higher than 45,000 ft Fly in the stratosphere. Flight hour more about than 24 hours.	SAR, Etc.	Global Hawk, Theseus, BQM-34, Altus2

EO stands for Electro Optical

IR stands for Infra Red

FLIR stands for Forward Looking InfraRed

SAR stands for Synthetic Aperture Radar

Table 2.5: UAV classification by weight.

Designation	Weight Range (kg)	Example
Super Heavy	more than 2000	Global Hawk
Heavy	200 to 2000	A-160
Medium	50 to 200	Raven
Light	5 to 50	RPO Midget
Micro	0.1 to 5	Dragon Eye
Nano	less than 0.1	Black Hornet

Based on their geometric dimensions, three classes of UAVs may be considered. These categories include small size, medium size and large size UAVs. These three classes are directly related to the classification based on weight. Man-portable UAVs are briefly discussed below. The smallest unmanned aerial vehicles are Nano and Micro UAV's (MUAV) such as the Black Hornet (Figure 2.1) and the AV Black Widow developed for military surveillance, law enforcement, and civilian rescue efforts. Their weight and payload are just a few grams with vehicle size in the order of few centimeters. Larger than MUAVs are the Small UAVs (SUAV). Their size ranges from tenths of decimeter to a few meters, with platform weights in the order of a few kilograms. They are hand-launched or launched from a mobile launch station. SUAVs including Raven, Pointer, and the Force Protection Aerial Surveillance System (FPASS) are man-portable, low-altitude, short-range systems assisted in providing base security, force protection, reconnaissance, and targeting. Small UAVs are rapidly growing in type and offer a versatile family of capabilities. They provide a unique target approaching capability. Their small size, quiet propulsion systems, and ability to feed information directly to battlefield airmen enhance the combat effectiveness [63].

2.2 Mission Aspects of UAVs

As mentioned earlier, the majority of UAVs is military orientated. Different military mission requirements have created various types of UAVs including [14]:

1. Intelligence, Surveillance, Target Acquisition and Reconnaissance (ISTAR). Examples include most UAVs.
2. Unmanned combat aerial vehicles (UCAV). Examples include X45A, X45C, X46, and X47.
3. Multi-Purpose. Examples include MQ-1 Predator, MQ-5B Hunter, and MQ-9 Predator B.
4. Vertical Take-Off and Landing (VTOL). Examples include Fire Scout, Killer Bee, and X50.
5. Radar and Communication Relay. Examples include Tethered Aerostat Radar System, and Near Space Maneuvering Vehicle (NSMV)/Ascender/V-Airship.
6. Aerial Delivery and Resupply. Examples include CQ-10 Snow Goose.

ISTAR is a system using UAVs to gather enemy information, locate a target, or patrol hostile air space without risking lives of the operators. Often in battle grounds, combat commanders require real time information of the upcoming enemy forces. As an illustration, to be aware of the potential enemy defense, gathering information via reconnaissance UAVs is more effective in saving soldier lives. This category contains most UAVs.

Chapter 3

Morphing Concepts

Following the introduction of the morphing shape alternatives, this Chapter describes morphing concepts including the planform alternation, out-of-plane transformation, and airfoil adjustment. Section 3.5 is dedicated to the two most successful morphing UAV programs launched by NextGen Aeronautics and Martin Lockheed. Friswell [15] defines four applications of the wing morphing concept:

1. Improvement of the aircraft performance to expand its flight envelope,
2. Replacement of conventional control surfaces for flight control to improve the performance and stealth characteristics,
3. Reduction of the drag to improve the range,
4. Reduction of the vibration or the control of flutter.

Structural morphing is not a new concept in aircraft design. The Wright Brothers, for example, used wing warping through structural deformation to control the roll of the aircraft [65], Parker [64] proposed a variable camber wing to increase the flight speed.

Significant amount of investigations have been conducted since [28, 29, 30] on the wing structural morphing to achieve optimum aircraft performance by altering wing aerodynamic parameters. Thus, based on the changes induced by the structural changes in the aerodynamics of the wing, the morphing concepts are classified as [51]:

1. Large morphing to produce global aerodynamic effects: Examples include large aspect ratio changes of the order of 50 - 60% or more.
2. Small morphing to produce global aerodynamic effects: Efforts like the synthetic jet actuation to produce hingeless trailing edge and morphing wing via twisting the airfoil section come under this category.
3. Small morphing to produce local aerodynamic effects: Examples include groups of synthetic jets for induced drag reduction and active skins to reduce the induced drag.
4. Intermediate morphing: Morphing for any other purposes like medium changes in span for flight in subsonic velocities.

By wing morphing, the author refers to a planform that is able to transform smoothly its shape or any other characteristic affecting significantly its aerodynamic properties. It is evident that a conventional aircraft has a wing matching the mission it is dedicated to. As a general observation, the concept of morphing wings is inspired from birds; but also from bats at its early stage as illustrated by the flying machines of Clement Ader [33] depicted by Figure 3.1.



Figure 3.1: Ader's Eole [33].

In fact, birds are able to adapt their wings to the conditions that need to be met at a given time. Thus, they can fold their wings tightly to dive for a prey, or fully extend them to glide; saving thus energy as it can be seen in Figure 3.2. Additionally, they use the camber and wing twist to control their flight. By changing the area of the wing, birds and other flying insects are able to alter the lift generated.

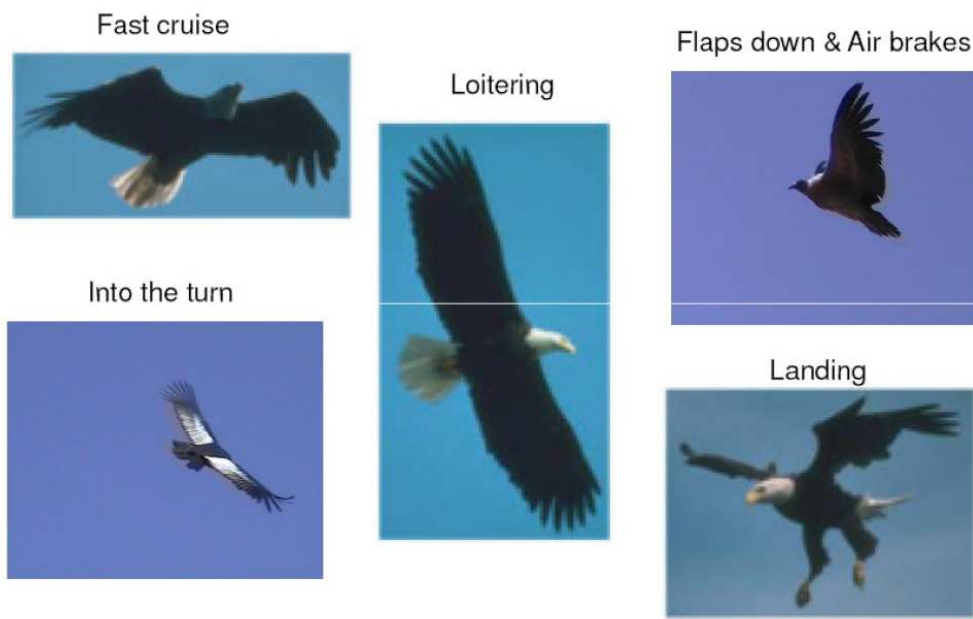


Figure 3.2: Eagle in various wing configurations [109].

Research [2, 15, 48] in the aircraft industry investigates the development of an aircraft wing that is able to mimic the bird wing morphing ability. Such an aircraft would perform dissimilar missions. Thus, a fighter aircraft or unmanned aerial vehicle could have multiple roles including reconnaissance, fighting and heavily bombing with an increased stealth capability. Furthermore, a commercial aircraft could adapt its wings smoothly for a high lift during takeoff and landing, extend them fully for optimum cruising, and fold them slightly for an efficient descent.

In order to morph the wing, approaches using the wing twist, leading and trailing edge deformations [31], and the airfoil camber control [30] have been given particular attention as efficient methods of mission optimization while minimizing the structural weight and induced drag. There are two approaches to achieve shape changes on a morphing aircraft [26]:

1. Planform changes using rigid mechanisms. The variable sweep on aircraft including F-14 and XF 10F Jaguar is based on this technique [32].
2. Compliant mechanisms. Compliant mechanisms are single-piece flexible structures that deliver the desired motion by undergoing elastic deformation as opposed to jointed rigid body motions of conventional mechanisms [110, 28]. Therefore, compliance in design leads to jointless, no-assembly, monolithic mechanical devices. The advantages of compliant mechanics include a reduced complexity, zero backlash and wear, sub-micron accuracy, and embedded actuation and sensing devices. They are particularly adequate for applications with small range of motions. Such mechanics have been used on the modified F-111 named Mission Adaptive Wing (MAW) [31]. However, the design of the F-111 suffers from weight penalty due to the use of several servo motors, transmission components and accessory equipment. Additionally, the actuators require energy for changing the shape of a structure. Furthermore, power is needed by the actuator to overcome its stiffness. Thus, using electric or pneumatic actuators combined with complex mechanisms might be inadequate to take full advantage of the morphing concept. Significant aerodynamic performance gains are effectively achieved through large overall changes in the aircraft planform using recent morphing technology combining novel materials and actuation systems [28].

3.1 Morphing Shape Alternatives

Significant geometric variations of an aircraft wing in-flight can allow efficient performance during different flight segments, or permit multi-role missions that are impossible without the aircraft reconfiguration. Conventional aircraft use mechanisms to change discretely the wing area in different flight configurations. These configurations include takeoff, climb, cruise and landing. The discrete shape change is achieved by extending or retracting flaps, slats, tabs, ailerons to either modify the wing area and the airfoil camber for additional lift or the aircraft controllability characteristics.

Several methods exist to increase the efficiency of different flight aspects of an aircraft through changing the aerodynamic characteristics of the wing. Firstly, changing the span or the aspect ratio of the aircraft wing alters the aircraft lift characteristics, and stealth characteristics for military aircraft. Secondly, loitering can be performed more efficiently by changing the airfoil shape through drooping the wings, increasing the airfoil camber, or twisting the wing. Performing any of these changes by morphing during a mission would give increased efficiency in the loiter stage [34]. Table 3.1 defines the aerodynamic advantages of varying the wing geometry.

Table 3.1: Effects of the change type on the aerodynamic characteristics in the scale 1-5 [34].

		Max. Speed	Range	Landing Dist.	Take-off Dist.	Maneuverability	State Change Effectiveness	Relative Numeric Total
Physical State Change	Span	5	4	4	4	3	4	24
	AR	3	4	3	3	2	3	18
	Sweep	5	3	5	5	4	4	26
	taper ratio	1	2	1	1	1	1	7
	t/c	1	2	1	1	1	1	7
	camber	2	2	5	5	5	4	23

It is evident from the table above that changing the sweep, the span or the airfoil camber provides significant aerodynamic and economic advantages.

Considering aircraft performance parameters such as range and endurance, it can be shown that these parameters are strongly dependent on $\left(\frac{C_L}{C_D}\right)$ and $\left(\frac{C_L^{\frac{3}{2}}}{C_D}\right)$ respectively. Furthermore, these ratios are directly proportional to the wing aspect ratio. It is thus obvious that an increase in the wing aspect ratio will result in a rise of both endurance and range. Therefore, by tailoring the wing geometry through morphing concepts, its lift and drag characteristics can be adjusted to a variety of missions or flight segments.

Sofla et al.[111] classify the wing morphing concepts into three major types:

1. Planform alternation,
2. Out-of-plane transformation,
3. Airfoil adjustment.

The planform alternation is performed through the wing area resizing by changing parameters including the span, chord length, and sweep angle. The out-of-plane transformations include the wing twist, the chord and span-wise camber changes. The airfoil adjustment regroups designs that can alter the wing profile with no significant change in the wing camber; the wing thickness control comes under this category. Figure 3.3 shows the classification mentioned above.

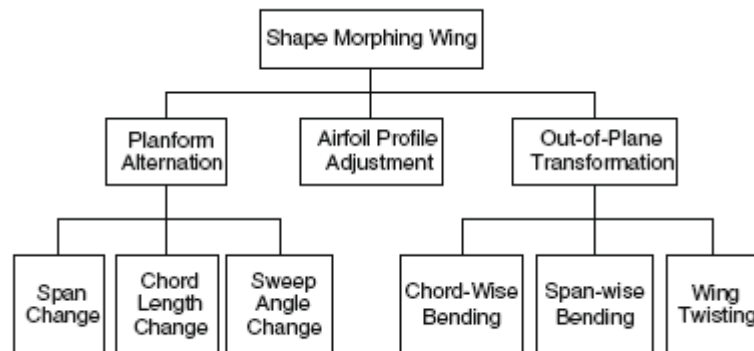


Figure 3.3: Classification for shape morphing of wing [111].

3.2 Wing Planform Alternations

The planform alternation can be realized by tailoring the win span, chord length, and sweep angle as shown in Figure 3.3. Thus, the wing sweep and span changes are designed to alter the wing configuration of an aerial vehicle for various flight conditions.

3.2.1 Wing Span Morphing

The telescoping wing design was proposed as an approach for the wing span change. It is known that the telescoping wing design is equivalent to the concept of changing the lift with conventional chord-wise flaps except that the span-wise flap increases the span and the area instead of only the camber. Additionally, it increases the aspect ratio; thus, improving efficiency and safety significantly.

In 1931, Ivan Makhonine's [20] telescoping wing concept produced the MAK-10 with an outer wing section telescoping into the inner section to reduce the span and the wing area for a high speed cruise. The wing is extended for economic cruise and landing. The sliding wing of the MAK-10 was actuated pneumatically combined with a manual stand-by system.

Recently, Blondeau et al.[112] realized the morphing of the aspect ratio of a wing using an inflatable telescopic spar. Their design consisted of three segmented telescopic wing with inflatable actuators replacing the traditional spars. These pneumatic spars consisted of three concentric cylindrical aluminum tubes that could achieve variation span configurations. The alignment of the sliding tubes was ensured using ceramic linear bearings. The prototype achieved a change of 114% of the wing aspect ratio. The wing maximum value of the lift to drag ratio (L/D) was approximately 15% higher than its rigid fixed wing counterpart when fully extended. Currently, Gevers Aircraft Inc. [22] holds a patent of the telescoping wing design. The proposed aircraft, the Genesis, is expected to cruise over 450 km/h and stall at a velocity of approximately 101 km/h with the wing fully extended. The advantages of the Genesis wings when they are retracted include:

1. A span reduction raises the wing strength to aerobatic rating,
2. A higher stiffness and resistance to bending and twist enhancing flutter resistant,
3. A small wing area improves the flight quality in rough air conditions,
4. The hangar space is minimized,
5. The drag reduction improves the speed and the efficiency,

while the advantages of the wings when they are extended include:

1. The rate of climb is improved, especially during single engine operation,
2. The endurance for instance during search and rescue operations or surveillance is improved,
3. The range is improved,
4. The touchdown speed is lowered,
5. Takeoff and landing lengths are reduced.

Nevertheless, challenges faced by this concept include the ability of the structure to resist bending under the loading due to large wing deflections, a weight penalty, actuator issues, and the energy required to drive the system. Due to an increase in the parasitic drag caused by discontinuous seams, telescoping wings have a lower aerodynamic efficiency (lift to drag ratio) than rigid fixed-wings [90].

3.2.2 Inflatable Wing Concept

In 1950s, Goodyear produced the first successful inflatable wings on their inflatoplane [45]. New materials address issues of leaking and deflation. Such wings can be constructed of rigidizable fabric composites that harden, after deployment and exposure to ultra violet radiation, or of rugged woven materials to prevent damage. Thus, simply inflatable wings require constant pressurization to maintain their shape, while inflatable/rigidizable wings harden into a persistent shape once inflated. The simply inflatable wings present a smooth surface compared to the rigidizable wings. This characteristic has a significant influence on the aerodynamic characteristics of the wing in terms of a higher lift and lower drag coefficients as it can be seen in Figure 3.5.

The first use of inflatable wings in a UAV was applied to the Apterion vehicle that was developed in the 1970s by ILC Dover, Inc. Apterion had a 1.55 m wingspan, 373 W engine, 3.18 kg gross weight and was remotely controlled via elevons mounted on the trailing edge. It was successful flight tested, but was never put into production [113].

Recently, Simpson et al.[114] designed and constructed non-rigidizable inflatable wings to provide the roll control through the wing camber morphing. This is referred to as wing warping. Since the wings were non-rigid, it was possible to manipulate their shape to induce a roll moment. The wing design took advantage of the presence of internal span-wise baffles (inflation cavities) to maintain the structural stiffness at a lower internal pressure. The outer wing and internal baffles were constructed from high strength fibers such as Kevlar.

Shape Memory Alloys (SMA), Electro-Active Polymers (EAP), and servo actuated systems represent good actuator candidates for inflatable wings. Cadogan et al.[115], for example, used SMA wires integrated to a multi-functional inflatable aerial vehicle. They actuated the aft end of the wing to achieve changes in section camber, leading to the aircraft roll control.

Benefits of inflatable wings include wing morphing to alter aerodynamic characteristics in-flight, stowing when the wing is not in use to keep the vehicle size small, robustness, low mass, and low deployment time. Their applications include UAVs such as High Altitude Long Endurance (HALE) vehicles. The wing planform can be either full or partial span design, allowing a large design space and possible mission adaptability. These wings are deployed to either provide new lifting surfaces or change the geometry of rigid lift surfaces. Their deployment increases both the span and wing area, hence, the aspect ratio of the wing. This deployment can occur in a relatively short time depending on the size of the wing and on the type of the inflation system.

Figure 3.4 illustrates the deployment in-flight of NASA Dryden I2000 [56] inflatable wing. Nitrogen gas pressurization of 1380-1725 kPa was applied to maintain a suitable wing strength and stiffness for the Dryden I2000.

Apart from the use as a stand alone aerodynamic surface on a morphing UAV, the inflatable system can also be used as an aspect ratio increasing device on a larger aircraft to enable a more radical change in the wing configuration. This technique improves the system efficiency across changing flight regimes, allowing the transition from a high speed target approach to a low speed loitering [47].



Figure 3.4: In-flight deployment of I2000 inflatable Wing [46].

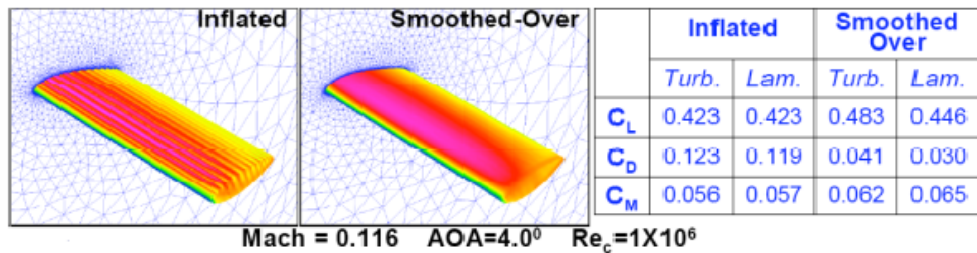


Figure 3.5: Aerodynamic coefficients of an inflatable wing [12].

3.2.3 Sweep Angle Variation

The concept of variable sweep started during World War II with the variable wing Messerschmitt P.1101 and was implemented by the US army on the Bell X-5 [21]. In this design, the aerodynamic forces on the wing are carried by a complex and heavy pivoting mechanism. The concept attempts in the supersonic range to have a small compact wing for high speed flights and one with larger area and span for takeoff climb and cruising. The design allows an aircraft to vary its aspect ratio and thickness to chord ratio (fineness ratio) to optimize the configuration for different flight Mach numbers [25].

This concept may be implemented using one of the three approaches including:

1. The whole wing outboard of fuselage moves,
2. The outer part of the wings moves,
3. The wings, when swept back are integrated with the tailplane to form a delta surface.

Generally, an increase of the sweep angle improves the aerodynamic performance at high speed regimes. Additionally, it significantly increases the flight envelope of an aircraft originally designed for low speed flights. However, the structural morphing is traditionally realized through complex and heavy mechanisms composed of pivots. These pivots must bear bending and torsion loads; they tend to be heavy due to their thickness, reducing thus the overall effectiveness of the design. The wing sweep mechanism of F-14 fighter is depicted in Figure 3.6.

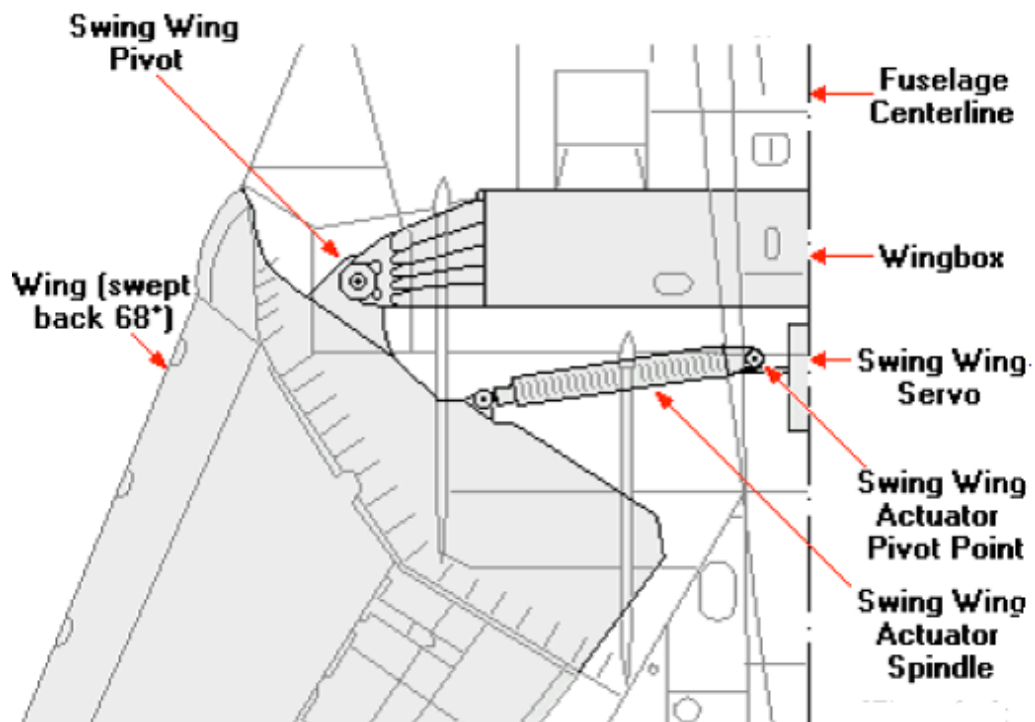


Figure 3.6: F-14 wing sweep mechanism [23].

The characteristics of variable sweep concept include [24]:

1. Delay in the drag rise. Thus, the subsonic speed and high altitude cruise speeds are increased.
2. Lower subsonic drag. Consequently, supersonic speeds can be reached without excessively low thickness ratios or high wing loading.
3. Lower lift slope. This implies a higher approach and cruise attitude, and a reduction in gust sensitiveness at high speed.

Nevertheless, the variable sweep concept involves difficulties including structural thickness, significantly high wing loadings and transonic and supersonic trim difficulties [19]. To eliminate penalties associated with this concept, the oblique wing approach was developed. The oblique wing flies supersonically with one wing swept forward and the other swept backward. At low speeds, the wing changes to an unswept design for a better subsonic efficiency. It is known to have a lower supersonic wave drag than conventionally designed symmetrically swept wings. Additionally, when flying at low speeds, the unswept wing has a higher efficiency than swept wings. An oblique wing can vary the wing sweep with a single pivot that is primarily loaded in tension, trading the aspect ratio for the fineness ratio by sweeping one wing tip forward and the other wing tip backward. Furthermore, the asymmetric sweep can increase the fineness ratio of the wing more significantly than a symmetric sweep design [25].

NextGen Aeronautics [59] developed UAVs based on scissors mechanism resulting in a variable sweep falling into the range of 15 to 35 degrees in-flight. NextGen's UAV is reviewed in section 3.5.

Alternatively, Friswell et al. [27] successfully demonstrated the use of unsymmetrical laminated composites to realize a variable sweep wing for morphing UAV applications. Their numeric analysis identified the bifurcation point referred to as a snapping point at which the geometry changes. This confirms the possibility of eliminating mechanical joints to obtain different geometries. In their design, the wing spars are made of bi-stable composites. When a bending moment is applied on the spar, it causes the spar to snap to a second stable position around the bifurcation point which acts as a hinge. Therefore, the application of multistable composites simplify the complex mechanical systems required to modify the geometry of conventional wings [44]. However, the use of bi-stable composite materials may suffer from fatigue at the bifurcation point. Furthermore, the compliance of the wing skin may interfere with the snapping motion [111]. Multi-stable composite materials are reviewed in Chapter 5.

3.3 Out-Of-Plane Transformations

An alternative approach to modifying the aerodynamic characteristics of a wing is to alter the wing out of its original plane. Several researches [83, 30, 111] have shown the potential of smart materials to accomplish the out-of-plane alternation of a morphing wing through camber change. This section presents the wing camber, chord, and twist controls.

3.3.1 Camber And Chord Control

In the camber control approach, the adaptive airfoil can alter its camber to obtain the desired lift. This eliminates the need for conventional control surfaces. Experimental and computational results show a high promise for variable camber geometries [31]. Camber change is performed either by the reconfiguration of the wing internal structure or the alternation of the wing skin. However, variable geometry airfoils such as the one developed for the Mission Adaptive Wing (MAW) [48] are complex structurally and consequently heavy and maintenance intensive.

Recently, Diaconu et al.[49] intensively investigated the use of bi-stable or multi-stable structures as a morphing approach for the airfoil chord and camber changes. The bi-stability behaviour of the composite is the result of the simultaneous effects of residual stress resulting from cooling and the non-linear deflections in the structure [50]. In Diaconu's design, such a bi-stable composite plate was embedded chord-wise and vertically in the airfoil cross section. This plate snapped from one stable position to another under moments applied alternatively by actuators on the edges of the laminate. Thus, the chord-wise composite member controlled the airfoil camber, while the vertical element altered its chord length.

Furthermore, Ursache et al.[52] demonstrated that by using structures that are acting in the post-buckling regime, it is possible to obtain significant changes in shape with very modest changes in the applied load. Thus, by making use of non-linear structural responses, camber control of deformable airfoils can be achieved by using a carefully designed pre-loaded internal spinal structure. Such a structure is expected to move through the desired shape changes under the control of a single actuator. This actuator will deliver aerodynamic characteristics that match a set of pre-specified target shapes and also give improved aero-elastic properties.

Sofla et al.[132] developed a series of SMA-actuated flexural structures which could be used to deform wing sections. Their actuated structures were based on a concept called antagonistic flexural unit cell (AFC). In this concept, a pair of one-way SMA actuators are placed at either side of a highly flexible unit core structure with large in-plane stiffness. The contraction of one SMA actuator upon heating results in the extension of the opposing SMA actuator mechanically. The contraction by heating of the now-extended actuator, later in the cycle, reverses the actuation.

High authority shape morphing beams can be made by the linear replication of the AFCs. Such actuated beams can be used to make reconfigurable wing boxes for shape morphing wing structures. Although the slow cooling rate of the SMA actuation is not appropriate for the flight control applications, the achievable aerodynamic changes are still suitable for in-flight mission adaptation of the wing. The AFC based actuated structures are attractive for wing morphing applications because the distributed SMA actuators carry aerodynamic loads and therefore reduce the weight penalty. Additionally, the new wing shapes after the cooling of each SMA actuator are retained without requiring power. This can eventually result in saving fuel and increasing the aircraft endurance [111].

Figure 3.7 illustrates a wing section prototype that is capable of undergoing camber changes when actuated by antagonistic SMA actuators.

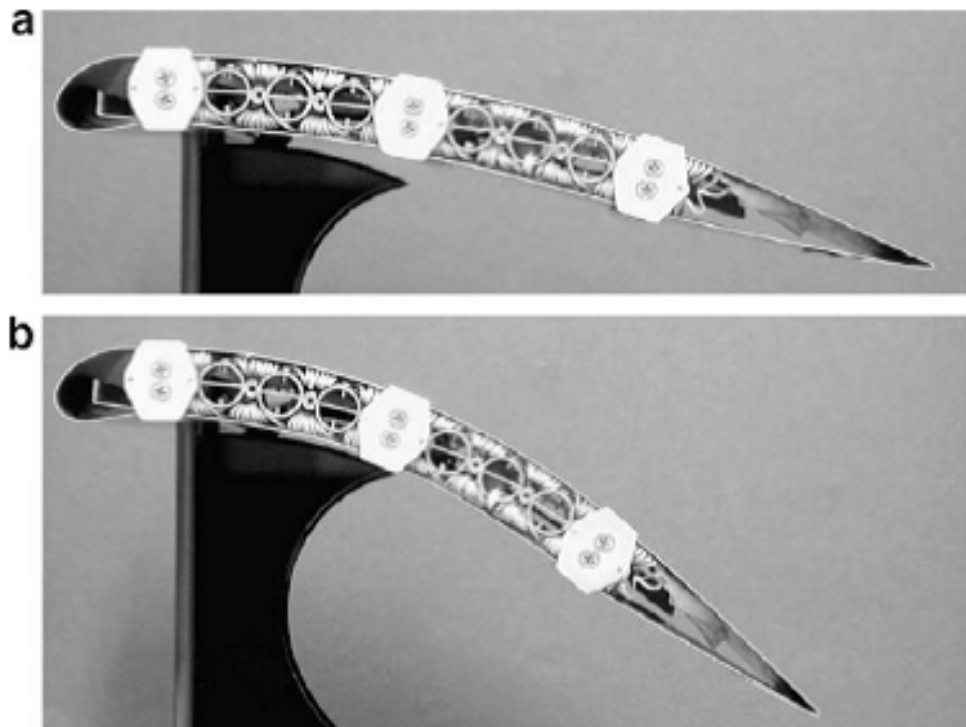


Figure 3.7: Chord-wise bending achieved by the heating of SMA strips in an antagonistic design. (a) Un-morphed and (b) morphed [133].

3.3.2 Wing Twist Control

In morphing via variable twist, the wing is configured to optimize the twist angle to obtain low drag and high lift aerodynamic characteristics. Sofla et al.[111] report the gradual changes of the airfoil chamber along the span as a method to create a controllable twisting of the wing. In their design, an antagonistic wing was prototyped using shape memory alloy (SMA) actuators. An antagonistic structure is based on a pair of one-way SMA actuators as described in the previous section. Thus, the wing undergoes twisting by the asymmetric actuation of its SMA actuators.

In an alternative approach, Mujahid et al.[116] controlled the roll of a mini UAV by twisting its flexible wing. In their design, torque rods ran spanwise. These rods were rotated separately by two servo-motors mounted in the fuselage. Commanding a deflection of the servo induces the rods to rotate by acting against the wing leading edge. Their results for flight characteristics for the roll and spinning showed that the vehicle was easier to fly using morphing instead of the conventional rudder as lateral directional effector.

Figure 3.8 presents the twisting of a wing section using antagonistic SMA actuation.

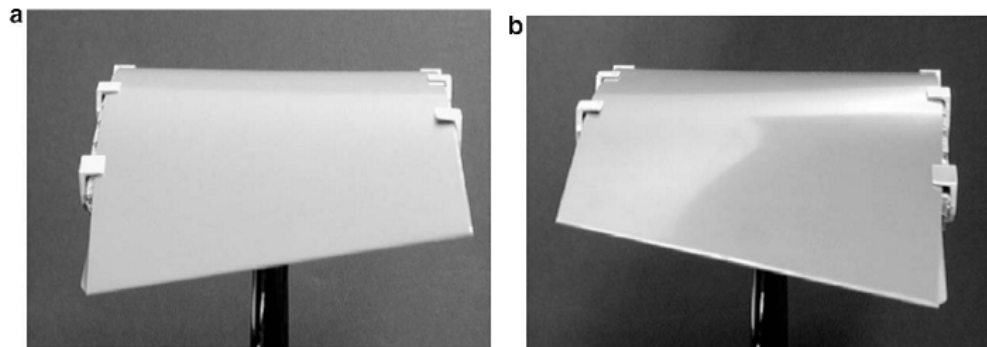


Figure 3.8: Twisting of a wing section achieved by antagonistic SMA actuation. (a) The left rib is flexed downward and right rib upward. (b) The left rib is actuated upward and the right one downward [133].

Figure 3.9 illustrates the nominal wing and the morphed wing when each servo-motor is commanded to its equal but opposite value.

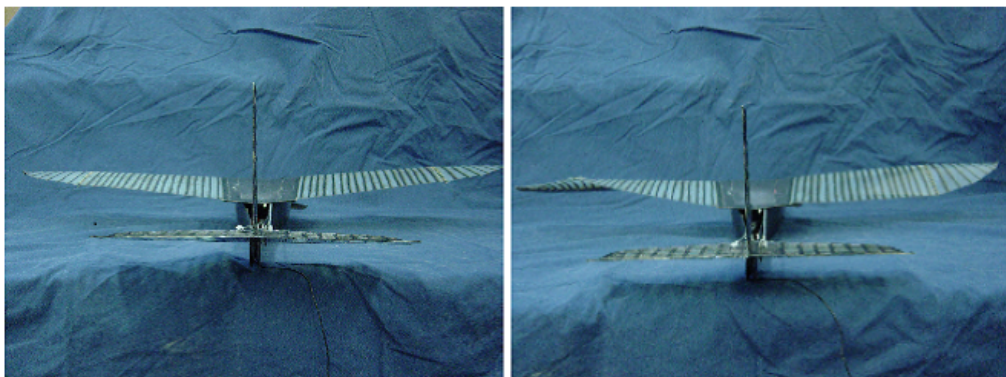


Figure 3.9: Nominal wing (left) and morphed wing (right) [116].

Moreover, adaptive aero-elastic structures offer potential solutions to achieve wing morphing through out-of-plane transformation. This approach uses the aerodynamic forces acting upon the wing to provide the necessary forces and moments to bend and twist the wing. These structures are reviewed in Chapter 5.

3.4 Airfoil Profile Adjustments

An airfoil significantly influences the aerodynamic characteristics of any aircraft. By tailoring the shape of the airfoil, the aircraft efficiency can be modified by tuning an optimum airfoil configuration. Thus, if an airfoil section can be changed accordingly with the shift of flight conditions, benefits may result that include the improvements of the Mach number, aerodynamic efficiency, aerodynamic performances such as the range, endurance, and the expansion of the flight envelope. The airfoil profile adjustments to alter the aerodynamic characteristics of the wing, as described in Figure 3.3, reshape the wing profile with no significant change of its camber. Austin et al.[117] developed a theoretical method which was experimentally validated. Their purpose was to control the static shape of flexible structures by employing internal translational actuators. In their design, 14 linear actuators were attached diagonally to form a wing rib structure as depicted in Figure 3.10. The diagonal elements are translational actuators that expand and contract to deform the airfoil. A prototype of the adaptive rib with the actuators was constructed to demonstrate the shape-control concept.

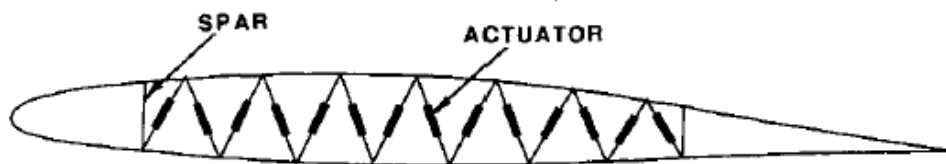


Figure 3.10: Airfoil profile control [117].

Dong et al.[118] designed and manufactured a changeable airfoil model using SMA springs between the wing skin and its supporting wing-box. Thus, by changing the constraint condition of the skins, they can achieve large deformation without overstepping their strain allowance. Shape memory alloy springs with the help of stop structures were used to actuate accurately certain points on the skins to approach the target airfoil. The wing-box consisted of rigid steel ribs and spars. The covering skin was allowed to slide over a cushion at the leading edge spar as illustrated by Figure 3.11. Cushions were used in order to avoid dislocation between the skins which were level with that of the trailing edge box. The resizing of the SMA spring length upon heating and cooling could alter the wing thickness.

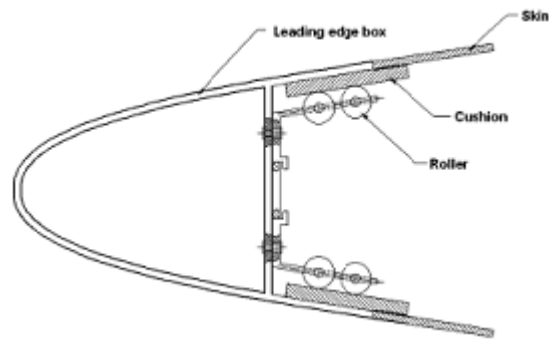


Figure 3.11: Position of the wing skins [118].

Table 3.2 summarizes actuation and skin types associated to a typical wing morphing.

Table 3.2: Morphing concepts, actuation and skin types.

Morphed aspects	Actuation types	Skin types
Sweep	Pneumatic Linear actuator Electric DC motor	Rigid segmented Stretchable
Span	Pneumatic DC motor Servo motor Linear actuator	Rigid segmented Stretchable
Chord	SMP Servo motor Linear actuator Pneumatic	Stretchable Flexible
Camber	PZT SMA Servo motor Pneumatic Ultrasonic	Rigid segmented Stretchable Flexible
Twist	SMA Electrical PZT DC motor Electric pneumatic	Rigid segmented Stretchable Flexible

3.5 Morphing UAVs

Several researchers [111, 114, 115, 118] have investigated, designed and prototyped morphing UAVs. The two most successful flight-tested vehicles are described in this section.

A large scale of wing morphing is achieved using either rigid mechanisms or smart materials embedded in the wing structures. Rigid mechanisms were used to achieve large shape changes in DARPA [2] morphing program under which NextGen Aeronautics and Lockheed Martin built full-scale wind-tunnel models as well as the subscale flying models. Lockheed's morphing concept is performed by folding the wings upwards and inwards to reduce its area and increase the sweep for a high-speed dash. In contrast, NextGen uses a movable scissors structure, covered with a flexible silicone skin reinforced with metal mesh, enabling the wing to reduce in area as it is swept back.

As a result of their intensive investigations, the first in-flight demonstration of a shape changing, or morphing wing was performed by NextGen with the UAV named MFX-1 [59]. The geometry change was implemented using an internal electro-mechanical actuation system. Approximately 200% change in aspect ratio, 70% change in area, 40% change in span, while independently controlling the sweep and area, and a wing sweep varying from 15 degrees to 35 degrees were demonstrated at various flight speeds around 50 m/s [96]. The model has a 3 meters semi-span when fully extended; but it reduces to 2.2 meters when the wing is retracted for high speed flights [61]. This successful test represents the first step in the development of a morphing UAV whose wing geometry can be rapidly and reversibly changed to optimize the aircraft for dramatically different flight conditions.

Following their previous success, NextGen completed the first autonomous flights of a morphing unmanned aerial vehicle named MFX-2 [59], a scaled version of MFX-1 weighting 135 kg and powered by twin-jet engines. The MFX-2 is capable of independently varying the wing area and sweep. The flight tests were the demonstrations of the morphing technology for a Hunter-Killer (Predator B) UAV, combining the loiter endurance of a surveillance platform with the high-speed dash capability of an attack aircraft. MFX-2 has the ability to create substantial in-plane shape changes and a surface area reduction to transform the wing from an efficient, high-aspect-ratio loiter shape to an efficient, swept, reduced-wing-area transonic, low altitude dash shape [62]. Its wing has flexible, stretchable skin panels attached to an articulated lattice structure with actuators in the joints. Thus, morphing is achieved through the adjustable framework to allow in-plane reconfiguration of highly flexible skins and internal components that create wing area and span changes, including changing leading edge sweep to control aerodynamic drag [62].

The variable geometry wing has the ability to move between five different wing planforms as illustrated in Figure 3.12. An increase of 36% in the aerodynamic efficiency from the cruise flight to the loiter configuration is noticeable from Figure 3.12, while the wing surface increases 51% from the cruise regime to dash maneuver configuration. The wing mechanism is described in Chapter 5.






High Lift	Climb	Cruise	Loiter	Dash/Maneuver (baseline)
				
Wing design L/D ratio 1.45 $b/2 = 8.8$ ft. $S = 17.0$ sq. Ft.	Wing design L/D ratio 1.39 $b/2 = 9.8$ ft. $S = 22.8$ sq. ft.	Wing design L/D ratio 1.23 $b/2 = 7.2$ ft. $S = 15.8$ sq. ft.	Wing design L/D ratio 1.60 $b/2 = 9.8$ ft. $S = 17.4$ sq. ft.	Wing design L/D ratio 1.00 $b_{dash}/2 = 7.2$ ft. $S_{dash} = 23.9$ sq. ft.
$b = \text{wing semi-span}$ $S = \text{wing semi-span area}$				

Figure 3.12: NextGen's morphing wing planform configurations [62].

Lockheed's morphing UAV was designed to investigate interactions between aerodynamics and structures (an aero-elasticity analysis and testing research and development project). This design uses wing folding in several positions to reduce the wetted area and change the sweep at critical points in the mission [62]. The flight tests demonstrate long loiter time and high dash speed in a single shape-changing aircraft. The hinges of the folding wing are covered by flexible silicone skins, and small flaps on the inboard leading edges close the gaps between the inward-folded wing and the fuselage. This flap is the first surface to be powered by a thermopolymer actuator which can fit inside the wing thin leading edge. The model has a 2.9 meters semi-span when unfolded for loiter and a 1.8 meters when folded for high speed flights [61].

Figure 3.13 shows the folding wing concept with wings fully extended and retracted. The wing mechanism is described in Chapter 5.

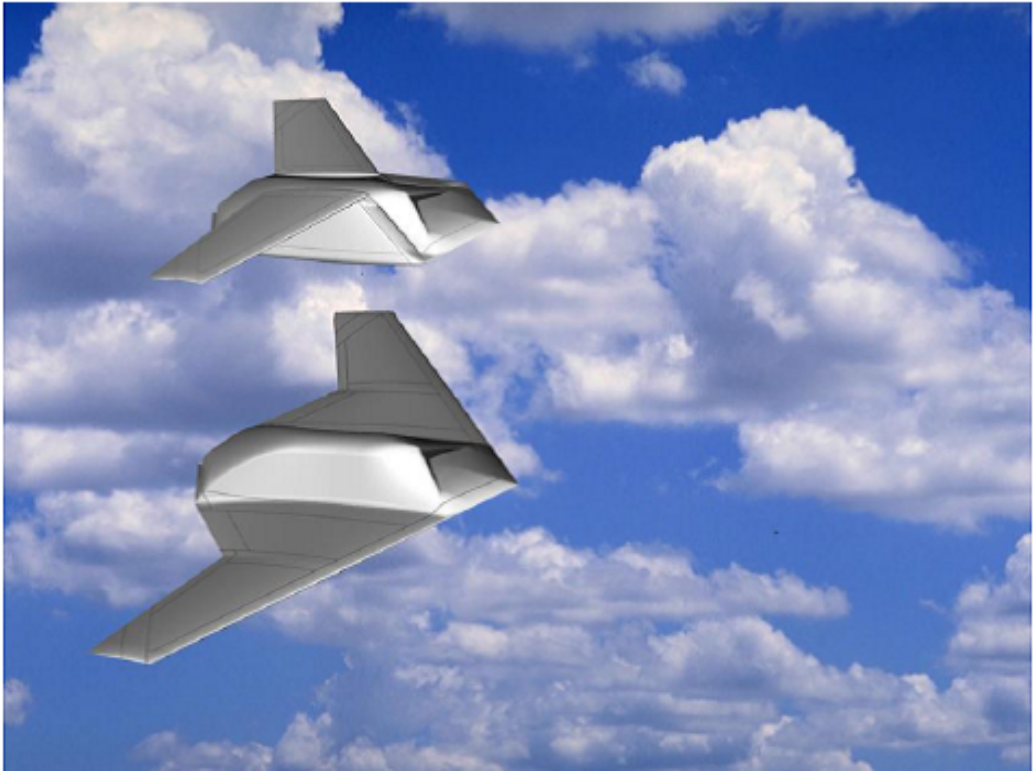


Figure 3.13: Lockheed's folding wing concept [62].

Chapter 4

Actuators And Sensors

This Chapter presents sensors and actuators. Additionally, it reviews the common smart materials. Smart materials require power supply or temperature regulation to induce deformations and maintain a stable state.

4.1 Fiber Optic Sensors

In 1990s, Dunphy et al.[42] identified number of benefits in combining optical fibers and composites. Compared with other sensing methods, optical fibers provide several compelling advantages. One of the most important benefit is their immunity to electro-magnetic interference. This eliminates the need for the costly and heavy shielding normally required to minimize electrical noise picked up when using electrically active sensors. Additionally, fiber optic sensors provide a high bandwidth, high sensitivity, and high dynamic range measurement capability. Additional advantages of this technology include fatigue, corrosion resistance, and the inherent strength of glass fibers [40]. These features enable fiber optic sensors to perform efficiently in extremely hostile environments of high temperatures, erratic vibrations, and shock loadings. The use of optical fiber technology with smart structures enables both the realization of multiplexed arrays of fiber sensors inter-connected by other fibers and the implementation of distributed sensors. Thus, Wood [43] mentioned the fiber Bragg grating sensor as an example in spacecraft application.

Recently, Yin et al.[40] distinguishes two basic classes of fiber optic sensors referred to as extrinsic optic sensors and intrinsic sensors. They are embedded into or attached to materials during the manufacturing process to enhance process control systems, augment the non-destructive evaluation once the parts have been made. Additionally, they form health and damage assessment systems once the parts have been assembled into the structures, and enhance control systems.

A basic fiber optic smart structure system is depicted by Figure 4.1.

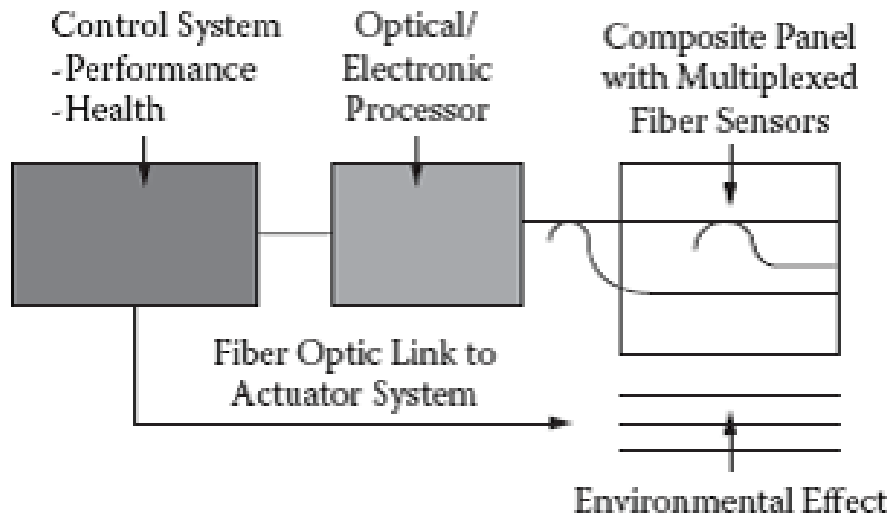


Figure 4.1: Basic fiber optic smart structure system [40].

In the figure above, fiber optic smart structure systems consist of optical fiber sensors embedded or attached to parts. These parts sense environmental effects that are multiplexed and directed down. The effects are then sent through an optical or electronic signal processor. The signal processor in turn feeds the information to a control system that may or may not act on the information via a fiber link to an actuator.

4.2 Smart Materials

Advances in material technology have enabled the development of devices which can serve as both sensors and actuators. By integrating these devices into a structure together with a controller, the material becomes “Smart”. In fact, the materials themselves are not “smart” since they passively react to an input rather than making decisions. By incorporating actuators within a composite structure to make the structure bend, the concept of shape control or morphing can be implemented. A smart structure should possess the ability to sense its internal and external environment. It should then be able to communicate the sensory signals via appropriate pathways (Figure 4.1) to one or several signal processing and control modules, where the information is analyzed and appropriate actions are decided. If necessary, the decisions must be conveyed to actuators incorporated within the structure, which respond by altering its characteristics such as the shape, size, stiffness, position, or natural frequency [41].

The actuators incorporated in the composite wing structure may induce the wing twist, camber shaping and control surface deformations. Additionally, these materials may produce structures with variable stiffness. The aerodynamic efficiency of a control surface may also be controlled and improved by changing the flow conditions over the lifting surface. The expected benefits from such concepts include a reduced drag over a broad range of flight conditions, increased payload, greater range, improved aerodynamic performance, and improved stealth characteristics [35].

It is common to classify smart materials as:

(a) Intrinsically adaptive materials. This category includes Shape Memory Alloys (SMA) and Shape Memory Polymers (SMP). When stimulated, these materials are subjected to transformations in their molecular or microscopic structures. These transformations induce changes in material mechanical properties.

(b) Active materials. This class includes electro-active polymers (EAP), Piezoelectric ceramics (PZT), and magnetostrictive materials. They act as transducers converting electrical, magnetic, or thermal energy into a mechanical energy.

The material choice depends on the specific morphing purpose. If the morphing is dedicated to flight control, the morphing system should exhibit [55]:

1. Relatively fast dynamic,
2. Capability to operate over a wide range of flight conditions,
3. High reliability,
4. Capability of repetitive actuation,
5. Robustness against uncertainties and disturbances such as gust loads,
6. Low power consumption.

Therefore, the ideal material should respond quickly to the external stimuli, be capable of large and recoverable free strains, transform effectively the input energy into mechanical energy. Additionally, it should not be affected by fatigue issues.

The use of smart materials simplifies mechanical systems and thus reduces operating costs. Moreover, it significantly expands the functionality or operating range so that a single system can have multiple uses with a substantial adaption to different conditions. Furthermore, these materials increase the resilience of the system by improving diagnostics, addressing unforeseen problems, and enabling new capabilities.

Table 4.1 reports the main characteristics of the most common smart materials in terms of maximum free strain, maximum stress, deformation energy density, efficiency, and relative speed of response.

Table 4.1: Most common smart materials [54].

Material	Max strain (%)	Max stress (MPa)	Elastic energy density (J/g)	Max effic. (%)	Relative speed
Dielectric Polymer					
Acrylic	215	16.2	3.4	60-80	Medium
Silicone	63	3	0.75	90	Fast
Electrostrictor Polymer P(VDF-TrFE)	4	15	0.17	--	Fast
Piezoelectric Ceramic (PZT)	0.2	110	0.013	>90	Fast
Single Crystal (PZN-PT)	1.7	131	0.13	>90	Fast
Polymer (PVDF)	0.1	4.8	0.0013	n/a	Fast
SMA (TiNi)	>5	>200	>15	<10	Slow
SMP	100	4	2	<10	Slow
Terfenol-D	0.2	70	0.0027	60	Fast
Conducting polymer (Polyaniline)	10	450	23	<1	Slow

From the table above, SMAs and SMPs can undergo large free strains¹ and exhibit large blocking forces². Nevertheless, they have a slow response and a limited efficiency. PZT and single crystal Piezo-ceramics exhibit a much lower free strain but they are capable of producing quite high blocking forces, and sensibly more efficient.

¹Free displacement or free strain refers to the maximum displacement an actuator can develop when there is no restraint against it.

²Blocking force refers to the maximum force an actuator can develop when it is reacting against a fixed constraint.

Electro-active polymers exhibit good properties, although they can produce low blocking stress [55]. Whilst hydraulic actuators can develop large displacements, they have a low blocking force. Piezo-electric stack actuators can develop large forces but they cannot induce large displacements.

Bending type actuators provide high displacements of the order of $1mm$ with low blocking force about $0.5N$. The stack actuators provide low displacements of the order of $1\mu m$ with high blocking force appropriately $1kN$. These two actuator types represent the extreme ends of the current Piezo-electric actuation technology. In the intermediate range, there is a deficiency of the actuator designs that would provide high displacement with high blocking force in the frequency range of few kilohertz [66].

4.3 Shape Memory Alloys

Modern morphing research intends to identify, explore and prototype new materials or mechanisms for active deformations of a high performance vehicle wings with the ultimate goal of a fully integrated adaptive wing structure for shape and maneuver control, performance improvements, stability augmentation, gust load alleviation, and health and usage monitoring [36]. Therefore, in the new approach to morph a wing efficiently, scientists and engineers envision a wing that will sense its environment and adapt its shape to perform optimally in a wide range of flight conditions [37]. Such a wing will spread out on command using shape memory metal alloys or other novel smart materials. It is expected that the material of the wing itself will bend to create the new shape.

Shape memory alloys (SMAs) are metallic alloys which undergo solid-to-solid phase transformations induced by appropriate temperature and/or stress changes. During these changes, the materials can recover permanent strains. Such alloys include NiTi, NiTiCu, and CuAlNi [53]. They have the unusual property of snapping back to their original shape with a high force when a certain amount of heat is applied. Therefore, any shape can be modeled into the alloy as its original shape. These alloys are effective for low frequency applications. They have been utilized to realize the hingeless control surfaces in the Smart Wing program of DARPA [48].

The shape memory materials exhibit some novel performances including sensing (thermal, stress or field), large stroke actuation, high damping, adaptive responses, shape memory, and super-elasticity capability which can be utilized in various engineering approaches to smart systems.

4.4 Piezo-Electric Materials

Piezo-electric materials are able to produce an electrical response when mechanically stressed and inversely a high precision motion can be obtained with the application of an electrical current. Developments in adaptive composite structures, by incorporating integrated Piezo-electric elements, open the possibility to adaptively modify the behavior of a structure. This offers potential benefits in a wide range of engineering applications including wing morphing, vibration damping, precision positioning, and buckling control. Piezo-electric materials are the most popular because their bandwidth covers most of the important aero-elastic modes [36].

4.4.1 Active Fiber Composites

Active fiber composites (AFC) constituted of unidirectional Piezo-electric ceramic fibers sandwiched between two electrodes and embedded in a polymer matrix present major advantages over conventional Piezo-electric materials like ceramics and polymers. AFCs provide a novel method for large scale actuation and sensing in active structures. They have demonstrated distinct advantages over current monolithic Piezo-ceramic actuators. These advantages include [36]:

1. Higher planar actuation strains,
2. A directional actuation or tailorable orthotropic actuation,
3. A robustness to damage,
4. A conformability to curved surfaces,
5. A potential for large area distributed actuation/sensing systems.

4.4.2 Macro Fiber Composite

The Macro Fiber Composite (MFC) proposed by NASA [39] is a material expected to act like muscles and nerves. It can be attached to a structure to bend it, reduce the vibrations and monitor the forces. The composite material is composed of ceramic fibers that can bend when a current is applied to them. By applying voltage to the MFC, the ceramic fibers change shape to expand or contract and turn the resulting force into a bending or twisting action on the material. Likewise, voltage is generated in proportion to the force applied to the MFC material. The material also generates a current when it is vibrated or flexed.

Chapter 5

Structure Solutions

This Chapter introduces the factors that need to be considered when designing a morphing structure. Additionally, it reviews the structural solutions to achieve the morphing of a planform. The two last sections of this Chapter discuss the limitations set by the square-cube law on the use of materials in term of scalability and address the control issues of morphing vehicles.

5.1 Design Aspects of Morphing Structures

As mentioned earlier, the wing is mainly responsible for the aerodynamic loads acting on the aircraft. Hence, most of research on morphing aircraft investigates the possibility of effectively changing the wing geometry. The design of a morphing aircraft is a multidisciplinary and interactive process since the idea is to design a structure that is capable of withstanding predetermined loads and to change its shape in order to bear random loads during operation.

McGowan [12] mentioned design key factors including weight as a primary requirement, followed by functionality since each mission and therefore the associated vehicle has different requirements and constraints. Figure 5.1 illustrates the smart morphing design concept which is the interaction of conflicting design perspectives including flight control, aero-elasticity and power requirements. For instance, the engines supplying the system power are expected to be efficient at low and high speed operations at any altitude. The actuator performance power and actuator force capability are essential to design success. The size, weight and volume of the actuators are important factors [62].

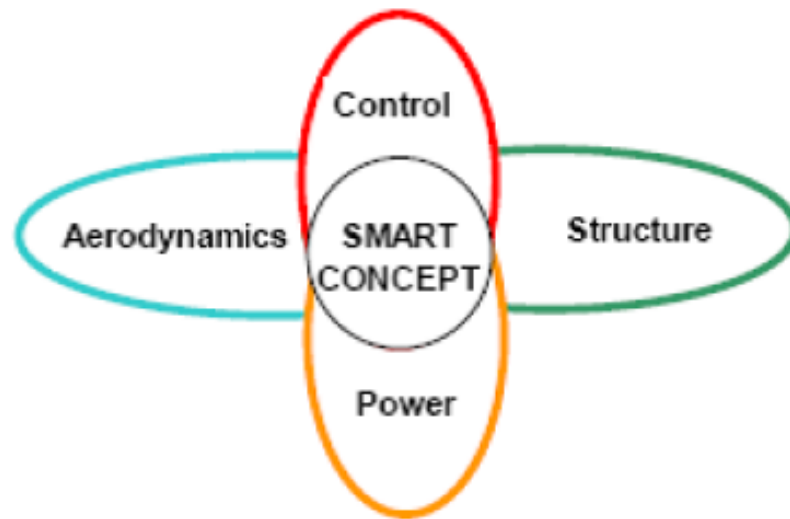


Figure 5.1: Morphing smart design concept [98].

Morphing can be implemented using motors or complex mechanisms distributed through the wing. However, to reduce the complexity of the structure, the actuation system consisting of active materials should be embedded in the structure so that no clear distinction can be made between the structure and actuation systems. Therefore, what is envisaged to produce and carry the loads is also capable to change its own shape or a limited part of it. Thus, design considerations should include [78]:

- (a) Aerodynamic vs. structural shaping: It ranges from pure aerodynamics (synthetic jets) to the heavily structural conforming flap.
- (b) Static vs. dynamic: This will determine the working “bandwidth” of the morphing structure by considering how fast is the shape change required and how often it needs to be changed. Thus, the speed and the frequency at which the shape change occurs are significant design parameters. Slow, quasi-static changes may be sufficient for some missions; rapid changes to increase aircraft maneuverability will make future morphing aircraft even more capable [32].
- (c) Small vs. large deformation: This should clarify how several degrees equivalent rotation and strain levels are induced by the morphing. Small and large morphing have been discussed in Chapter 3.

It is obvious that prior to morphing there is no actuation and the wing exhibits a high stiffness state. However, during morphing, a minimal actuation is required and the wing is in a low stiffness state with changes in aerodynamic loads and actuation forces. Following the morphing, the system returns to its initial conditions of actuation and stiffness. The structural integrity of the wing must be preserved under all circumstances.

Depending on the expected performance, the following elements should be considered [98]:

- (a) Extent of the shape change,
- (b) Type of actuation,
- (c) External work,
- (d) Evaluation of deformation energy involved,
- (e) Speed of actuation,
- (f) Evaluation of power required,
- (g) Level of reliability needed,
- (h) Actuation occurrence,
- (i) Necessity to operate in different conditions.

Moreover, optimization investigations can be performed for drag reduction [29, 99, 100, 101] and to minimize the power needed for actuation [17].

5.2 Multi-Stable Composite Materials

To minimize the structural weight and the complexity of a flying vehicle, composite materials provide a promising solution. Generally, composite materials present high specific strength and stiffness ratios. The high degree of design flexibility of fiber reinforced composites has increased their applications in aerospace structures. This is due to their superior performance compared to metals. It is known that the properties of a composite depend on factors including the choice of the constituent materials, the method of combining them, and the process of fabrication. This design flexibility, though complex, enables the designer to tailor the material to obtain a desired structural response. Subsequently, to obtain a span-wise morphing wing using flexible matrix composite (FMC), it is common to orientate the fibers along the chord, with the matrix direction aligned along the span as depicted in Figure 5.2. This configuration produces large strains at low actuation force and the fibers provide reinforcement and out-of-plane load carrying ability. In contrast, for chord or camber changes, the fibers are orientated along the span while the matrix direction is aligned with the chord. This direction may undergo large strains at low actuation force. Thus, the fibers aligned with the span provide reinforcement and out-of-plane load carrying ability [78].

However, these basic orientations are weak to resist shear loading. Therefore, the stacking sequences of the laminate should consider orientations including 45 degrees.

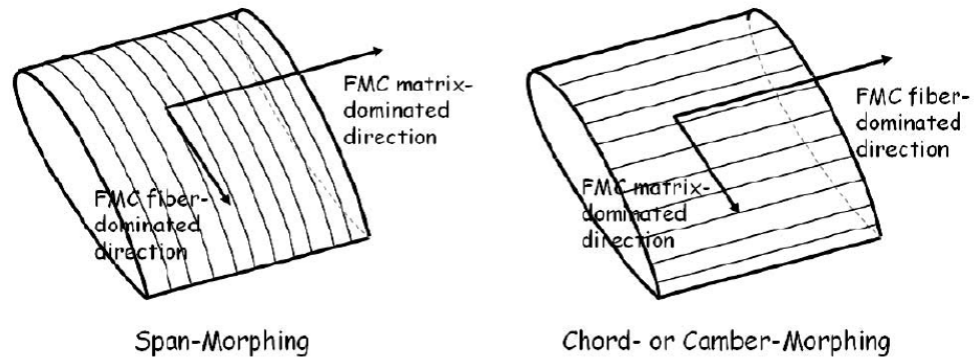


Figure 5.2: One dimensional morphing concept [78].

Generally, fiber reinforced flexible matrix composites utilize the high elongation capability of elastomers such as polyurethane to withstand large strains in the matrix material while retaining strength and stiffness in the fiber direction. One of the potential applications of FMCs is the construction of flexurally compliant, torsionally stiff composite drive-shafts [97]. Thermoplastic elastomers including elastane, a member of alternative thermoplastic polyesters, polyethylene and polyurethane elastomers possess a high chemical adjustability with good robust mechanical properties. These materials together with Shape Memory Polymers (SMP) are good candidate materials for smart skins.

It is known that bi-stable composites exhibit large deformations but only require low actuation forces. This makes them in the current form difficult to be used as morphing skins since aerodynamic loads may be greater than the forces needed to snap the laminates from one stable configuration to the other [103].

Actuator and sensor technologies require energy to change and maintain the morphed shape. Thus, their use implies a continuous electric power supply or temperature regulation for operation. Therefore, recent research [27, 28, 57] indicates that multi-stable composite materials are a promising technology to the structure morphing. These structures consist of non-symmetric fiber reinforced laminated composites. They possess the ability to remain in a natural equilibrium following the occurrence of change in shape. It is known that if a composite laminate does not have any symmetrical stacking sequence, thermally induced stresses develop during the curing process and cause an out-of-plane curvature as the laminate cools to its operational temperature [57]. These stresses are caused by thermal effects, moisture absorption and chemical shrinkage. The out-of-plane curvature can be tailored by adjusting the stacking sequences and ply thickness. Depending on the plate geometry, the thermally induced stresses may cause the laminate to have more than one stable configuration or shape. Therefore, morphing can be obtained by alternating between these states.

The main advantage of using these structures is that they will maintain one of the stable shapes with the need of no force holding them in that position. This means that power is required only to transform the structure from one stable configuration to another. Hence, they can carry loads in both states as long as they do not reach the critical snap-through load. Figure 5.3 illustrates examples of bi-stable materials.

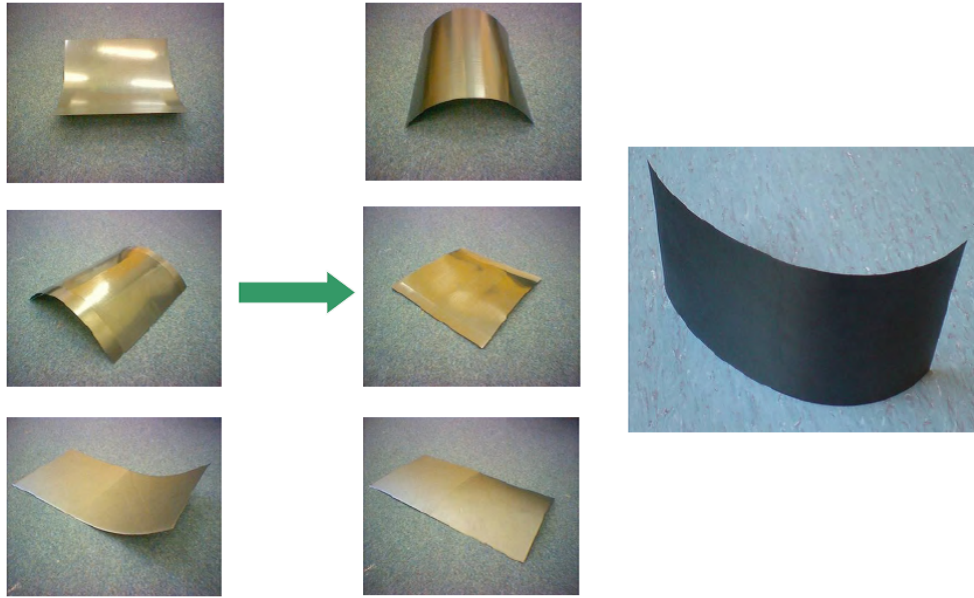


Figure 5.3: Bi-stable composite materials [88].

If composite materials with multiple stable states are to be used for morphing aircraft, adequate actuation system must be defined so that these materials may snap from one stable state to another. Thus, in his PhD dissertation, Schultz [119] used Piezo-electric patches (Macro Fibre Composite (MFC)) bonded to the surface of the laminate to induce snap-through with a shear force. Schultz successfully produced a morphing laminate based on the MFC actuator and obtained good predictions of the snap-through loads for a patch bonded in the middle of the plate. Additionally, Schultz et al.[120] discussed the concept of using a Piezo-ceramic actuator bonded to a side of a two-layer asymmetric cross-ply laminate to provide the moments necessary to snap the laminate from one stable equilibrium shape to another. Their experimentally measured stable shapes of the laminate-actuator combination were predicted very well using a model, and the predicted actuation voltage needed to initiate the snap-through behavior was reasonably close to the experimental value. Schultz et al model is reviewed in Chapter 6. Furthermore, Dano and Hyer [121] but also Hufenbach et al.[122] used shape memory alloy (SMA) wires to apply a bending moment to a plate as a demonstration of the snapping-through of multi-stable composite materials for morphing applications. These wires require to be heated in their operating ranges.

Friswell et al.[28] investigated a variable sweep wing concept based on bi-stable composite spars. The wing-box in their design consisted of two spars with an interconnected truss-rib structure. Applying a bending moment on the spar caused the spar to snap to a second stable position. The snapping point therefore acts as a hinge. The actuation type used was not mentioned in their work. In an electronic mail correspondence with the author, Professor Friswell comments the difficulties encountered in the actuation of multi-stable composites. This correspondence is quoted below:

" Actuating the multi-stable structures is very difficult. For multi-stable plates there has been some work involving SMAs or Piezo-electric patches, but the big problem is that actuating plates using actuators on the plate surface is very difficult and requires large strains and/or high stresses. Some of the concepts we tried at Bristol involved plates - for example the winglet - but generally we didn't consider excitation - in the case of the winglet the aerodynamic load was used. We also looked at more general multi-stable structures (for example the trailing edge) - although we didn't build a system with actuators. For 3D structures there are more possibilities to include conventional actuators within the internal volume of the structures - although we didn't get that far. The thrust of the work at Bristol was to develop tools to model the multi-stable behaviour. You can see there is still a lot of work to do before multi-stable structures could be used in aircraft!"

5.3 Adaptive Aero-Elastic Structures

The adaptive aero-elastic structures approach uses the aerodynamic forces acting upon the wing to provide the forces and moments to bend and twist the wing. Thus, the structure contains no actuator. Generally, these structures exploit the energy on the fluid (aerodynamic forces), rather than directly using the smart actuators to change the shape of the wing. In this solution, the airfoil camber may be controlled through the shear center position and stiffness tailoring. Nevertheless, the adaptive internal structures concept is inadequate for high frequency applications including flutter or buffet load suppression. The approach is best applied to the tip end of the lifting surface where the structural stiffness is less and the influence upon the aerodynamic forces is significant. Additionally, some elements of the wing internal structure would need to be adaptive [104].

5.3.1 Variable Geometry Truss

The Variable Geometry Truss (VGT) is a statically determinate truss that contains some members capable of length variation. A schematic diagram of a simplest VGT unit is shown in Figure 5.5. It consists of top and bottom rigid triangular sections, ABC and $A_1B_1C_1$, which are connected to the mid section DEF by six fixed length bars, respectively. The mid section is composed of three variable length members, DE , EF and FD . The relative positions between top and bottom triangles can be varied by changing the length of DE , EF and FD . A chain of such members can form a long beam which can be shortened, elongated or tilted. The VGT can almost be directly used as front and rear spars as depicted in Figure 5.4. A synchronised elongation of all the actuated members leads to the shortening of both front and rear spars. This results in the shortening of the wing. More complex motion of the actuated members can cause upwards or downwards motion of the wing. Moreover, because the top and the bottom triangles remain rigid, the units can be easily connected with rigid trusses so that the shape changing units can be placed only at locations where shape changing is required [95].

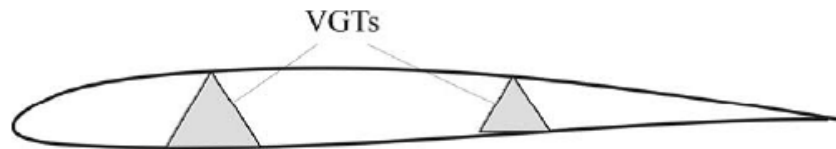


Figure 5.4: Wing with two VGTs as spars [95].

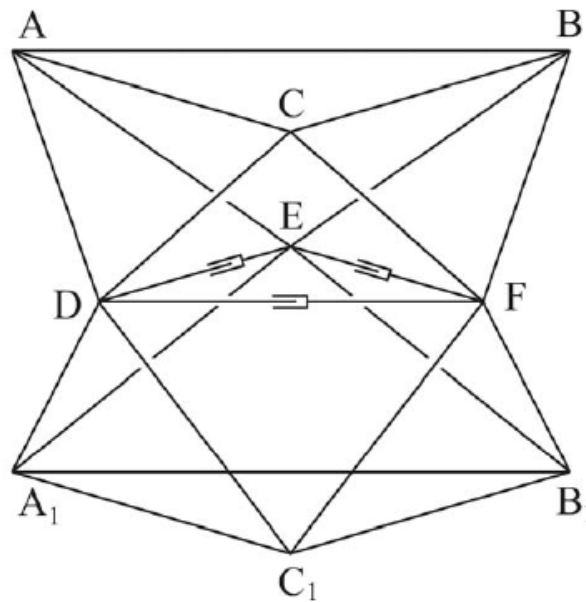


Figure 5.5: Double octahedral VGT unit [95]

5.3.2 Variable Stiffness Spar

The Variable Stiffness Spar (VSS) concept demonstrates the use of moving spars for the aircraft roll control by rotating the spars as shown in Figure 5.7. Additionally, the torsional stiffness of the wing and the position of the local shear center can be controlled by moving the chord-wise position of a central spar as illustrated in Figure 5.6. As such, VSS is proposed in order to increase the maneuverability of a flexible aircraft. A reduced torsional stiffness leads to larger deflections and reduced flutter speeds [92]. This spar controls the wing torsional stiffness and twist to enhance the roll performance.

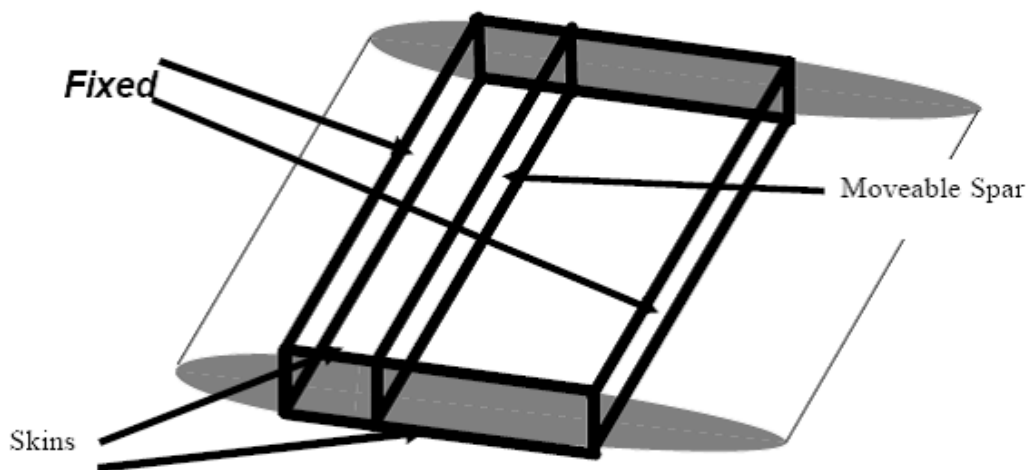


Figure 5.6: Wing box with movable central spar [92].

The chord wise motion of the central spar not only alters the torsional stiffness but also the location of the local shear center. The wing twist is reduced as the spar is moved from forwards to aft. However, the bending stiffness remains constant.

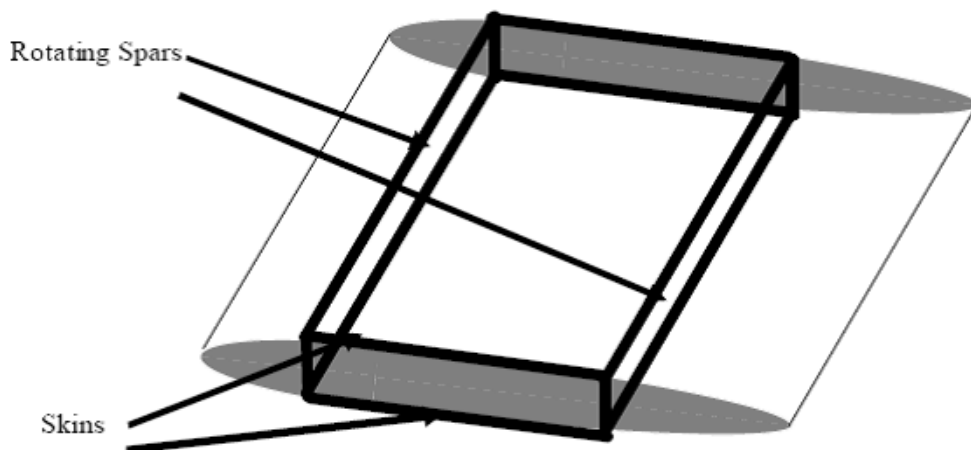


Figure 5.7: Wing box with rotating leading and trailing edge spars [92].

The rotation of the spars alters their bending stiffness in both vertical and horizontal directions as well as the torsional stiffness and shear center location.

The cylindrical VSS as proposed by Chen et al.[123] consisted of a segmented spar linked with hinges to the rib. The bending stiffness of their spar was different about its normal axis at each cross section of the spar. Therefore, the bending stiffness of the wing can be altered by rotating the spar about its own longitudinal axis. This results in the twisting of the wing under load. Their spar was mechanically actuated. This mechanical actuation system may cause an additional weight increase of the entire structure. Therefore, Changho et al. [91] demonstrated successfully the use of shape memory alloy spars for aero-elastic performance enhancement.

5.3.3 Bend-Twist Coupled Beams

An example of a coupled beam is a box beam so tailored that an imposed cantilever load results in twisting as well as bending, although no torsional load is imposed. Reversible behaviour would be exhibited if, in addition, an imposed torsional load results in bending as well as twisting, although no cantilever load is imposed. Such a structure is said to exhibit bend-twist coupling. The elastic coupling can be varied over the span with composites by appropriate selection of ply angles, thicknesses and the span-wise layup [93].

For conventional laminated composites constructed of orthotropic layers, the level of anisotropy is determined by the fiber orientation with respect to the primary loading direction. Therefore, the fibers oriented at an angle ϑ , as shown in Figure 5.8, can be used to produce either bend-twist coupling or extension-twist coupling. Bend-twist coupling requires the mirror lay-up as depicted by Figure 5.8(a) and the helical layup, Figure 5.8(b), is required for extension-twist coupling to be exhibited. In the case of coupled spars, it is considered beneficial to use braided planforms rather than a more conventional lamination method.

A key advantage in using braided planforms is the relative ease of manufacturing compared to conventional laminated composites. Moreover, the structural box is continuous, and fatigue or damage tolerance performance is better than will conventional laminated composites [94].

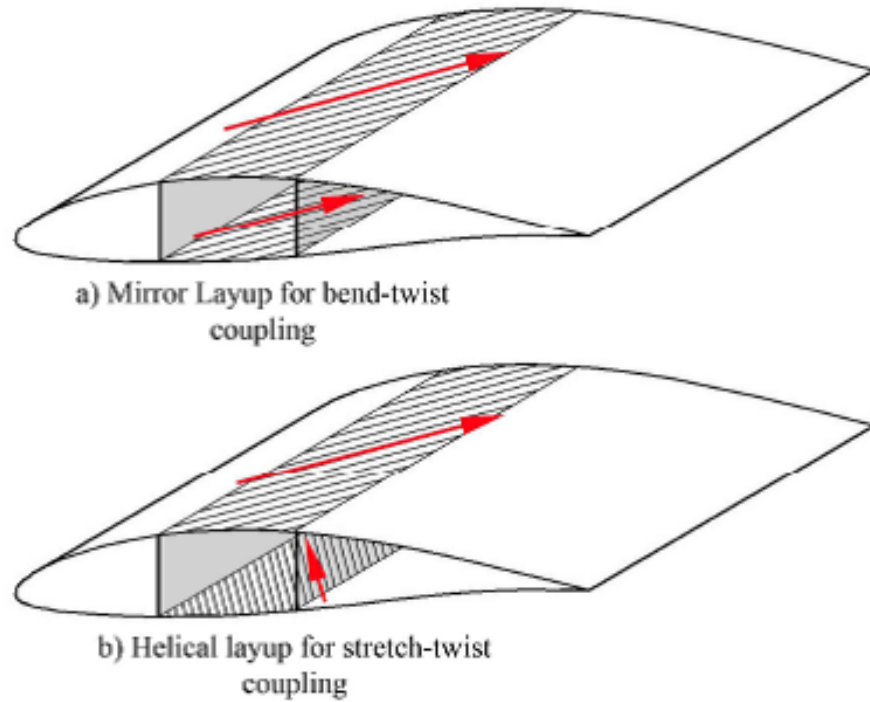


Figure 5.8: a) Layup for bend-twist coupling and b) layup for extension-twist coupling [93].

The use of a single braided pre-form would produce the helical layup as illustrated in Figure 5.9(a). If, however, a single pre-form is cut and used in two halves to create a double box beam, the mirror layup can be achieved as shown by Figure 5.9(b). This is thought to be significantly more robust than the patch layup technique for creating bend-twist coupling, which has joint strain incompatibilities and is prone to delamination when exposed to cyclic loads. Figure 5.9(c) depicts a patch layup [94].

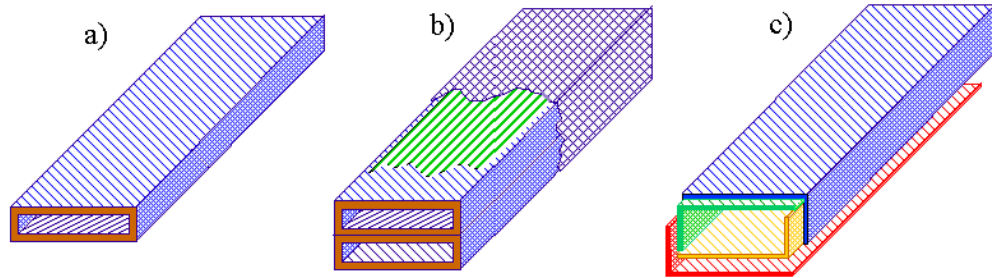


Figure 5.9: a) Single box layup, b) double box layup and c) patch layup [93].

Distributed Piezo-electric materials are shown to be a very attractive element for the control of vibration in flexible structures. Lead zirconate titanate (PZT) ceramic and the orthotropic polyvinylidene fluoride (PVF2 or PVDF) are widely used Piezo-electric materials. Lee, in his PhD dissertation [124], showed that PVF2 laminae can sense and produce both bending and twisting motions in laminated plates. However, PVF2 is very compliant and available only in very thin forms; this makes it a poor actuator candidate for most engineering applications. On the other hand, PZT is very stiff and has larger Piezo-electric coefficients than PVF2 [125]. PZT is a transversely isotropic material that can detect and generate only bending motion when positioned parallel to the structure axes. To make PZT supply bending as well as twisting motion, Park et al.[128] attached directionally rectangular patches on the host structure surfaces. Yang and Bian [126] sensed experimentally and actuated the bending and twisting motion in laminated plates by using embedded parallel PZT patches. The patches supplied bending and twisting when they induced identical and opposite strains, respectively.

5.3.4 Preloaded Internal Spine Structures

A deformable internal spinal structure can be used to achieve shape control with a limited number of low-power actuators [93]. Buckling of structural members leads to a reduction in their structural stiffness, hence, a reduction in the demand on the actuator force to induce a given displacement. Bi-stability provides another alternative approach to achieve a softer host structure against which actuators have to work to produce a shape change.

Post-buckling of single strut components has been successfully utilized to magnify the performance of Piezo-electric actuators used to control a UAV with morphing wing by Ursache et al [52]. They present a global shape control accomplished by distorting a slender internal spinal structure. This structure is attached to a hyper-elastic outer cladding that forms the aerodynamic surface of the morphed airfoil. The approach proposed consists of a partially buckled simply supported Euler strut subjected to an eccentric end load, as depicted in Figure 5.10. Such a strut, when made of an isotropic material, takes up a half sine wave shape whose amplitude is controlled by the end loading. Therefore, with an appropriate choice of material properties, the buckled shape can be made to conform to the camber line of an airfoil [93]. The actuation type used in their design was not identified.

Similarly, Vos et al.[83] used a new type of Piezo-electric flight control mechanism which relied on axial precompression to magnify control deflections and forces simultaneously. Their Post-buckled precompressed bending actuator was oriented in the plane of the 12% thick wing and mounted between the end of a tapered D-spar at the 40% chord and a trailing-edge stiffener at the 98% chord. Furthermore, Phani et al.[71] used Piezo-actuation system under three forms including a linear actuator, composite beam, and a composite strut to deduce a closed-form relationship between actuator force and displacement. The main advantage of such structures is that a modest variation in the force applied can result in large deformations. Vos and Phani models are reviewed in Chapter 6.

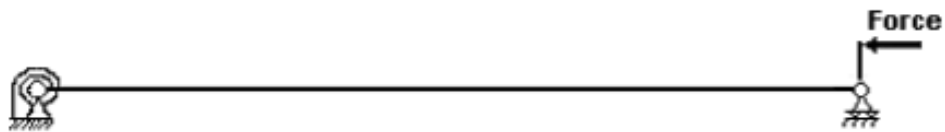


Figure 5.10: A beam column with eccentric load [52].

5.3.5 Kagome Lattice Structures

A Kagome lattice is an arrangement of laths composed of interlaced triangles such that each point where two laths cross has four neighboring points. Figure 5.11 illustrates a planar Kagome lattice. Several researches [26, 38, 105] show that the Kagome lattice has promise as the basis of active structures. Its shape can be changed by linear actuators replacing some of the bars of the lattice. By altering the length of these actuators changes the macroscopic shape of the structure.

Kagome trusses are special because they are statically indeterminate and are effectively isotropic and stiff in-plane [103]. The feature making the Kagome planar truss exceptional for actuation is that any of its members (if considered as pin-jointed) can be actuated to achieve arbitrary in-plane nodal displacements with a minimal internal resistance [38, 105].

This attribute arises because the infinite, pin-jointed model satisfies most of the requirements for static determinacy, permitting a minimal elastic energy storage in bending even when the joints are welded. This truss is known to be of an infinite planar truss amenable to assembly from repeat units having both isotropic stiffness and the properties desired for actuation [105].

Such a truss pattern has several useful properties for morphing structures. In the case of the three dimensional manifestation, two forms are possible: a Kagome plane with solid face sheet and two Kagome face sheets connected by a double tetragonal pattern core [26].

Hutchinson et al.[105] conclude that the single Kagome plate with solid face sheet may be deformed via truss actuation to form any long wave-length deformation. However, practical limits of actuation energy restrict deformations to small Gaussian curvatures¹. In the case of the twin Kagome face structure, it is suggested that no restriction is placed upon the Gaussian curvature of the desired form. According to [105], by removing the mid-plane symmetry from the structure, it is possible to create a statically and kinematically determinate structure. Furthermore, by [26], in the case of a finite Kagome truss, it is possible to add additional members to the boundaries in order to make it both statically and kinematically determinate. An airfoil was created in [26] using a repeating network of the Kagome lattice structure, with upper and lower nodes displaced. Linear actuators replaced selected truss sections to allow active camber control.

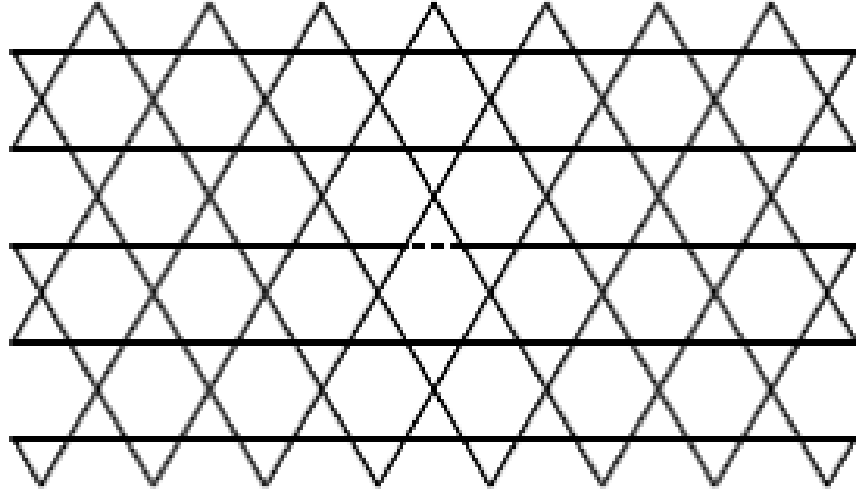


Figure 5.11: A planar Kagome lattice [38].

¹Only surfaces that can be curved in both direction possess a Gaussian curvature which is defined mathematically as the product of the extreme curvatures in the orthogonal principal directions.

5.3.6 Auxetic Materials

Auxetic materials are cellular materials or structures composed of periodic or semi-periodic cells in the three spatial directions with set topological connectivity [127]. They have a negative Poisson ratio and can be foams, ceramics, long fiber composites or micro porous polymers as well as honeycomb. In honeycombs, the negative Poisson's ratio behaviour implies a stiffening geometric effect.

A chiral honeycomb structure is composed of circular elements (nodes) of equal radius joined by straight ligaments (ribs) which are tangent to the nodes [106]. This structure provides compliance and allows a continuous deformation of the airfoil. As a result of a Poisson ratio close to -1, chiral honeycomb allows large deflections, while the material remains in elastic range [130]. The in-plane deformation mechanism of the honeycomb is provided by the rotation of the nodes. This results into the bending and axial deformation of the attached ligaments. This type of honeycomb is dominated by in-plane properties rather than out-of-plane like a conventional honeycomb. Such a structure presents advantages such as a high in-plane indentation resistance, shear modulus, and compressive strength [107]. It also allows a high deformability whilst still recovering its original dimensions.

Generally, a wing-box is mainly subjected to torsional and shear loads. These loads are carried by internal structure such as spars and ribs, and the wing skin. The hexa-chiral wingbox concept investigated in [106, 107] replaces the rib with a cellular network. Such a honeycomb has in-plane special orthotropic properties, because of the combined action of the bending of the ligaments and their axial deformation.

To assess the feasibility of having a completely passive morphing airfoil, without using any external power supply or actuation system, Bornengo et al. [107] applied their investigation of the hexa-chiral honeycomb to the wing of a race-car having an Eppler 420 airfoil. Eppler420's camber provides significant lift at low speed [130]. The problem faced by making passive morphing wing is to allow the internal structure to flex whilst still maintaining the structural integrity. They demonstrated that the hexagonal chiral honeycomb internal layout of such an airfoil can achieve passively the required deformation pattern in order to produce the desired aerodynamic down-force. They evaluated the aerodynamic pressure distribution over the airfoil using Vortex Lattice Method (VLM). VLM calculates the external aerodynamic loading and transfers it into an equivalent structural loading applied to a finite element model. This structural loading induces a global deformation of the original airfoil profile. This deformation alters the aerodynamic configuration of the wing of the race-car. The deformation mechanism, given by the rotation of the circles and the combined bending and axial deformation of the ligaments, allows the airfoil to undergo substantial displacements within the elastic range of the material. This allows the airfoil to passively morph under aerodynamic loading. The shape of the airfoil can be changed at selected speeds only. However, these speeds must provide sufficient dynamic pressure to activate the structural deformation mechanism. Thus, the airfoil alters its camber whilst still resisting the shear and torsion loads.

Figure 5.12 illustrates an airfoil based on hexagonal chiral honeycomb.



Figure 5.12: Chiral airfoil structure [130].

5.3.7 Belt Rib Concept

The Belt Rib concept as shown in Figure 5.13 is proposed by DLR in Germany for a continuous camber variation. In this solution, the continuous camber variation is achieved by transferring the stroke of an actuator into a geometric change of the airfoil shape through a closed belt and an internal networked structure simulating the ribs inside the airfoil section [18]. The orientation of the spars makes the camber change possible due to the low stiffness. The skin of the airfoil which defines the shape, is essentially like a belt and the spars like spokes or ribs [103].

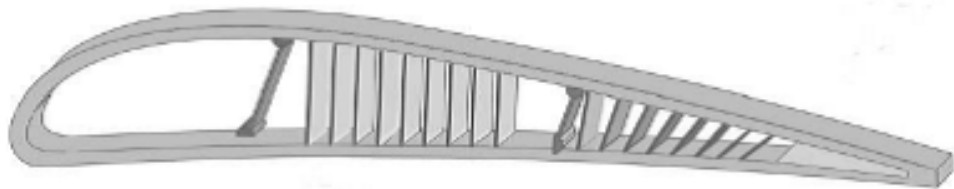


Figure 5.13: The belt rib concept [103].

5.3.8 Finger Concept

The rotating rib concept, referred to as the finger concept, has been developed at the Politecnico di Milano based on the solution proposed by DLR. Its goals include the possibility to be embedded into high lift devices with the expectation of adding a certain degree of adaptiveness to a classical control surface, a maximum span wise trailing edge camber angle variation of ± 5 degrees, and a gapless camber variation allowing a smooth deformed wing surface. Thus, a variable camber is achieved for a trailing edge.

In this approach, the classical connection between the skin and the ribs, traditionally based on rivets, is substituted by a discrete number of linear slides allowing the skin to glide over the rib contour. On the trailing edge of the airfoil, the upper and lower skins are not rigidly connected each to another; but they are able to glide into a linear slide bearing. The actuator torque deforms the skin panels as well as gaining friction forces inside the slide bearings [102]. Thus, the airfoil is composed of a flexible rib made of separated plate like elements connected through revolute joints. The rotation of the driven element is transferred gradually from element to element by kinematics, providing the desired rib contour [18]. Figure 5.14 illustrates the concept.

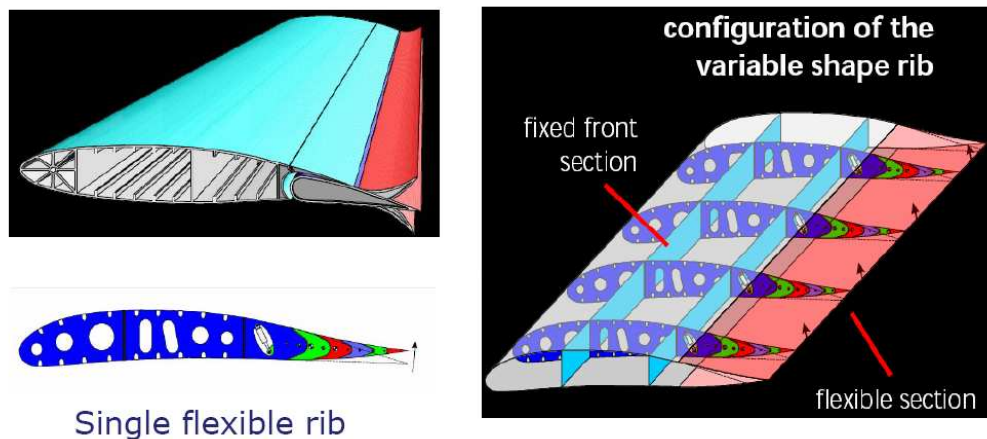


Figure 5.14: Finger concept [102].

5.4 NextGen's Wing Mechanism

Figure 5.15 shows the wing mechanism of the NextGen wing reviewed in Chapter 3. The wing contains a planar mechanism that can be actuated by a series of linear actuators. A highly flexible skin (elastomeric skin) is attached to the mobile frame that completes the morphing wing. NextGen used an electric motor to deform the wing box structure that was stiffened by means of ribbons [111]. To hold a particular configuration, the structure makes use of worm gear mechanisms or other lockouts, without continuous power supply to the actuators [11].

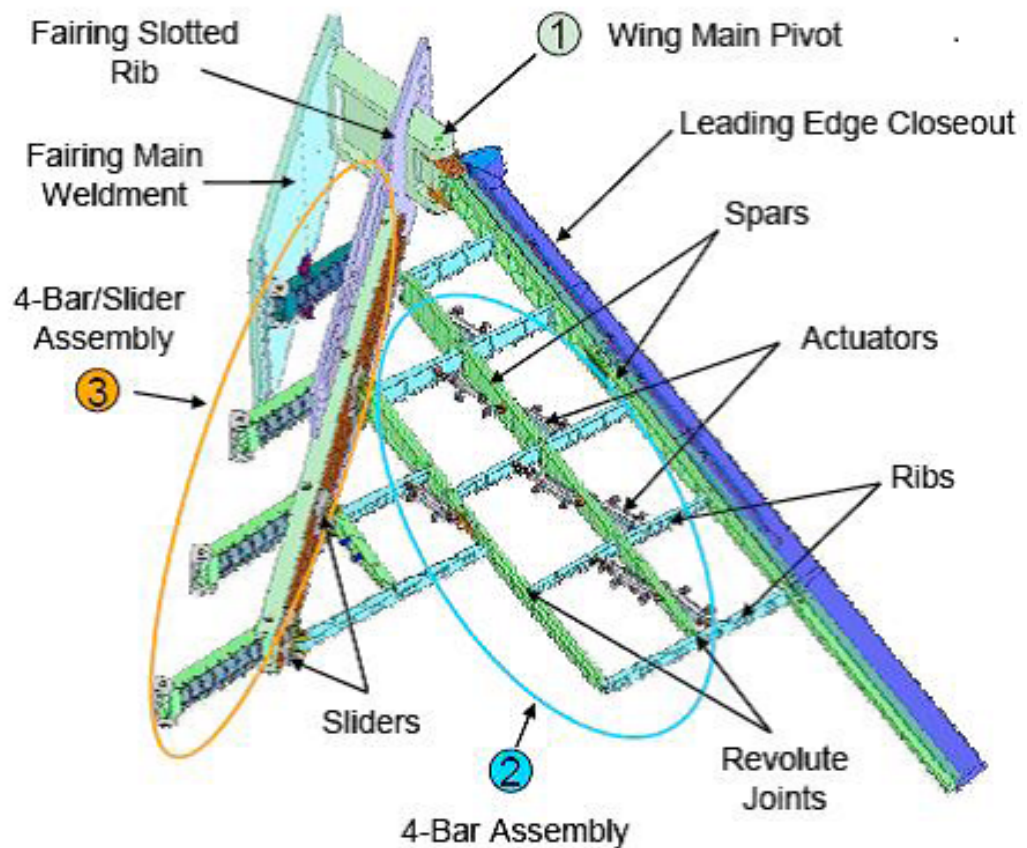


Figure 5.15: NextGen's bat wing mechanism [89].

5.5 Lockheed's Wing Mechanisms

From Figure 3.11, it can be seen that Lockheed's wing has a dihedral angle change and a change in gull² configuration for shape morphing. In gull designs, the wing is divided into two hinged segments that rotate with respect to each other and at the wing root. Lockheed's folding wing concept is referred to as the most innovative. Their design uses electrical actuators to fold the wing [111].

Figure 5.16 illustrates the wing structure. The design is unique because of its challenging joint requirements. The joint must be strong, lightweight, able to change shape while maneuvering, and maintain a smooth exterior surface to avoid disturbing flow around the airfoil. This problem has been successfully addressed through the use of embedded actuators and a knuckle joint capable of providing the necessary shape continuity regardless of the joint position [96].

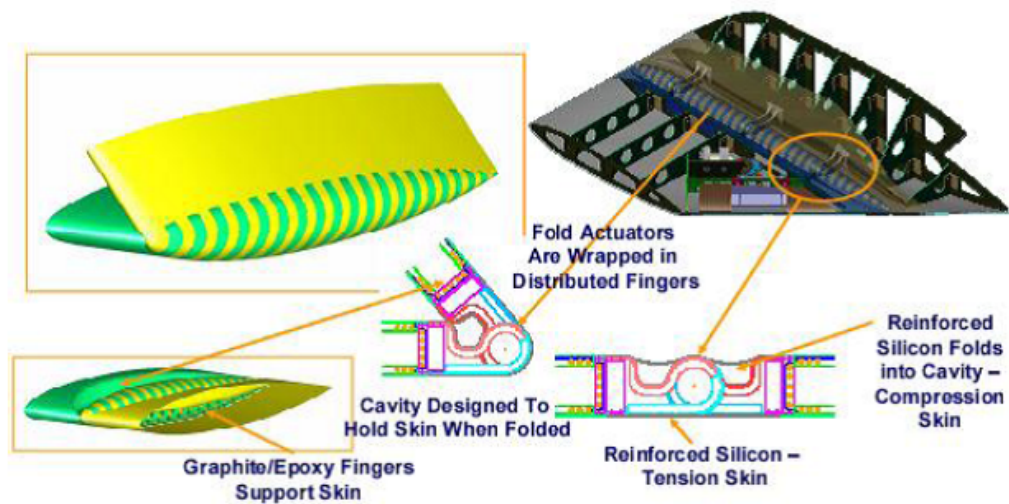


Figure 5.16: Lockheed's morphing wing joint design [62].

²The gull wing is an aircraft wing configuration with a prominent bend in the wing somewhere along the span, generally near the wing root. Its name is derived from the seabirds which it resembles.

5.6 Scaling Limitations

According to [79], the square-cube law is a principle drawn from the mathematics of proportion and applied in engineering and biomechanics. It was first demonstrated by Galileo in the *Two New Sciences* [80] and states as:

“When an object undergoes a proportional increase in size, its new volume is proportional to the cube of the multiplier and its new surface area is proportional to the square of the multiplier”. This statement is represented mathematically as:

$$V_2 = V_1 \left(\frac{l_2}{l_1} \right)^3 \quad (5.1)$$

$$S_2 = S_1 \left(\frac{l_2}{l_1} \right)^2 \quad (5.2)$$

Where V_1 , l_1 and S_1 are respectively the original volume, length and surface area while V_2 , l_2 , and S_2 denote the new volume, length and surface area in this order. The square-cube law limits biological materials to similarly be used in high-performance vehicles [36]:

1. Stresses vary with the square of the length.
2. Loads vary with the cube of the length for self-loaded structures by weight; but vary with the square of the length in the case of a pressure load.

Therefore, for the same material ultimate stress, the structural system is significantly loaded as the size increases. Additionally, the aerodynamic pressure would scale with $length^0 = 1$ for the same dynamic pressure. However, Torenbeek [19] reports that the square-cube law has been defeated by the ingenuity of designers. Thus, aircraft will not be scaled up according to a geometric similarity and the stress levels have increased considerably. Nevertheless, the actual wing structural weight fraction will tend to increase with the size of the aircraft, unless the wing loading is increased. Thus, statistical materials from Torenbeek show that for an aircraft powered by jet engines, the wing loading is approximately proportional to $W^{\frac{1}{5}}$. This factor becomes $W^{\frac{1}{3}}$ for propeller propulsion. W denotes the weight of the aircraft.

5.7 Control Issues Of Morphing UAVs

A radical change in planform is accompanied with dramatic changes in aerodynamic center. Consequently, the morphing aircraft must be stable while morphing. Therefore, simultaneous combination of the flight control and morphing control become an import issue to be addressed.

Friswell et al.[26] report that Raytheon Corporation uses the wing asymmetry on a morphing UAV based on the concept of wing extension to control the roll motions. Their UAV has two motors and gear set so that each wing could be extended separately. In addition to using wing extension for planform change, the extension was used asymmetrically for roll control. The roll moment is produced by the span differential.

Currently, morphing vehicles are based on separating shape morphing and stability control in order to maintain stability. With the exception of using anti symmetric wing extension, separate control effectors have been used to change the shape, to those used to maintain stability [26]. Nevertheless, UAVs designed to mimic basic morphing mechanisms commonly observed on bird wings should have the ability to twist their wings at the tip or at the root for roll control and vary the gull wing angle. Fortunately, NextGen's has addressed successfully this concern through their folding wing reviewed in previous sections.

However, any morphing approach will involve large rigid-body motions of the UAV's flexible structures under aerodynamic and distributed actuation system loads. Therefore, the response of the UAV will be governed by the time-varying aerodynamic forces and moments which will be a function of the wing shape changes by the morphing command. Dynamic models for the morphing UAV must properly take into account its inherent time-varying nature due to the dynamic coupling between inertial aerodynamics, structural, and distributed control forces. Unfortunately, such a complex dynamic behavior is difficult to analyze theoretically. One possible approach is to assume that the time-varying dynamics could be represented by a linear parameter-varying plant model that approximately captures the morphing UAV's complex behavior [108].

Chapter 6

Modeling Principles of Morphing Structures

This Chapter presents the basis of finite element formulation of a morphing structure. Additionally, it includes the methods that may be used to model a camber and span morphing wing; it establishes the relationship between the actuation force and the structural displacement using the differential and energy methods. Furthermore, this Chapter reviews the modeling of a continuously morphing flying wing and the snap-through of unsymmetric composite laminates. Finally, it presents the Theodorsen's function as a means to express the pressure distribution over a morphing wing.

6.1 Basic Static And FE Formulations

The objective of a morphing airfoil or wing is to change lift with minimum weight and energy requirement using actuation forces or moments applied to the ribs which transfer them to the skin causing changes in the airfoil shape. This change in shape involves large displacements resulting into a non-linear problem to be analyzed. Distributed non-linearities such as geometric non-linearity and buckling should be considered when deformations including translations, rotations, and the associated strains are large enough so that the equilibrium equations have to be written with respect to the deformed geometry. The equilibrium equation for larger displacement can be expressed using the updated Lagrangian formulations¹ [69]. Worth is mentioning the fact that material non-linearity is excluded from the present discussion. Moreover, typical model will be described using Lagrangian formulations. Additionally, concentrated non-linearities including free-play, friction, and hysteresis may be caused by loose structural joints. These non-linearities require investigations. The influences of the actuator non-linearities on the actuator dynamics and the aero-elastic characteristics should be addressed as well. The actuator non-linearities are expected to play an important role in the non-linear aero-elastic characteristics of the morphing structure.

¹The updated Lagrangian formulation refers to the current configuration, often called the deformed configuration; while the total Lagrangian formulation refers quantities to the original configuration [74]

Furthermore, gust loads have a significant impact on the aircraft dynamic behavior. Thus, they are relevant loading conditions for aircraft design. It is known that winds are seldom present in a stable direction or at a constant speed. This variation leads to the generation of vertical wind loading on the aircraft.

Although gusts are less pronounced at higher altitudes, they must still be taken into account. Such gust activity leads to dynamic changes in the aircraft lift. Air vehicles with a low wing loading or with a high value of lift-curve slope are more susceptible to gust disturbance [19]. Those UAVs designed for high altitude operation are likely to require both of these aerodynamic characteristics. The influence of gusts on the aircraft flight behaviour will need to be carefully assessed especially when operating at low altitudes for example during take-off and landing flight segments. At low altitude, the average wind speed can be almost double that at the operating height [6]. To reduce the effects of gusts on the UAV dynamic behaviour, it is necessary to equip the aircraft with powerful gust load alleviation and auto-stabilizing systems. The gust statical analysis can be performed using panel method applied to an aero-elastic model.

Numbers of authors including Cook [67], Bathe [68], and Crisfield [69] have developed finite element theories considering non-linearity applied to practical problems. Thus, structural and aerodynamic analysis of morphing structure can be performed using non-linear Finite Element Method (FEM). However, it is not straight forward to mathematically optimize a structure with non-linear behavior, because calculation of non-linear sensitivity is extremely difficult [70].

Gürdal [78] described a generic model of a morphing airfoil to be subjected to:

1. Aerodynamics forces denoted by $f_a = f + A.u$
2. Actuation forces/moments considered as input and denoted by f_m
3. Internal structural forces expressed as $f_{in} = K.u$

where f , A , u , and K denote respectively the aerodynamic force without actuation, aerodynamic influence coefficient matrix, displacement due to the actuation, and the stiffness matrix.

The loads expressed above lead to the equilibrium and displacement equations:

$$f_{in} = f_a + f_m \quad (6.1)$$

$$u = u_0 + \Delta u \quad (6.2)$$

where u_0 is the displacement without actuation, and Δu the displacement with actuation. The problem can be modeled using the governing equations below.

$$(K - A).u_0 = f_a \quad (6.3)$$

$$(K - A).\Delta u = f_m \quad (6.4)$$

So that the incremental lift which is a function of the displacement due to the actuation (Δu) is maximized; while the compliance under aerodynamic loading written as $f_a^T u_0$ and the work done by the actuators written as $f_m^T \Delta u$ are minimized. It must be beared in mind that the structure should be stiff enough to resist load but flexible enough to provide shape morphing and the integrity of the structure preserved under all circumstances. The total volume constraint would be the best approach.

6.2 Force-Displacements Relationship

To give a closed form relationship between the actuator force and structural displacements, Phani et al.[71] performed the analysis of single and multi-element structural assemblies using two methods:

1. The differential approach referred to as the exact element theory based on stability functions.
2. The Rayleigh-Ritz approximate energy method based on an assumed trial function for the displacements.

A multi-element structure could describe the trailing edge of a wing, while a single element may represent the rib or spar of the wing of a micro vehicle. The differential method and the approximate energy minimization technique were preferred over the conventional finite element analysis (FEA) due to their ability to pin-point the initial buckling load, and trace the buckling path more accurately than FEA method.

6.2.1 Differential Method

Starting from a single strut subjected to an actuation force F inclined at an angle Φ as depicted in Figure 6.1; with the free body-displacement diagram in Figure 6.2, the analytical methods are extended to the trailing edge of a morphing wing as illustrated by Figure 6.3.

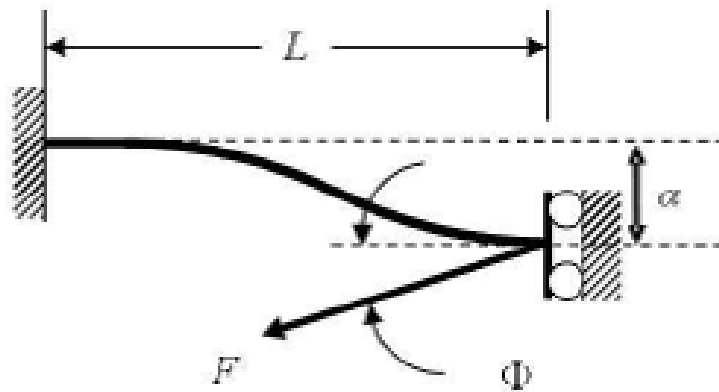


Figure 6.1: Member with actuator force [71].

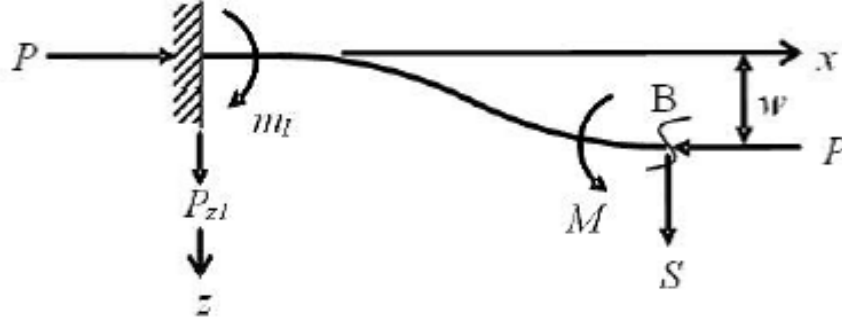


Figure 6.2: Forces and displacements for a post-buckled member [71].

The moment equilibrium about a cut along the member at point B yields:

$$M(x) = -EI \frac{d^2 w}{dx^2} = F \cos(\Phi) w + m_1 - F \sin(\Phi) x \quad (6.5)$$

with E and I denoting respectively the material elastic modulus and the second moment of area of the beam. The differential equation above has the displacement curve as a general solution:

$$w(x) = C_1 \cos(\beta x) + C_2 \sin(\beta x) - \frac{m_1}{P} + \frac{-P_{z1} x}{P} \quad (6.6)$$

where C_1 and C_2 are coefficients defined by the end conditions:

1. At the fixed end, the displacement and the slope of the displacement curve vanish.
2. At full length of the strut, the displacement is assumed to be α according to Figure 6.1, while the slope of the displacement curve is zero.

and $\beta = \sqrt{\frac{P}{EI}}$, $P = F \cos(\Phi)$, and $P_{z1} = -F \sin(\Phi)$.

Using stability functions which take into account the non-linear effect due to the axial load in the member based on the moment distribution method described by Livesly and Chandler² [72], the solution of equation 6.6 can be determined, and the flexural end-shortening can be obtained by integrating the displacement curve as:

$$\epsilon = \frac{1}{2} \int_0^L \left[\frac{dw}{dx} \right]^2 dx \quad (6.7)$$

The net displacement along the actuator is given in terms of α and ϵ by a suitable coordinate transformation from strut axes to actuator axes as:

$$\delta(\Phi) = \alpha \sin(\Phi) + \epsilon \cos(\Phi) \quad (6.8)$$

²Their publication “Stability functions for structural frameworks” was found as a non printable google electronic book.

6.2.2 Rayleigh-Ritz Energy Method

Alternatively, the Rayleigh-Ritz method based on the energy approximation or the total potential energy of the structure expressed as:

$$V = \frac{1}{2} \int_0^L EI \left(\frac{d^2w}{dx^2} \right)^2 dx - F \sin(\Phi) \alpha - F \cos(\Phi) \epsilon \quad (6.9)$$

is minimized by assuming a suitable trial function for the displacement field $w(x)$ parametrized by α . The derivative of the potential energy equation with respect to α is set to zero, giving a close form expression for α .

In the multi-element structures illustrating a morphing trailing edge (Figure 6.3), translations are produced using a hybrid system comprising of Piezo-electric stacks controlling struts AB and DE, and conventional actuators within inclined bracing elements to monitor the displacements. Additionally, the rotations are achieved by three methods: bending the individual struts BC and CD, introducing a post-buckled precompressed element FC, and differential end-shortening of the two struts AB and DE. The energy approach, though approximate, was found to be sufficient.

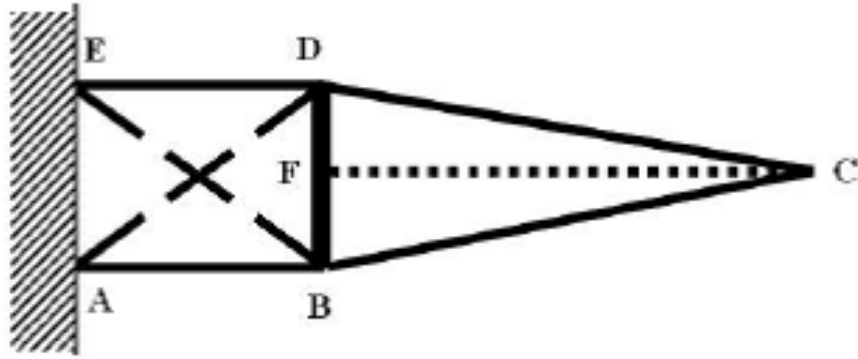


Figure 6.3: Trailing edge framework for morphing wing [71].

6.3 Span Morphing Wing Model

A variable span morphing wing alters its wing span for various flight conditions to improve performance by reducing the drag. The wing geometric characteristics such as the aspect ratio and the wing area increase with the wing span expansion; while the span-wise lift distribution decreases for the same lift, inducing a decline in the drag which results in performance improvement measured as an increase in range. However, the wing span-wise extension generates significant increase in the wing root bending moment. Therefore, an analysis of a span-wise morphing wing must couple aerodynamic and aero-elastic investigations [75]. The aero-elastic response of flight vehicles with a concentrated structural non-linearity such as free-play, typically includes flutter (a dynamic aero-elastic phenomenon), divergence (a static aero-elastic phenomenon), limit-cycle oscillation (a non-linear aero-elastic phenomenon), and chaotic motion.

For the telescoping wing analysis, the wing configuration including wing retracted and wing fully extended together with basic wing geometric characteristics should be clearly presented and the computational tools stated. The doublet-hybrid method (DHM) can be used to calculate unsteady aerodynamic forces in subsonic flight regime while MSC/NASTRAN can be used for modeling the wing box structure consisting of the main wing box and the sliding wing section. Appropriate constraints should be applied to the wing structure with a particular attention to the moving part; since the structural characteristics of the variable span morphing wing are significantly dependent on the boundary conditions at the joint. The telescoping wing contains concentrated non-linearities such as free-play at the junction [75]. free-play, which is a local structural non-linearity rising at the wing section interface, can be addressed using fictitious mass method³.

6.3.1 Aero-Elastic Model

Aero-elastic modeling involves two aspects including a structural model, and an aerodynamic model. But in some cases, a control model is added to represent the effects of actuators and other control elements. Thus, the exact modeling of the aero-elastic behaviour of an air vehicle implies the coupled solution of:

1. The full compressible Navier Stokes equations,
2. The full structural vibration equations.

The structural model leads to the equations of motion obtained by inserting the expression of the system total energy (sum of the kinetic energy and potential energy which is composed of the internal and external energy) into Lagrange's equation written as:

$$\frac{d}{dt} \left(\frac{\partial T}{\partial \dot{q}} \right) - \left(\frac{\partial T}{\partial q} \right) + \left(\frac{\partial U}{\partial q} \right) = \frac{\partial V}{\partial q} \quad (6.10)$$

where T, V, U, and q denote respectively the kinetic energy, the potential energy, the internal energy, and the generalized coordinate.

³Fictitious masses are used to improve the accuracy and efficiency of modal based structural analyzes that involve substructure synthesis, local excitation, and local structural changes.

Thus, the aero-elastic equations of the wing structure are given in a matrix form as:

$$[M] \{\ddot{x}\} + [K] \{x\} = \{f\} \quad (6.11)$$

where $[M]$ and $[K]$ denote the mass and stiffness matrices respectively, while $\{f\}$ and $\{x\}$ are the aerodynamic load and structural displacement vectors respectively. The aerodynamic load vector can be written as:

$$\{f\} = \{\{f\}\} + \{f_0\} \quad (6.12)$$

where $\{\{f\}\}$ is due to the wing deflection and $\{f_0\}$ resulting from the airfoil shape or angle of attack.

For the determination of a static deformation of the structure ($\ddot{x} = 0$), the vectorial equations

$$[K] \{x\} = \{f\} \quad (6.13)$$

have to be solved using for instance the modal approach.

6.3.2 Aerodynamic Model

Aerodynamic models depend on flow regime and simplicity. Four flow regimes may be considered for aero-elasticity investigations [76]:

1. Incompressible,
2. Subsonic,
3. Transonic,
4. Supersonic.

The aerodynamic loads can be computed using Vortex Lattice Method (VLM). VLM provides a platform considering linearized and non-linearized compressible flow approaches. Additionally, compressibility effects can be accounted for by correcting the airflow density using Prandtl-Glauert correction [81]. A simplified modeling consists of ignoring the effect of the wake vortices⁴. Thus, a quasi-steady model is performed with the assumption that there are only the lift placed on the quarter chord, and the pitching moment around the flexural axis, contributing to the aerodynamic forces. Both lift and pitching moment coefficients can be computed using integral equations from thin airfoil theory.

In addition to the aerodynamic forces mentioned above, the air exerts another force on the airfoil: the wing forces a mass of air during its acceleration or deceleration motion. The air reaction force is known as the added mass effect⁵ [76]. This force causes both lift and moment contributions.

⁴The instantaneous aerodynamic forces depend not only on the instantaneous position of the airfoil but also on the position and strength of the wake vortices [76].

⁵Added mass or virtual mass is the inertia added to a system because an accelerating or decelerating body must move some volume of surrounding fluid as it moves through it [77].

6.4 Camber Morphing Model

Vos et al.[83] describe a semi analytical method and the Theodorsen theory to compute the pressure distribution over a camber morphing airfoil to predict the lift over the morphing part of a laminate wing actuated by post-buckled precompressed (PBP) actuators.

6.4.1 Structural Model

PBP actuators belong to a subset of low net passive stiffness or zero net passive stiffness class actuators. These actuators work on the fundamental principle expressed as:

$$F_{piezo} = (K - K_{sp}) \Delta x \quad (6.14)$$

where K_{sp} , K , and Δx denote respectively a negative spring rate mechanism, the passive stiffness of the structure, and the generated deflection. The morphing wing panel employing PBP actuators on the camber is depicted in Figure 6.4.

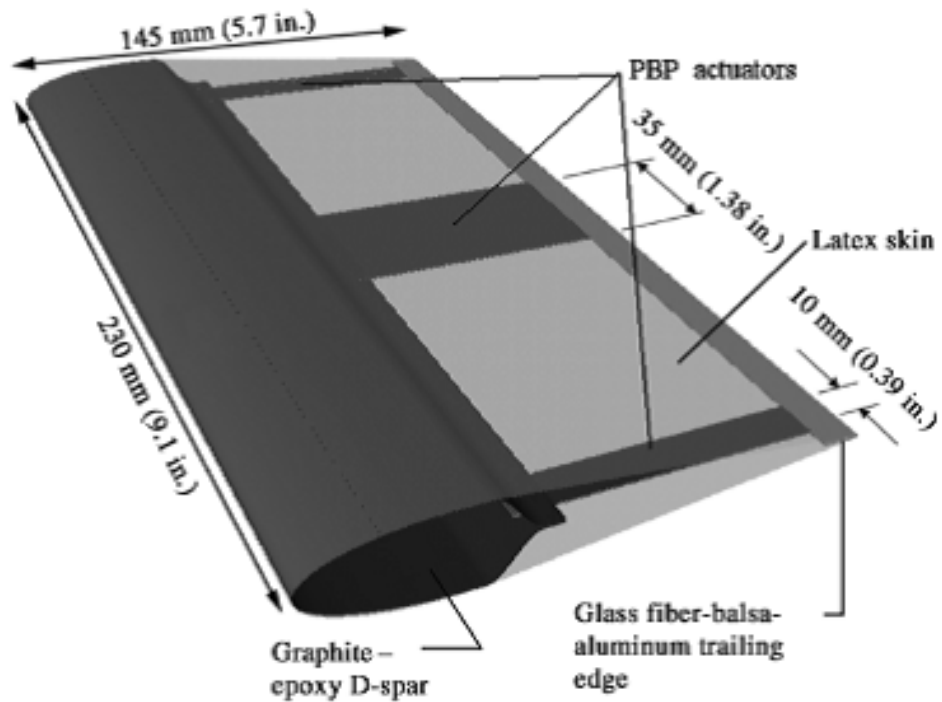


Figure 6.4: Camber line with PBP [83].

Figure 6.5 illustrates the schematic model for the analysis.

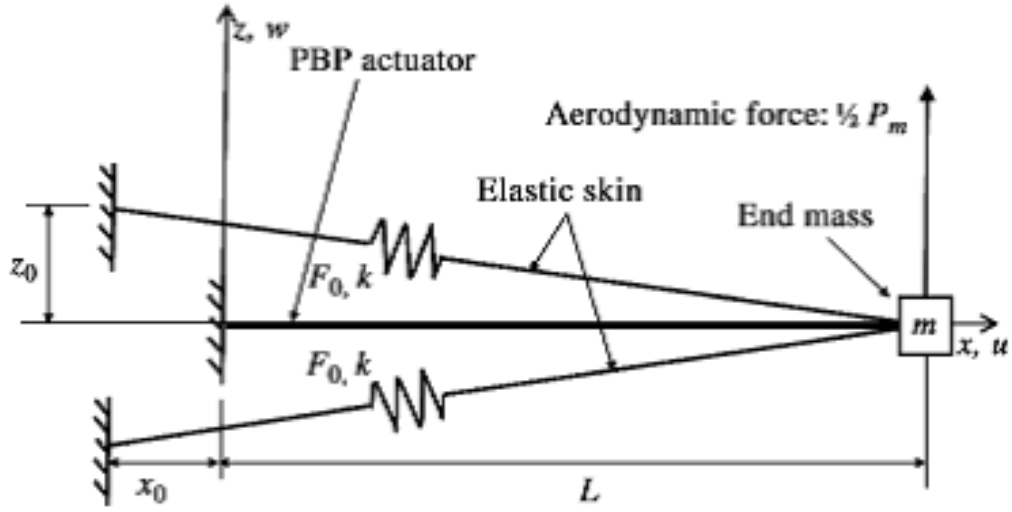


Figure 6.5: Wing morphing part model [83].

From Figure 6.5, the morphing part of the airfoil is loaded by the skin modeled as spring with tension force F_0 and spring stiffness K and the aerodynamic end force, $\frac{P_m}{2}$, resulting from the pressure distribution over the airfoil. The trailing edge is modeled as a mass positioned at the end of the actuator. It is assumed that the skin can be modeled as a membrane which will not exhibit any out-of-plane displacement due to the aerodynamic force since the precompressed force in the skin is larger than the aerodynamic load. Therefore, a uniform stress distribution is expected through the skin. Hence, half of the aerodynamic load is carried by the morphing part and the other half by the rigid part.

Subsequently, resultant forces and moments from the actuator in the laminate wing skin are obtained by integrating the stress over the skin thickness according to [84], by applying the laminate notations illustrated in Figure 6.6.

$$N = \int_{-\frac{t}{2}}^{\frac{t}{2}} \sigma dz \quad (6.15)$$

$$M = \int_{-\frac{t}{2}}^{\frac{t}{2}} \sigma z dz \quad (6.16)$$

The stress resultant is in the form of forces per unit length and moments per unit length.

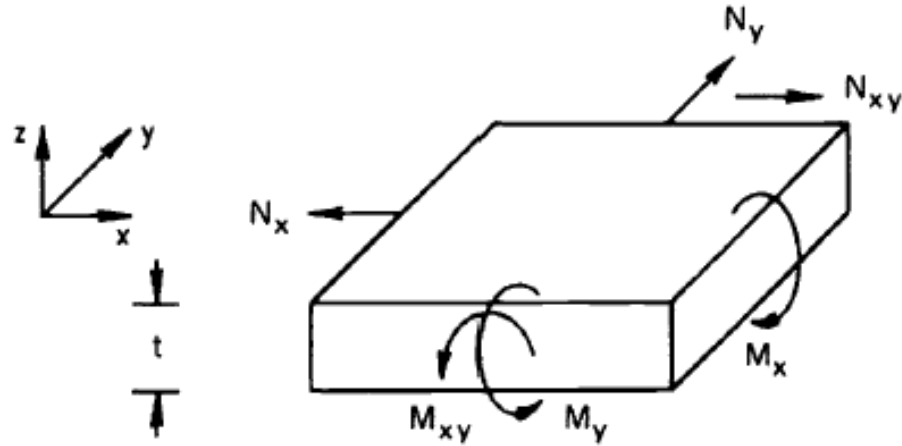


Figure 6.6: Stress and moment resultants for a laminate element [84].

The forces and moments in the laminate that are induced by the actuator elements are a function of the Piezo-electric zero (virgin) strain denoted by Λ . Assuming no external loading, and neglecting thermal effects, the in-plane laminate strains and curvatures are described by:

$$\begin{bmatrix} A & B \\ B & D \end{bmatrix}_a \begin{pmatrix} \Lambda \\ 0 \end{pmatrix}_a = \begin{bmatrix} A & B \\ B & D \end{bmatrix}_l \begin{pmatrix} \varepsilon \\ \kappa \end{pmatrix}_l \quad (6.17)$$

where the subscript a and l stand for actuator and laminate respectively. The equations above allow to define the relationship between the actuation zero strain Λ and the laminate curvature κ once the values of D and B are known from the classical laminate plate theory. The free strain of the actuator in the laminate is one of the driving parameters of the eventual deflection of the morphing wing [83]. The out-of-plane displacement due to external loading on the PBP can be accessed through Euler-Bernoulli beam⁶ equation and by applying Rayleigh-Ritz method⁷ [86] using assumed shape functions ψ_i . The principle of assumed shapes is somewhat akin to using a Fourier series to represent a time signal by the summation of a series of sinusoids of different amplitude and phase.

⁶The Euler-Bernoulli equation describes the relationship between the beam's deflection and the applied load [85]: $\frac{\partial^2}{\partial x^2} \left(EI \frac{\partial^2 u}{\partial x^2} \right) = w$

⁷The Rayleigh-Ritz approach is used to represent the deformation of the system by a finite series of known assumed deformation shapes multiplied by unknown coefficients. The idea is that this combination of shapes represents the true deformation of the system as closely as possible. The more shapes used, the more accurate will be the approximation.

For a system where the deformation varies in only one dimension, the bending deformation is given by:

$$w(x, t) = \sum_{i=1}^N q_i(t) \psi_i(x) \quad (6.18)$$

where $\psi_i(x)$ is the i th assumed deformation shape (a function of x), $q_i(t)$ is the i th unknown coefficient (the generalized coordinate), which is a function of time, and N is the number of terms in the series. Applying the partial differential equation 6.10 leads to the beam state equation:

$$M\ddot{q} + Kq = \frac{P_m}{2} \psi(L) \quad (6.19)$$

which yields, when solved for N number of shape functions, an approximate solution for the aerodynamic load represented at the right side of the equation above. The exact solution is given by equation 6.10. Furthermore, a Vortex Lattice code can be used to evaluate the present semi analytical method.

6.4.2 Theodorsen's Model

Theodorsen's function $C(k)$, a complex quantity⁸, is used to model the changes in amplitude and phase of the sinusoidal unsteady aerodynamic forces relative to the quasi-steady forces for different reduced frequencies [86]. This function is an important component in predicting the starting of flutter in the frequency domain and in the analysis of the response to continuous turbulence.

The solution of the flow around the airfoil undergoing harmonic oscillations can be divided into two parts [86]:

- (a) Circulatory terms: the lift and moment terms occurring due to the vorticity in the flow are related to Theodorsen's function.
- (b) Non-circulatory terms: the apparent inertia forces whose creation is not related to vorticity. These internal forces are also referred to as added masses as seen in the previous section. For example as the airfoil moves, a cylindrical mass of air accelerates with the airfoil and introduces a reactive force and moment upon the airfoil. These terms are of minor importance for bending or torsion type flutter of cantilever wings at low reduced frequencies, but they are significant for flutter of control surfaces at higher reduced frequencies.

⁸ $C(k) = F(k) + iG(k)$, where k is the reduced frequency defined as $k = \frac{\omega b}{U}$

Therefore, the net pressure distribution over the airfoil can be written as:

$$\Delta p = \Delta p_c + \Delta p_{nc} \quad (6.20)$$

with the subscripts c and nc standing for circulatory and Non-circulatory respectively.

The Non-circulatory pressure contribution can be solved using unsteady Bernoulli equation, following the determination of the disturbed velocity potential using conformal mapping. Additionally, the circulatory pressure is determined by applying the Kelvin circulation theorem⁹ and imposing the Kutta condition¹⁰ to the airfoil. Vos et al. give the solution for both terms as:

$$\Delta p_c = -2\rho U \left(\frac{\partial \phi}{\partial x_0} + \frac{\partial \phi}{\partial x} \right) \quad (6.21)$$

with the assumption that a vortex at location x_0 in the wake moves with the undisturbed flow velocity U . ϕ denotes the perturbation velocity potential.

$$\Delta p_{nc} = -2\rho \left(\frac{\partial \phi}{\partial t} + U \frac{\partial \phi}{\partial x} \right) \quad (6.22)$$

These equations lead to the lift expressed as:

$$L = \int_0^c \Delta p dx = - \int_0^c \left[2\rho U \left(\frac{\partial \phi}{\partial x_0} + \frac{\partial \phi}{\partial x} \right) C(k) + 2\rho \left(\frac{\partial \phi}{\partial t} + U \frac{\partial \phi}{\partial x} \right) \right] dx \quad (6.23)$$

Equation 6.23 has to be solved with an appropriate assumption on the Theodorsen function $C(k)$.

⁹The Kelvin Circulation Theorem states that, for any flow governed by Euler's Equation, the circulation round a material loop is conserved [87]. Thus, $\frac{\partial \Gamma}{\partial t} = 0$

¹⁰The rear stagnation point at the trailing edge allows the flow leave the upper and lower surfaces smoothly at the trailing edge. This is the essence of the Kutta condition [87].

6.5 Continuously Morphing Wing Model

Ameri et al.[131] whose work is reviewed in this section, present a conceptual approach for the modeling of a small-scale flying wing with active winglets actuated via a distribution of actuators. The conceptual approach allows the tailoring of the main parameters influencing the flexibility of the structures. The goal of their work was to modify the flying wing from its discrete surfaces concept, actuated via single torque actuator, to a seamless continuous concept actuated via a distribution of actuators. They used equivalent plate continuum models to simulate morphing structures with the assumption that only global quantities of the response are of concern. An equivalent plate model approach was chosen instead of the widely used equivalent beam model because the beam model is not suitable for low aspect ratio wings made of composite materials.

The challenges with equivalent plate models is the difficulty of capturing local effects. When simple polynomial Ritz based functions are used, the resulting numerical analysis is significantly simplified leading to explicit expressions of stiffness and mass matrix in terms of system design variables.

The plate representation of a structure is considered as a bridge between the simple beam model and the complex, but accurate Finite Element (FE) model. Existing solutions for plates are classified according to the deformation theory used:

- a) The Classical Plate Theory (CPT). The CPT is based on the Kirchhoff-Love hypothesis. This hypothesis states that a straight line normal to the plate middle surface remains straight and normal during the deformation process. The CPT approach works well when through-thickness shear deformations are negligible. This is applicable to thin isotropic plates.
- b) The First-order Shear Deformation Theory (FSDT). The FSDT is based on the Reissner-Mindlin model. It relaxes the constraint that a normal to the mid-surface stays normal to the mid-surface after deformation. It allows a uniform transverse shear strain. Due to its simplicity, the FSDT has a low computation requirement.
- c) The Higher-order Shear Deformation Theory (HSDT). The HSDT is based on a more accurate representation of the local distribution of the transverse shear.

6.5.1 Structural Model

The wing is modeled by applying the First-order Shear Deformation Theory (FSDT). The wing geometry is defined by a small number of sizing and shape design variables. Particularly, the skin depth and thickness, spar caps, ribs and spar thicknesses are all defined through polynomials with respect to the coordinates of a reference plane where the wing trapezoid is defined. Similarly, displacements are defined by polynomials whose coefficients represent the time-dependent generalized coordinates. The minimization of the total energy leads to the Lagrange equations and the mass and stiffness matrices are evaluated by analytical integration.

Geometry Definition

The geometry of the wing is depicted in Figure 6.7. It represents a generic trapezoidal wing shape defined over a global left-handed coordinate system x , y and z . It is composed of spars, ribs and caps.

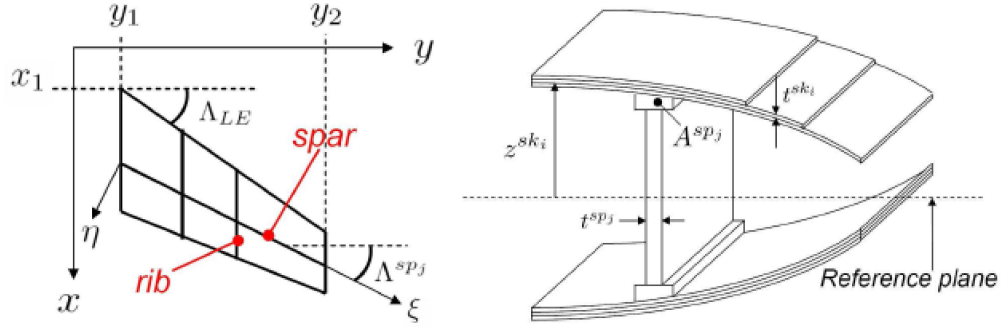


Figure 6.7: Generic trapezoidal wing (left) and wing-box (right)[127].

The wing is defined over the following bounded set:

x :

$$\{x_1 + y \tan(\Lambda_{LE}) < x < x_1 + y \tan(\Lambda_{LE}) + c(y)\} \quad (6.24)$$

y :

$$\{y_1 < y < y_2\} \quad (6.25)$$

where Λ_{LE} is the leading edge sweep angle and $c(y)$ is the local chord.

A depth distribution is defined over the bounded region of the wing. This depth distribution is the height of each composite skin layer forming the wing shape with respect to a reference plane $z = 0$. The i -th layer height z^{sk_i} is described by a polynomial series in the x and y global coordinates as follows:

$$z^{sk_i}(x, y) = \sum_{k=1}^{N_k} H_k^{sk_i} x^{m_k} y^{n_k} \quad (6.26)$$

where the H^{sk_i} coefficients are used as design variables. Under the hypothesis of a small thickness-to-depth ratio, two sets of depth are taken into account. These are the upper z^{up} , and the lower surfaces z^{lo} .

Similarly, a distribution of the i -th composite layer thickness is defined over the wing planform:

$$t^{sk_i}(x, y) = \sum_{j=1}^{N_j} T_j^{sk_i} x^{m_j} y^{n_j} \quad (6.27)$$

Each spar is identified by a spar line having the general expression:

$$x^{spj}(y) = a_1 y + a_2 \quad (6.28)$$

This linear equation locates the η axis of a local coordinates system (ξ, η, z) which is rotated with respect to the global system by an angle Λ^{spj} . The thickness distribution and cap area of the spars are expressed as simple polynomials in y , as $t^{spj}(y)$ and $A^{spj}(y)$ respectively. Each rib is modeled as parallel to the longitudinal axis, and thus is identified simply by the line $y = y^{rbk}$, with thickness distribution $t^{rbk}(x)$ and spar cap area $A^{rbk}(x)$.

Material Properties

Each skin layer has its own fibre direction in the x - y plane and the constitutive equations reflect a plane strain behavior:

$$\boldsymbol{\sigma}^{sk_i} = \mathbf{Q}^{sk_i} \boldsymbol{\epsilon}^{sk_i} \quad (6.29)$$

where $\boldsymbol{\sigma}^{sk_i} = [\sigma_{xx} \ \sigma_{yy} \ \sigma_{xy}]^T$ and $\boldsymbol{\epsilon}^{sk_i} = [\epsilon_{xx} \ \epsilon_{yy} \ \gamma_{xy}]^T$ are the stress and strain vectors respectively. \mathbf{Q}^{sk_i} is the constitutive matrix of the i -th layer.

The constitutive behaviour of each spar is defined in the local (ξ, η, z) coordinate system so that

$$\tilde{\boldsymbol{\sigma}}^{spj} = \tilde{\mathbf{Q}}^{spj} \tilde{\boldsymbol{\epsilon}}^{spj} \quad (6.30)$$

where $\tilde{\boldsymbol{\sigma}}^{spj} = [\sigma_{\eta\eta} \ \sigma_{xz}]^T$ and $\tilde{\boldsymbol{\epsilon}}^{spj} = [\epsilon_{\eta\eta} \ \gamma_{\eta z}]^T$

This means that the spars sustain only axial stress and the transverse shear. The spar strain vector in global coordinates $\boldsymbol{\epsilon}^{spj} = [\epsilon_{xx} \ \epsilon_{yy} \ \gamma_{xy} \ \gamma_{xz} \ \gamma_{yz}]^T$ is related to the strain in local coordinates by means of the following relation:

$$\tilde{\boldsymbol{\epsilon}}^{spj} = \mathbf{T} \boldsymbol{\epsilon}^{spj} \quad (6.31)$$

where \mathbf{T} is the global-to-local rotation matrix for the spar strain vector defined as

$$\mathbf{T} = \begin{bmatrix} s^2(\Lambda^{spj}) & c^2(\Lambda^{spj}) & s(\Lambda^{spj})c(\Lambda^{spj}) & 0 & 0 \\ 0 & 0 & 0 & s(\Lambda^{spj}) & c(\Lambda^{spj}) \end{bmatrix} \quad (6.32)$$

where $s = \sinus$ and $c = \cosinus$

The spar caps sustain only axial stress, and thus the constitutive equation is simply

$$\sigma_{\eta\eta} = E \epsilon_{\eta\eta} \quad (6.33)$$

A rotation vector gives the global-to-local transformation:

$$\epsilon_{\eta\eta} = \mathbf{t}^T \boldsymbol{\epsilon}^{spcr} \quad (6.34)$$

where $\boldsymbol{\epsilon}^{spcr} = [\epsilon_{xx} \ \epsilon_{yy} \ \gamma_{xy}]^T$ is the spar cap strain vector in global coordinates and the rotation matrix is given by

$$\mathbf{t} = \begin{bmatrix} s^2(\Lambda^{spj}) & c^2(\Lambda^{spj}) & s(\Lambda^{spj})c(\Lambda^{spj}) \end{bmatrix}^T \quad (6.35)$$

Similar relations are obtained for the ribs and the rib caps. They behave in a similar way to the spars and spar caps previously described, but the local η axis is rotated by an angle $\Lambda^{rbk} = 90^\circ$ and coincides with the x axis.

First-Order Shear Deformation

The first-order shear deformation plate theory (FSDT) is based on the Reissner-Mindlin assumption where the u , v and w displacements of the wing are approximated as

$$u(x, y, z, t) = u_0(x, y, t) + z\psi_x(x, y, t) \quad (6.36)$$

$$v(x, y, z, t) = v_0(x, y, t) + z\psi_y(x, y, t) \quad (6.37)$$

$$w(x, y, z, t) = w_0(x, y, t) \quad (6.38)$$

where u_0 , v_0 and w_0 denote the corresponding mid-plane displacements in the x , y , z directions; ψ_x and ψ_y are unknown functions giving contributions to the transverse shear deformations in the $x - z$ and $y - z$ planes respectively.

Under the hypothesis of small surface curvatures, the wing skins are modeled as a thin plane stress panel, and the strain field is given by:

$$\epsilon_{xx} = u_{,x} \quad (6.39)$$

$$\epsilon_{yy} = v_{,y} \quad (6.40)$$

$$\gamma_{xy} = u_{,y} + v_{,x} \quad (6.41)$$

while the transverse shear fields captured by the spars and ribs are:

$$\gamma_{xz} = u_{,z} + w_{,x} \quad (6.42)$$

$$\gamma_{yz} = v_{,z} + w_{,y} \quad (6.43)$$

Substituting equations (6.36) through (6.38) into equations (6.42) and (6.43) shows that ψ_x and ψ_y are the actual rotations of the sections about the y and x axes respectively:

$$\psi_x = \gamma_{xz} - w_{0,x} \quad (6.44)$$

$$\psi_y = \gamma_{yz} - w_{0,y} \quad (6.45)$$

Mass And Stiffness Matrices

The equivalent plate theory is based on the assumption that the deformation field is approximated by a series of Ritz polynomials. Thus, the unknowns in equations (6.36) through (6.38) are expressed as:

$$u_0(x, y, t) = \mathbf{a}_1(x, y)^T \mathbf{q}_1(t) \quad (6.46)$$

$$v_0(x, y, t) = \mathbf{a}_2(x, y)^T \mathbf{q}_2(t) \quad (6.47)$$

$$\psi_x(x, y, t) = \mathbf{a}_3(x, y)^T \mathbf{q}_3(t) \quad (6.48)$$

$$\psi_y(x, y, t) = \mathbf{a}_4(x, y)^T \mathbf{q}_4(t) \quad (6.49)$$

$$w_0(x, y, t) = \mathbf{a}_5(x, y)^T \mathbf{q}_5(t) \quad (6.50)$$

where $\mathbf{a}_i = [\dots, x^{n_p} y^{m_p}, \dots]^T$ are vectors containing the polynomial terms or shape functions, which may be of different lengths. The \mathbf{q}_i are vectors of the time-dependent generalized coordinates.

Substituting equations (6.46) through (6.50) into equations (6.36) through (6.38) and defining the displacement vector $\mathbf{u} = \begin{bmatrix} u & v & w \end{bmatrix}^T$ and the vector of generalized coordinates $\mathbf{q} = \begin{bmatrix} \mathbf{q}_1^T & \mathbf{q}_2^T & \mathbf{q}_3^T & \mathbf{q}_4^T & \mathbf{q}_5^T \end{bmatrix}^T$, leads to:

$$\mathbf{u} = \mathbf{S}\mathbf{q} \quad (6.51)$$

where $\mathbf{S} = \mathbf{S}(x, y, z)$ is the matrix relating the generalized coordinates to the physical displacements. Substituting equations (6.46) through (6.50) into equations (6.39) through (6.41) and equations (6.42) and (6.43) leads to:

$$\boldsymbol{\epsilon}^{sk_i} = \mathbf{E}\mathbf{q} \quad (6.52)$$

$$\boldsymbol{\epsilon}^{sp_j} = \mathbf{W}\mathbf{q} \quad (6.53)$$

where $\mathbf{E} = \mathbf{E}(x, y, z)$ and $\mathbf{W} = \mathbf{W}(x, y, z)$ are matrices providing the deformation field for the skin layers and for the spars respectively.

Finally, the mass and stiffness matrices for each element of the wing are obtained using an energy approach. Specifically, the kinetic (T) and elastic potential (ε) contributions to the total energy of the wing are defined for the skin, spar and spar caps (the procedure is identical for ribs and rib caps) and the application of the Lagrange equations

$$\frac{d}{dt} \left(\frac{\partial T}{\partial \dot{q}_n} \right) - \left(\frac{\partial T}{\partial q_n} \right) + \left(\frac{\partial \varepsilon}{\partial q_n} \right) = 0 \quad (6.54)$$

with $n = 1, 2, \dots, N_q$ minimizes the total energy with respect to the generalized coordinates, and gives the mass and stiffness matrices. In practice, this procedure requires the computation of integrals over the geometric domain. Since the nature of the shape functions and the definition of depths, thicknesses and areas are all polynomials in x and y , the integrals may be calculated in closed form, and no numerical evaluation is required.

Wing Skins

The contribution to the kinetic energy of an infinitesimal skin element of volume $t^{sk_i}(x, y) dx dy$ and of density ρ , is given by

$$dT^{sk_i} = \frac{1}{2} \rho t^{sk_i}(x, y) \dot{\mathbf{u}}^T \dot{\mathbf{u}} dx dy \quad (6.55)$$

Substituting equation (6.51) and integrating over the wing domain defined by equations (6.24) and (6.25), gives the total kinetic energy as:

$$T^{sk_i} = \frac{1}{2} \dot{\mathbf{q}}^T \left(\int \int \rho t^{sk_i}(x, y) \mathbf{S}(x, y, z^{sk_i})^T \mathbf{S}(x, y, z^{sk_i}) dx dy \right) \dot{\mathbf{q}} \quad (6.56)$$

$$T^{sk_i} = \frac{1}{2} \dot{\mathbf{q}}^T \mathbf{M}^{sk_i} \dot{\mathbf{q}}$$

Similarly, the potential energy of the infinitesimal skin element is

$$d\varepsilon^{sk_i} = \frac{1}{2} t^{sk_i}(x, y) \boldsymbol{\epsilon}^{sk_i T} \boldsymbol{\sigma}^{sk_i} dx dy \quad (6.57)$$

Substituting equations (6.29) and (6.52) and integrating over the wing domain, gives the total potential energy as

$$\varepsilon^{sk_i} = \frac{1}{2} \mathbf{q}^T \left(\int \int t^{sk_i}(x, y) \mathbf{E}(x, y, z^{sk_i})^T \mathbf{Q}^{sk_i} \mathbf{E}(x, y, z^{sk_i}) dx dy \right) \mathbf{q} \quad (6.58)$$

$$\varepsilon^{sk_i} = \frac{1}{2} \mathbf{q}^T \mathbf{K}^{sk_i} \mathbf{q}$$

Wing Spars

The contribution to the kinetic energy of an infinitesimal spar element of volume $t^{spj}(\eta)d\eta dz$ and of density ρ is given by:

$$dT^{spj} = \frac{1}{2}\rho t^{spj}(\eta) \dot{\mathbf{u}}^T \dot{\mathbf{u}} d\eta dz \quad (6.59)$$

Substituting equation (6.50) and considering the global-to-local coordinate system relation,

$$d\eta = \frac{dy}{\cos(\Lambda^{spj})} \quad (6.60)$$

the double integration over the wing length and between the lower and upper limit of the spar leads to the following expression for the mass matrix:

$$\mathbf{M}^{spj} = \frac{\rho}{\cos(\Lambda^{spj})} \int_{z^{lo}(x^{spj},y)}^{z^{up}(x^{spj},y)} \int_{y_1}^{y_2} t^{spj}(y) \mathbf{S}(x^{spj},y,z)^T \mathbf{S}(x^{spj},y,z) dy dz \quad (6.61)$$

where $x^{spj} = x^{spj}(y)$ is the spar line as defined in equation (6.28). The potential energy of the infinitesimal spar element is defined as:

$$dU^{spj} = \frac{1}{2} t^{spj}(\eta) \tilde{\boldsymbol{\epsilon}}^{spjT} \tilde{\boldsymbol{\sigma}}^{spj} d\eta dz \quad (6.62)$$

Equations (6.30), (6.31), (6.53) and (6.60) give the expression for the spar stiffness matrix

$$\mathbf{K}^{spj} = \frac{1}{\cos(\Lambda^{spj})} \int_{z^{lo}(x^{spj},y)}^{z^{up}(x^{spj},y)} \int_{y_1}^{y_2} t^{spj}(y) \mathbf{E}^T \mathbf{T}(\Lambda^{spj})^T \tilde{\mathbf{Q}}^{spj} \mathbf{T}(\Lambda^{spj}) \mathbf{E} dy dz \quad (6.63)$$

with $\mathbf{E} = \mathbf{E}(x^{spj},y,z)$

Spar Caps

The volume of an infinitesimal spar cap element, belonging to the j -th spar, is $A^{spcr}(y)d\eta dx$. Thus, following the procedure adopted in the previous section, expressions for the mass and stiffness matrices for the spar caps are:

$$\mathbf{M}^{spcr} = \frac{\rho}{\cos(\Lambda^{spj})} \int_{y_1}^{y_2} A^{spcr}(y) \mathbf{S}(x^{spj},y,z^*)^T \mathbf{S}(x^{spj},y,z^*) dy \quad (6.64)$$

$$\mathbf{K}^{spcr} = \frac{\mathbf{E}}{\cos(\Lambda^{spj})} \int_{y_1}^{y_2} A^{spcr}(y) \mathbf{W}(x^{spj},y,z^*)^T \mathbf{t} \mathbf{t}^T \mathbf{W}(x^{spj},y,z^*) dy \quad (6.65)$$

where $z^* = z^{up/lo}(x^{spj},y)$ is the height at which the spar cap is defined.

Finally, mass and stiffness matrices of the whole structure are given by summing the contributions of all the elements of the wing.

$$\mathbf{M} = \sum \mathbf{M}^{sk_i} + \sum \mathbf{M}^{spj} + \sum \mathbf{M}^{spcr} + \sum \mathbf{M}^{rb_k} + \sum \mathbf{M}^{rbc_s} \quad (6.66)$$

$$\mathbf{K} = \sum \mathbf{K}^{sk_i} + \sum \mathbf{K}^{spj} + \sum \mathbf{K}^{spcr} + \sum \mathbf{K}^{rb_k} + \sum \mathbf{K}^{rbc_s} \quad (6.67)$$

Multiple Plate Capability

If the system comprises more than one plate, each of them with arbitrary orientation in space, a global coordinate system has to be set up. A local coordinate system, fixed with respect to the undeformed reference state, is defined for each plate. Thus, if the same set of polynomial is used for each plate, the global number of degrees of freedom will be $N_P \times N_q$ where N_P is the number of plates and N_q is the number of degrees of freedom of each plate. Finally, each plate will add to the system a contribution to the kinetic and potential energies that is evaluated with respect to the local coordinate system and thus, the formulation obtained in previous sections is used for this purpose.

Ameri et al. formulated the displacement compatibility between contiguous plates by means of stiff springs. Both rotational and longitudinal springs are used in their work. The displacement compatibility is imposed in global coordinates; but expressed in local coordinates as follows: Consider the contiguous plates i and j and let R^i and R^j be respectively the global-to-local transformation matrix of each plate. In order to impose the displacement compatibility of the point A_i belonging to body i and the point A_j belonging to body j , the following expression leads to the potential energy of the springs linking A_i and A_j :

$$\varepsilon = \frac{1}{2} (\bar{\mathbf{u}}_{A_i}^i - \bar{\mathbf{u}}_{A_j}^j)^T \begin{bmatrix} k_x & 0 & 0 & 0 & 0 \\ 0 & k_y & 0 & 0 & 0 \\ 0 & 0 & k_z & 0 & 0 \\ 0 & 0 & 0 & k_{rx} & 0 \\ 0 & 0 & 0 & 0 & k_{ry} \end{bmatrix} (\bar{\mathbf{u}}_{A_i}^i - \bar{\mathbf{u}}_{A_j}^j) \quad (6.68)$$

where $\bar{\mathbf{u}}$ collects the elastic displacements and the rotations of a point of the structure in global coordinates. Thus, the global displacement vector can be expressed in terms of the local displacement $\bar{\mathbf{u}}$, via a geometrical rotation matrix, and, consequently, in terms of the Lagrangian coordinates via the matrix of shape functions \mathbf{S} .

$$\bar{\mathbf{u}} = \mathbf{R}\mathbf{u} = \mathbf{R}\mathbf{S}\mathbf{q} \quad (6.69)$$

Substituting equation (6.69) in to equation (6.68) leads to the following expression for the potential energy

$$\varepsilon = \frac{1}{2} (\mathbf{q}_i^T \mathbf{K}_{ii}^s \mathbf{q}_i + \mathbf{q}_j^T \mathbf{K}_{jj}^s \mathbf{q}_j + \mathbf{q}_i^T \mathbf{K}_{ij}^s \mathbf{q}_j + \mathbf{q}_j^T \mathbf{K}_{ji}^s \mathbf{q}_i) \quad (6.70)$$

where the generic contribution to the stiffness matrix is defined as

$$\mathbf{K}_{lp}^s = \mathbf{S}_{Al}^T \mathbf{R}^{lT} \begin{bmatrix} k_x & 0 & 0 & 0 & 0 \\ 0 & k_y & 0 & 0 & 0 \\ 0 & 0 & k_z & 0 & 0 \\ 0 & 0 & 0 & k_{rx} & 0 \\ 0 & 0 & 0 & 0 & k_{ry} \end{bmatrix} \mathbf{R}^p \mathbf{S}_{Ap} \quad (6.71)$$

with $l = i, j$ and $p = i, j$

6.5.2 Piezo And Thermo Actuator Model

A patch of Piezo or thermo actuator undergoes a strain variation when an electrical field or a thermal variation respectively, is imposed through the thickness. Assuming that the patches are thin enough to be modelled as plates and assuming a plane-strain behavior, the previous relations can be expressed analytically as:

$$\tilde{\epsilon}_{\Delta T} = \begin{bmatrix} \epsilon_{11} \\ \epsilon_{22} \\ \gamma_{12} \end{bmatrix} = \begin{bmatrix} \alpha_1 \\ \alpha_2 \\ 0 \end{bmatrix} \Delta T \quad (6.72)$$

$$\tilde{\epsilon}_V = \begin{bmatrix} \epsilon_{11} \\ \epsilon_{22} \\ \gamma_{12} \end{bmatrix} = \begin{bmatrix} d_{13} \\ d_{23} \\ 0 \end{bmatrix} \frac{V}{t} \quad (6.73)$$

where $\tilde{\epsilon}_{\Delta T}$ and $\tilde{\epsilon}_V$ are the strains defined in the principal material coordinates of each patch, α_1 and α_2 are the thermal expansion coefficients in the 1 and 2 directions respectively, d_{13} and d_{23} [m/V] are the Piezo-electric constants; ΔT is the temperature variation input with respect to a reference temperature while the ratio V/t , between the input voltage V and the distance between the electrodes t , represents the through-the-thickness electric field.

The strain vectors in global coordinates $\epsilon_{\Delta T}$ and ϵ_V , is obtained by applying the rotation matrix \mathbf{T} which is a function of the angle θ . The angle θ defines the orientation of the principal material coordinate system with respect to the global, and is defined as follows:

$$\mathbf{T}(\theta) = \begin{bmatrix} m^2 & n^2 & mn \\ n^2 & m^2 & -mn \\ -2mn & 2mn & (m^2 - n^2) \end{bmatrix} \quad (6.74)$$

where $m = \cos(\theta)$ $n = \sin(\theta)$ such that

$$\tilde{\epsilon} = \mathbf{T}(\theta) \epsilon \quad (6.75)$$

Using this definition, the strain vectors in global coordinates is obtained as:

$$\epsilon_{\Delta T} = \mathbf{T}(\theta)^{-1} \mathbf{b}_{\Delta T} \Delta T \quad (6.76)$$

$$\epsilon_V = \mathbf{T}(\theta)^{-1} \mathbf{b}_V \frac{V}{t} \quad (6.77)$$

where $\mathbf{b}_{\Delta T} = [\alpha_1 \ \alpha_2 \ 0]^T$ and $\mathbf{b}_V = [d_{13} \ d_{23} \ 0]^T$

The strain due to the stress field ϵ_S is obtained by subtracting from the total strain field ϵ the contribution due to the thermal and the Piezo-electric strains.

$$\epsilon_S = \epsilon - (\epsilon_{\Delta T} + \epsilon_V) \quad (6.78)$$

Recalling equation (6.52), linking the total strain vector to the generalized coordinates vector for an infinitesimal skin element, and equations (6.76) and (6.77), the previous equation becomes

$$\epsilon_S = \mathbf{E}\mathbf{q} - \mathbf{T}(\theta)^{-1} \mathbf{b}_{\Delta T} \Delta T - \mathbf{T}(\theta)^{-1} \mathbf{b}_V \frac{V}{t} \quad (6.79)$$

The constitutive relations providing the stress vector $\boldsymbol{\sigma} = [\sigma_{xx} \ \sigma_{yy} \ \sigma_{xy}]^T$ is given by:

$$\boldsymbol{\sigma} = \mathbf{Q}\epsilon_S \quad (6.80)$$

where \mathbf{Q} is the constitutive matrix rotated in global coordinates.

The equations describing the interaction between the smart patches and the structure is obtained via a virtual work approach. The virtual work δW_ε done by the elastic forces on an infinitesimal element of Piezo-thermo actuator of volume $tdxdy$ is defined as:

$$\delta W_\varepsilon = \delta \boldsymbol{\epsilon}^T \boldsymbol{\sigma} t dx dy = \delta \mathbf{q}^T \left\{ \mathbf{E}^T \mathbf{Q} \left(\mathbf{E} \mathbf{q} - \mathbf{T}(\theta)^{-1} \mathbf{b}_{\Delta T} \Delta T - \mathbf{T}(\theta)^{-1} \mathbf{b}_V \frac{V}{t} \right) \right\} t dx dy \quad (6.81)$$

The inertial forces f_i acting on an infinitesimal element of mass $\rho t dx dy$ is defined using d'Alembert principle:

$$f_i = -\rho t \ddot{\mathbf{u}} dx dy = -\mathbf{S} \ddot{\mathbf{q}} \rho t dx dy \quad (6.82)$$

Thus, the virtual work δW_i done by the inertial forces becomes:

$$\delta W_i = \delta \mathbf{u}^T \mathbf{f}_i = -\delta \mathbf{q}^T \mathbf{S}^T \mathbf{S} \ddot{\mathbf{q}} \rho t dx dy \quad (6.83)$$

Similarly, the virtual work δW_{ext} done by the external forces f_{ext} per unit area is defined by:

$$\delta W_{ext} = \delta \mathbf{u}^T \mathbf{f}_{ext} dx dy = \delta \mathbf{q}^T \mathbf{S}^T \mathbf{f}_{ext} dx dy \quad (6.84)$$

The equilibrium condition states that the external and inertial virtual works must balance the internal work done by the stresses:

$$\delta W_{ext} = \delta W_i + \delta W_\varepsilon \quad (6.85)$$

Substituting in the previous equation, equations (6.81), (6.83), and (6.84), leads to:

$$\delta \mathbf{q}^T \left\{ \mathbf{E}^T \mathbf{Q} \mathbf{E} \mathbf{q} - \mathbf{E}^T \mathbf{Q} \mathbf{T}(\theta)^{-1} \mathbf{b}_{\Delta T} \Delta T - \mathbf{E}^T \mathbf{Q} \mathbf{T}(\theta)^{-1} \mathbf{b}_V \frac{V}{t} \right\} t dx dy \quad (6.86)$$

$$= \delta \mathbf{q}^T \left\{ -\rho t \mathbf{S}^T \mathbf{S} \ddot{\mathbf{q}} + \mathbf{S}^T \mathbf{f}_{ext} \right\} dx dy$$

which is integrated over the area S_A of the actuator patch, leading to

$$\mathbf{M}^A \ddot{\mathbf{q}} + \mathbf{K}^A \mathbf{q} = \mathbf{e}_{ext} + \mathbf{e}_V V + \mathbf{e}_{\Delta T} \Delta T \quad (6.87)$$

where

$$\mathbf{M}^A = \int \int_{S_A} \mathbf{S}^T \mathbf{S} \rho t dx dy \quad (6.88)$$

$$\mathbf{K}^A = \int \int_{S_A} \mathbf{E}^T \mathbf{Q} \mathbf{E} t dx dy \quad (6.89)$$

$$\mathbf{e}_{ext} = \int \int_{S_A} \mathbf{S}^T \mathbf{f}_{ext} dx dy \quad (6.90)$$

$$\mathbf{e}_V = \left(\int \int_{S_A} \mathbf{E}^T \mathbf{Q} \mathbf{T}(\theta)^{-1} dx dy \right) \mathbf{b}_V \quad (6.91)$$

$$\mathbf{e}_{\Delta T} = \left(\int \int_{S_A} \mathbf{E}^T \mathbf{Q} \mathbf{T}(\theta)^{-1} t dx dy \right) \mathbf{b}_{\Delta T} \quad (6.92)$$

where \mathbf{M}^A and \mathbf{K}^A are the mass and stiffness contributions of the strain actuator to be added to the total mass and stiffness matrices of the structure, while \mathbf{e}_V and $\mathbf{e}_{\Delta T}$ are the generalized vectors providing to the structure the effect of an applied voltage and a temperature variation, respectively. If N_A actuators are placed over the wing surface, the contribution of each actuator has to be included. If the patch dimensions are small compared to the whole skin area, then the previous equations can be discretized and evaluated with respect to the center point coordinates of the patch, namely x^A , y^A and z^A . For instance equation (6.88) becomes

$$\mathbf{M}^A = \mathbf{S} \left(x^A, y^A, z^A \right)^T \mathbf{S} \left(x^A, y^A, z^A \right) \rho t a b \quad (6.93)$$

where a and b are the width and length of the patch, supposed to be rectangular.

6.6 Snap-Through Model

Schultz et al.[120] discussed the concept of using a piezoceramic actuator (Macro-Fiber Composite (MFC) actuator) bonded to a side of a two-layer unsymmetric cross-ply $[0/90]_T$ laminate to provide the moments necessary to snap the laminate from one stable equilibrium shape to another. They developed a model based on the Rayleigh-Ritz technique and the use of energy and variational methods. An analytical model was developed in three steps including cooling the cured laminate, bonding the actuator to the laminate, and applying voltage to the laminate-actuator combination. These steps are reviewed in this section. Figure 6.8 illustrates the laminate-actuator geometry. The laminate is considered to be fixed at the geometric center, and with no external applied loads.

Accordingly, in each of the three steps, the three components of the displacement of the geometric mid-surface of the laminate (the reference surface in this analysis) are approximated by:

$$u^0 = c_5x + \frac{1}{3}c_6x^3 + c_7xy^2 - \frac{1}{6}c_1^2x^3 - \frac{1}{8}c_1c_3x^4 - \frac{1}{40}c_3^2x^5 \quad (6.94)$$

$$v^0 = c_8y + c_9x^2y + \frac{1}{3}c_{10}y^3 - \frac{1}{6}c_2^2y^3 - \frac{1}{8}c_2c_4y^4 - \frac{1}{40}c_4^2y^5 \quad (6.95)$$

$$w^0 = \frac{1}{2}(c_1x^2 + c_2y^4) + \frac{1}{6}(c_3x^3 + c_4y^3) \quad (6.96)$$

where u, v , and w are the displacements in the x, y , and z directions, respectively. The 10 parameters c_1 through c_{10} are unknown coefficients to be determined. Because of symmetry requirements on the displacement, the third order w -displacement polynomial can not be used to represent the w -displacement field over the entire laminate. However, a quarter-symmetry argument is applied to allow the use of this polynomial to represent the w -displacement field. Then, the total potential energy is calculated over only one-quarter of the laminate.

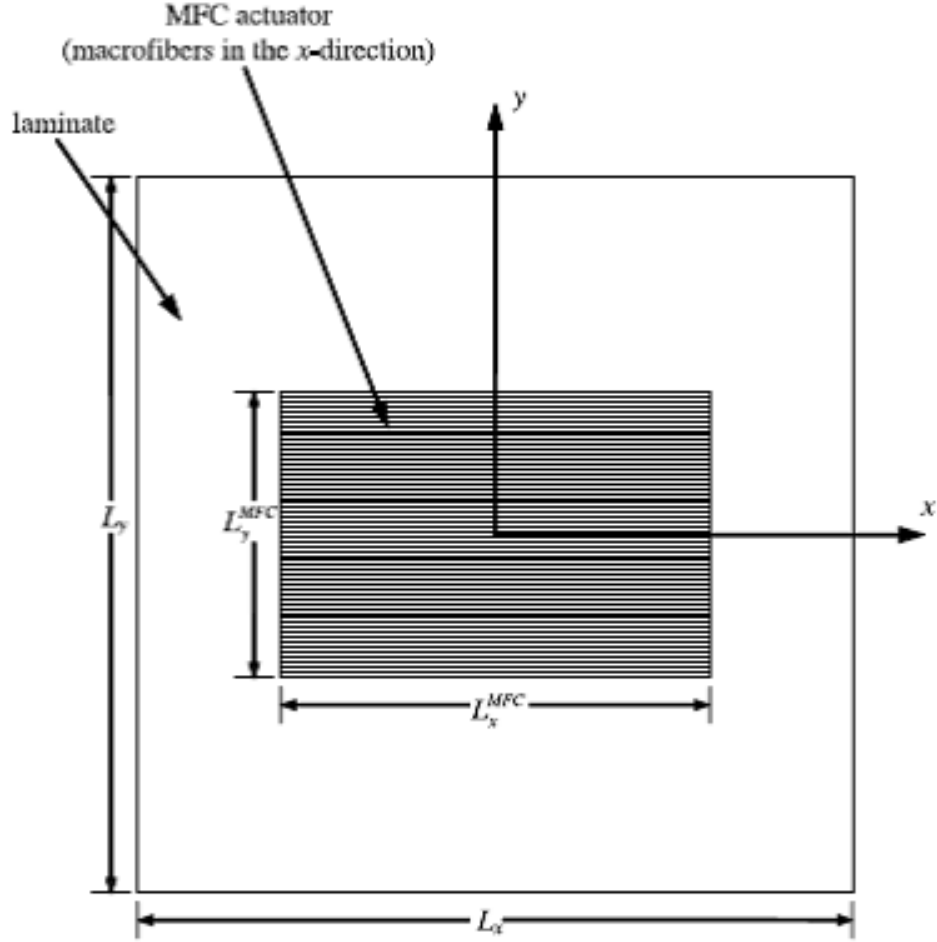


Figure 6.8: Geometry of laminate-actuator combination [120].

Step I: Laminate Cooling Model

The first step of the model is to determine the initial cooled shape of the two-layer $[0/90]_T$ laminate. Because this step does not include the actuator, and no forces are applied to the laminate, only thermal effects within the laminate are considered. Accordingly, the total potential energy, Π , in this step is the strain energy of the cooled laminate, Π_1 , given by:

$$\Pi = \Pi_1 = 4 \left(\frac{1}{2} \int_0^{L_x} \int_0^{L_y} \int_{z_0}^{z_2} [(\sigma_x - \sigma_x^T) \varepsilon_x + (\sigma_y - \sigma_y^T) \varepsilon_y + (\sigma_{xy} - \sigma_{xy}^T) \gamma_{xy}] dx dy dz \right) \quad (6.97)$$

where σ denotes the stress in the laminate, σ^T is the thermally induced stress, ε and γ_{xy} represent the strains. Additionally, L_x and L_y are the side lengths of the laminate as depicted in Figure 6.8, the thickness coordinates z_0 and z_2 are the coordinates for the bottom of the 0° graphite-epoxy layer and the top of the 90° graphite-epoxy layer, respectively.

The stresses are given by

$$\sigma_x = \bar{Q}_{11}\varepsilon_x + \bar{Q}_{12}\varepsilon_y + \bar{Q}_{16}\gamma_{xy} - \sigma_x^T \quad (6.98)$$

$$\sigma_y = \bar{Q}_{12}\varepsilon_x + \bar{Q}_{22}\varepsilon_y + \bar{Q}_{26}\gamma_{xy} - \sigma_y^T \quad (6.99)$$

$$\sigma_{xy} = \bar{Q}_{16}\varepsilon_x + \bar{Q}_{26}\varepsilon_y + \bar{Q}_{66}\gamma_{xy} - \sigma_{xy}^T \quad (6.100)$$

where \bar{Q} denotes the transformed reduced stiffnesses of the graphite-epoxy layers. The thermally induced stresses are given by:

$$\sigma_x^T = \bar{Q}_{11}\varepsilon_x^T + \bar{Q}_{12}\varepsilon_y^T + \bar{Q}_{16}\gamma_{xy}^T \quad (6.101)$$

$$\sigma_y^T = \bar{Q}_{12}\varepsilon_x^T + \bar{Q}_{22}\varepsilon_y^T + \bar{Q}_{26}\gamma_{xy}^T \quad (6.102)$$

$$\sigma_{xy}^T = \bar{Q}_{16}\varepsilon_x^T + \bar{Q}_{26}\varepsilon_y^T + \bar{Q}_{66}\gamma_{xy}^T \quad (6.103)$$

with

$$\varepsilon_x^T = \alpha_x \Delta T \quad (6.104)$$

$$\varepsilon_y^T = \alpha_y \Delta T \quad (6.105)$$

$$\gamma_{xy}^T = \alpha_{xy} \Delta T = 0 \quad (6.106)$$

where α denotes the coefficient of thermal deformation of the layer and ΔT the temperature change from the cure temperature to room temperature which is the operating temperature in the case in hands.

For small strains and moderate rotations, the mid-surface strains and curvatures in the laminate are given by the Von Kármán approximation through the more general strain-displacement relations:

$$\varepsilon_x^0 = \frac{\partial u^0}{\partial x} + \frac{1}{2} \left(\frac{\partial w^0}{\partial x} \right)^2 \text{ and } \kappa_x^0 = -\frac{\partial^2 w^0}{\partial x^2} \quad (6.107)$$

$$\varepsilon_y^0 = \frac{\partial v^0}{\partial y} + \frac{1}{2} \left(\frac{\partial w^0}{\partial y} \right)^2 \text{ and } \kappa_y^0 = -\frac{\partial^2 w^0}{\partial y^2} \quad (6.108)$$

$$\gamma_{xy}^0 = \frac{\partial u^0}{\partial y} + \frac{\partial v^0}{\partial x} + \frac{\partial w^0}{\partial x} \frac{\partial w^0}{\partial y} \text{ and } \kappa_{xy}^0 = -2 \frac{\partial^2 w^0}{\partial x \partial y} \quad (6.109)$$

According to the Kirchhoff hypothesis, the strains as a function of the thickness location, z , are given by

$$\varepsilon_x = \varepsilon_x^0 + z\kappa_x^0 \quad (6.110)$$

$$\varepsilon_y = \varepsilon_y^0 + z\kappa_y^0 \quad (6.111)$$

$$\gamma_{xy} = \gamma_{xy}^0 + z\kappa_{xy}^0 \quad (6.112)$$

By substituting equations (6.94) through (6.96) into equations (6.107) through (6.109) and equations (6.110) through (6.112) and, in turn, substituting these results into equations (6.98) through (6.100) and equation (6.97), taking into account equations (6.101) through and (6.106), and carrying out the integrations of equation (6.97), the total potential energy is reduced to an algebraic equation in terms of material properties, geometry, and the coefficients c_1 through c_{10} .

These coefficients are determined by solving the 10 simultaneous non-linear algebraic equations that result from equating to zero the first variation of total potential energy with respect to these coefficients, namely

$$\frac{\partial \Pi}{\partial c_i} = 0 \quad (6.113)$$

where $i = 1, \dots, n$

The stability of the solution is determined by checking the positive definiteness of the 10×10 matrix associated with the second variation of the total potential energy with respect to these 10 coefficients.

Step II: Actuator Bonding To Laminate

The total potential energy of the laminate and actuator bonded to it is the sum of the strain energy from equation (6.97), Π_1 , and the strain energy of the actuator, which is given as:

$$\Pi_2 = 4 \left(\frac{1}{2} \int_0^{\frac{L_x^{MFC}}{2}} \int_0^{\frac{L_y^{MFC}}{2}} \int_{z_2}^{z_3} [\sigma_x^{a2} \epsilon_x^{a2} + \sigma_y^{a2} \epsilon_y^{a2} + \sigma_{xy}^{a2} \gamma_{xy}^{a2}] dx dy dz \right) \quad (6.114)$$

where σ^{a2} is the stress, ϵ^{a2} and γ^{a2} denote the strain in the MFC actuator due to the bonding process. Additionally, the thickness coordinates z_2 and z_3 define the thickness of the actuator. The stress-strain relations for the bonded actuator are:

$$\sigma_x^{a2} = \bar{Q}_{11} \epsilon_x^{a2} + \bar{Q}_{12} \epsilon_y^{a2} + \bar{Q}_{16} \gamma_{xy}^{a2} \quad (6.115)$$

$$\sigma_y^{a2} = \bar{Q}_{12} \epsilon_x^{a2} + \bar{Q}_{22} \epsilon_y^{a2} + \bar{Q}_{26} \gamma_{xy}^{a2} \quad (6.116)$$

$$\sigma_{xy}^{a2} = \bar{Q}_{16} \epsilon_x^{a2} + \bar{Q}_{26} \epsilon_y^{a2} + \bar{Q}_{66} \gamma_{xy}^{a2} \quad (6.117)$$

For simplification, it is assumed that the curvatures of the mid-surface of the laminate and the mid-surface of the actuator (rather than the curvatures of the contacting surfaces) are the same. The strains in the actuator is then be approximated as

$$\epsilon_x^{a2} = \left(z - \left(\frac{z_3 - z_0}{2} \right) \right) \kappa_x^0 \quad (6.118)$$

$$\epsilon_y^{a2} = \left(z - \left(\frac{z_3 - z_0}{2} \right) \right) \kappa_y^0 \quad (6.119)$$

$$\gamma_{xy}^{a2} = \left(z - \left(\frac{z_3 - z_0}{2} \right) \right) \kappa_{xy}^0 = 0 \quad (6.120)$$

where the κ terms are not known, but will be the same in the actuator and the laminate. The displacement fields of the form in Step I are again assumed to be valid. For this step, the total potential energy of the laminate-actuator combination is given as:

$$\Pi = \Pi_1 + \Pi_2 \quad (6.121)$$

It is worth noticing that in the total potential energies of the laminate and actuator given above, the work terms due to the stresses between the laminate and actuator cancel each other. The coefficients c_1 through c_{10} for this step are again determined by finding stationary values of Π , as in equation (6.113), and the stability is checked by examining the second variation.

Step III: Actuation of The MFC

This step considers the laminate-actuator combination with no slipping between the laminate and the actuator, and includes the deformation due to voltage applied to the actuator. The initial shape is specified by the coefficients c_1 through c_{10} associated with the shape determined from Step II. For Step III, these known coefficients are renamed c_1^i through c_{10}^i , respectively. The superscript ‘i’ denotes ‘initial.’

The total potential energy of the model is broken into the laminate contribution, Π_1 , and the actuator contribution, Π_3 . The contribution to the total potential energy from the MFC actuator is then written as:

$$\Pi_3 = 4 \left(\frac{1}{2} \int_0^{\frac{L_x^{MFC}}{2}} \int_0^{\frac{L_y^{MFC}}{2}} \int_{z_2}^{z_3} [(\sigma_x^{a3} - \sigma_x^E) \epsilon_x^{a3} + (\sigma_y^{a3} - \sigma_y^E) \epsilon_y^{a3} + (\sigma_{xy}^{a3} - \sigma_{xy}^E) \gamma_{xy}^{a3}] dx dy dz \right) \quad (6.122)$$

where σ^{a3} denotes the stress, ϵ^{a3} and γ^{a3} are the strains in the actuator. The mid-surface of the graphite-epoxy laminate remains the reference surface. The stresses in the actuator are given by:

$$\sigma_x^{a3} = \bar{Q}_{11} \epsilon_x^{a3} + \bar{Q}_{12} \epsilon_y^{a3} + \bar{Q}_{16} \gamma_{xy}^{a3} - \sigma_x^E \quad (6.123)$$

$$\sigma_y^{a3} = \bar{Q}_{12} \epsilon_x^{a3} + \bar{Q}_{22} \epsilon_y^{a3} + \bar{Q}_{26} \gamma_{xy}^{a3} - \sigma_y^E \quad (6.124)$$

$$\sigma_{xy}^{a3} = \bar{Q}_{16} \epsilon_x^{a3} + \bar{Q}_{26} \epsilon_y^{a3} + \bar{Q}_{66} \gamma_{xy}^{a3} - \sigma_{xy}^E \quad (6.125)$$

where σ^E denotes the Piezo-electrically induced stresses given by

$$\sigma_x^E = \bar{Q}_{11} \epsilon_x^E + \bar{Q}_{12} \epsilon_y^E + \bar{Q}_{16} \gamma_{xy}^E \quad (6.126)$$

$$\sigma_y^E = \bar{Q}_{12} \epsilon_x^E + \bar{Q}_{22} \epsilon_y^E + \bar{Q}_{26} \gamma_{xy}^E \quad (6.127)$$

$$\sigma_{xy}^E = \bar{Q}_{16} \epsilon_x^E + \bar{Q}_{26} \epsilon_y^E + \bar{Q}_{66} \gamma_{xy}^E \quad (6.128)$$

where ϵ^E and γ^E are Piezo-electrically induced strains. The strains in the actuator, ϵ^{a3} and γ^{a3} are given by:

$$\epsilon_x^{a3} = \epsilon_x - \epsilon_x^s \quad (6.129)$$

$$\epsilon_y^{a3} = \epsilon_y - \epsilon_y^s \quad (6.130)$$

$$\gamma_{xy}^{a3} = \gamma_{xy} - \gamma_{xy}^s \quad (6.131)$$

The ϵ_x^s and γ_{xy}^s terms are considered shift strains and account for the discontinuous through-thickness distributions of the strains due to the room-temperature bonding of the actuator to the laminate. They allow the strain in the actuator to be defined by the reference surface strains and curvatures. They are Kirchhoff-like strains that are zero at the reference surface. After the actuator is bonded to the laminate, the strains in the laminate would be due to cooling and due to bending from adding the actuator. The strains in the actuator would be due only to bending. As a result, the strain distributions through the thickness of the laminate and actuator would not be continuous. When the laminate-actuator combination is snapped to the second actuator-added shape, the laminate and actuator would both have extensional and bending strains; the strain distributions would continue to be discontinuous between the laminate and actuator.

With actuation, it is assumed, in the spirit of the Kirchhoff hypothesis, that the strain increments in the laminate and actuator will be continuous through the thickness. Thus, the profiles of strains through the laminate and actuator would remain discontinuous. To account for this discontinuity, a set of coefficients c_1 through c_{10} is used to define the strains within the laminate and the actuator due to the application of voltage. The shift strains are given by:

$$\epsilon_x^s = \epsilon_x^{i0} + \left(\frac{z_3 - z_0}{2} \right) \kappa_x^{i0} \quad (6.132)$$

$$\epsilon_y^s = \epsilon_y^{i0} + \left(\frac{z_3 - z_0}{2} \right) \kappa_y^{i0} \quad (6.133)$$

$$\gamma_{xy}^s = \gamma_{xy}^{i0} + \left(\frac{z_3 - z_0}{2} \right) \kappa_{xy}^{i0} \quad (6.134)$$

where the ϵ^{i0} and γ_{xy}^{i0} terms are the initial strains and the κ^{i0} terms represent the initial curvatures.

The total potential energy for the actuation portion of the model is thus

$$\Pi = \Pi_1 + \Pi_3 \quad (6.135)$$

The shapes, actuated or unactuated, of the laminate-actuator combination are determined by solving for c_1 through c_{10} by equating to zero the first variation of the total potential energy given by equation 6.135. The stability is checked by examining at the second variation.

Chapter 7

Conclusion

7.1 Challenges

A morphing structure should be able to alter its shape, carry the required load and be lightweight. However, designers have been able to accomplish simultaneously only two of the three goals [60, 73]. Therefore, the goal of current research is to develop particular materials and devices that can enable morphing through time variant air frames whose changes in geometry will significantly influence aerodynamic performance as well as stealth characteristics for military applications.

As mentioned in the present review, there are several challenges in the design of morphing UAVs:

1. The integrity of compliant structures must be ensured under all circumstances. The structure should be rigid enough to withstand the loads but flexible enough to morph.
2. The system should be designed so that the required actuation force falls within the adequate limits. Thus, the morphing can occur efficiently.
3. The wing skin should provide a smooth and seamless aerodynamic surface whilst efficiently bearing the aerodynamic loads.
4. The design process should be extended to encompass multiple flight regimes.
5. The engines should be efficient at low and high speed flights at all altitudes.
6. The control systems should be efficient even with highly coupled control effectors.

Thus, the main challenge faced by the morphing technology is to design, fabricate and operate effective integrated combinations of deformable wing skins, actuators and mechanisms, and flight controls to provide the system designer of morphing UAV with the freedom to deal with future diverse, conflicting vehicle mission capabilities [96, 62].

The wing cover skins are subject to loads including compression, tension, and the shear and bending characteristics of aerodynamic loads taking into account the effects of added masses. The skins must therefore possess a high degree of deformability whilst maintaining the shape and structure integrity under all circumstances. In order to meet these requirements, thermoplastic elastomers and shape memory polymers are suggested as good candidate materials for smart skins. Nevertheless, an excessively flexible skin is exposed to the hazard of sagging under pressure loads. This may result into an inefficient torsional stiffness of the structure. Additionally, thermo-active polymers and advanced Piezo-electric actuators will provide the motion control while the flight dynamic, control system, and software will adapt to the radical shape changes.

7.2 Perspectives

Bio-inspired micro air vehicles characterize the aeromechanics and scalability of bat flight [60]. As a general observation, bat wing motion, unlike that of insects and birds, has several degrees of freedom. Therefore, the bat wing has a high degree of flexibility with anisotropy and non-linear elasticity. The wing surface is singular as it is composed of a thin wing consisting of a highly anisotropic, compliant skin membrane. It is therefore suggested that the incorporation of flexible wing membranes as lifting surfaces be examined as a potentially useful feature for engineered maneuverable micro flight vehicles.

Bibliography

- [1] R.W. Wlezein, G.C. Horner, A.R. McGowan, S.L. Padula, M.A. Scott, R.J. Silox, and J.O. Simpson, *The aircraft morphing program*, AIAA-98-1927.
- [2] DARPA, <http://www.darpa.mil/dso/archives/mas>, 15.12.2009
- [3] <http://www.defenseindustrydaily.com/the-advent-of-a-better-jet-engine-03623>, 15.12.2009
- [4] Kimon P. Valavanis, 2007, Springer, *Advances in Unmanned Aerial Vehicles, State of the Art and the Road to Autonomy*, ISBN 978-1-4020-6113-4.
- [5] <http://www.centennialofflight.gov/index.htm>. 10.2.2010
- [6] E.L. Carpenter, H.P.W. 2003, Burlington: Butterworth-Heinemann, *Aerodynamics for Engineering Students. 5th ed.*
- [7] <http://www.fas.org/irp/program/collect/pioneer.htm>, 07.3.2010
- [8] William Jangwhan, UAV CENTER Co, Introduction to UAV System, 2002-10-02
- [9] http://www.proxdynamics.com/products/pd_100_black_hornet, 07.03.2010.
- [10] <http://img259.imageshack.us/img259/7559/tabel1trnnc6.png>, 08.03.2010
- [11] Anna-Maria Rivas McGowan, Dan D. Vicroy, Ronald C. Busan, Andrew S. Hahn, Perspectives on highly adaptive or morphing aircraft, RTO-MP-AVT-168.
- [12] Anna-Maria Rivas McGowan, Morphing Background and Historical Perspective, Instituto Superior Tecnico Lisboa, Portugal, 17-20 November 2008.
- [13] <http://www.tandef.net/use-uav-target-designation-0>, 08.03.2010
- [14] OSD UAV Roadmap 2002-2027, Office of the Secretary of Defense (Acquisition, Technology, & Logistics), Air Warfare, December 2002.
- [15] <http://www.aer.bris.ac.uk/research/morphing/morph-intro.html>, 15.1.2010
- [16] <http://www.pbs.org/wgbh/nova/spiesfly/uavs.html>, 15.1.2010
- [17] Brian C. Porck, Terrence A. Weisshaar, William A. Crossley, September 2002, Morphing airfoil shape change optimization with minimum actuator energy as an objective, AIAA 2002-5401

- [18] D. Danieli, F. Scarpa, F. Gandhi, P. Anusonti-Inthra, STRUCTURAL ANALYSIS OF MORPHING WING USING ROTATIONAL ACTUATION, Laboratory, Aerospace Engineering, University of Sheffield, and Department of Aerospace Engineering, The Pennsylvania State University.
- [19] Egbert Torenbeek, 1988, Synthesis of subsonic airplane design, Delta University Press
- [20] <http://www.ww2aircraft.net/forum/other-mechanical-systems-tech/makhonine-telescoping-wing-8527.html>, visited on 9.2.2010
- [21] http://www.militaryfactory.com/aircraft/detail.asp?aircraft_id=658, visited on 12.2.2010
- [22] <http://www.geversaircraft.com/index.html>, visited on 9.2.2010
- [23] <http://www.anft.net/f-14/f14-detail-wsm.htm> visited on 12.2.2010
- [24] R. K. Page, Aircraft with variable sweep wings, October 1965, pages 295-299
- [25] Michael J. Hirschberg, David M. Hart, Thomas J. Beutner, A Summary Of A Half-Century of Oblique Wing Research, Defense Advanced CENTRA Technology and Research Projects Agency.
- [26] Michael I. Friswell, Daniel J. Inman Morphing Concepts for UAVs, 21st Bristol UAV Systems Conference April 2006.
- [27] Filippo Mattioni, Paul M. Wear, Kevin Potter, Michael I. Friswell, Multi-stable composites application concept for morphing aircraft, Bristol BS8 1TR
- [28] M. I. Friswell, D. Baker, J. E. Herencia, F. Mattioni and P. M. Weaver, Compliant Structures for Morphing Aircraft, 17th International Conference on Adaptive Structures and Technologies Oct. 16 ~ Oct. 19, Taipei, Taiwan.
- [29] J. Enrique Herencia, Paul M. Weaver and Michael I. Friswell, Morphing wing design via aero-elastic tailoring, 48th AIAA/ASME/ASCE/AHS/ASC Structures, Structural Dynamics, and Materials Conference, 23 - 26 April 2007, Honolulu, Hawaii
- [30] Cody Lafountain, Kelly Cohen, and Shaaban Abdallah, Camber Controlled Airfoil Design for Morphing UAV, 47th AIAA Aerospace Sciences Meeting Including The New Horizons Forum and Aerospace Exposition, 5 - 8 January 2009, Orlando, Florida
- [31] Sridhar Kota, Joel Hetricka, Russell Osborna, Donald Paul, Ed Pendleton, Peter Flick, Carl Tilmann, Design and application of compliant mechanisms for morphing aircraft structures, Smart Structures and Materials 2003: Industrial and Commercial Applications of Smart Structures Technologies, Eric H. Anderson, Editor, Proceedings of SPIE Vol. 5054 (2003) © 2003
- [32] Terrence A. Weisshaar, Morphing Aircraft Technology – New Shapes for Aircraft Design, NATO, RTO-MP-AVT-141.

- [33] <http://www.flyingmachines.org/ader.html> 18.2.2010
- [34] Cesnik, Carlos E.S. A Framework For Morphing Capability Assessment. Department of Aerospace Engineering, University of Michigan. 2004
- [35] Alan Baker, Stuart Dutton, Donald Kelly, Composite Materials for Aircraft Structures, American Institute of Aeronautics and Astronautics, Inc. 1801 Alexander Bell Drive, Reston, VA 20191-4344
- [36] Carlos E. S. Cesnik, Morphing and aero-elasticity for Very Flexible Aircraft, Presented at the Morphing Aircraft Materials, Mechanisms and Systems, Instituto Superior Tecnico Lisboa, Portugal, 17-20 November 2008
- [37] S. Ashley, Flying on Flexible Wings, Scientific American Magazine, pp.84-91, Nov. 2003
- [38] A.C.H. Leung D.D. Symons and S.D. Guest, Actuation of kagome lattice structures, Department of Engineering, University of Cambridge
- [39] http://www.nasa.gov/home/hqnews/2007/dec/HQ_07287_Invention_of_the_Year.htm 22.2.2010
- [40] Shizhuo Yin, Paul B. Ruffin, Francis T. S. Yu, Fiber Optic Sensors Second Edition, 2008 by Taylor & Francis Group, LLC.
- [41] D. Uttamchandani, Fiber-optic sensors and smart structures: Developments and prospects, Electronic & Commun. Engineering J., pp. 237–246, Oct. 1994.
- [42] J. R. Dunphy, G. Meltz, F. P. Lamm, and W. W. Morey, Multi-function, distributed optical-fiber sensor for composite cure and response monitoring, Proc. SPIE, 1370, pp. 116–118, 1990
- [43] K. Wood, T. Brown, R. Rogowski, and B. Jensen, Fiber optic sensors for health monitoring of morphing airframes. I. Bragg grating strain and temperature sensor, Smart Mater. Struct., 9, 2000.
- [44] <http://www.aer.bris.ac.uk/research/morphing/multistableStruct.html>, 15.1.2010
- [45] Cocke, B., Wind-Tunnel Investigation of the Aerodynamics and Structural Deflection Characteristics of the Goodyear Inflatoplane, NACA RM L58E09, September, 1958.
- [46] Jamey D. Jacob, Suzanne W. Smith, Dave Cadogan, Steve Scarborough, Expanding the Small UAV Design Space with Inflatable Wings, 2007 Society of Automotive Engineers, Inc. 07ATC-217
- [47] David Cadogan, Tim Smith, Frank Uhelsky, Matt MacKusic, ILC Dover, Frederica, DE 19946, Morphing Inflatable Wing Development for Compact Package Unmanned Aerial Vehicles
- [48] Sheryll Goecke Powers, Lannie D. Webb, Edward L. Firend, and William A. Kolos, Flight test results from a supercritical mission adaptive wing with smooth variable camber, NASA technical Memorandum 4415, November 1992.

- [49] Cezar Gabriel Diaconu, Paul M. Weaver, and Filippo Mattioni, Solutions for morphing airfoil sections using bi-stable laminated composite structures, 48th AIAA/ASME/ASCE/AHS/ASC Structures, Structural Dynamics, and Materials Conference 23 - 26 April 2007, Honolulu, Hawaii.
- [50] Hyer, M. W, Calculations of the Room-Temperature Shapes of Unsymmetric Laminates, *Journal of Composite Materials*, Vol. 15, Jul. 1981
- [51] http://dnc.tamu.edu/projects/flowcontrol/Morphing/public_html/index.htm, 10.2.2010
- [52] Narcis M. Ursache , Andy J. Keane and Neil W. Bressloff, On the Design of Morphing Airfoils using Spinal Structures, 47th AIAA/ASME/ASCE/AHS/ASC Structures, Structural Dynamics, and Materials Conference 1 - 4 May 2006, Newport, Rhode Island
- [53] K. Otsuka, C. M. Wayman, *Shape Memory Materials*, Cambridge University Press, Cambridge, 1999.
- [54] Bar-Cohen Ed., *electro active polymer (EAP) actuators as artificial muscles: reality, potential, and challenges*, 2nd Edition Vol. PM136, 2004, SPIE Press, Bellingham, WA.
- [55] A. Fontanazza, R. Talling, M. Jackson, R. Dashwood, D. Dye, L. Iannucci, *Morphing Wing Technologies Research*, Imperial College London, 1st SEAS DTC Technical Conference - Edinburgh 2006.
- [56] <http://www.nasa.gov/centers/dryden/news/NewsReleases/2001/01-67.html>, 10.2.2010
- [57] Pedro Portela, Pedro Camanho, Paul Weaver, Ian Bond, Analysis of morphing, multi stable structures actuated by Piezo-electric patches, *Computers and Structures* 86, 2008, 347–356
- [58] http://www.gyrodynehelicopters.com/qh-50_evolution.htm , 7.3.2010
- [59] NextGen Aeronautics, http://www.nextgenaero.com/success_mfx1.html, 09.03.2010
- [60] Major General Curtis M Bedke Commander, Air Force Research Laboratory, 6 January 2009.
- [61] <http://www.flightglobal.com/articles/>
- [62] Terrence A. Weisshaar, Purdue University, *New Aircraft Systems Concepts-Towards New Horizons in aero-elasticity*, RTO-MP-IST-999
- [63] The U.S. Air Force Remotely Piloted Aircraft and Unmanned Aerial Vehicle Strategic Vision, 2005
- [64] H. F. PARKER, *THE PARKER VARIABLE CAMBER WING*, Report N0. 77
- [65] Anderson, J. D., *Introduction to Flight*, 2nd ed., McGraw-Hill, 1985.

- [66] Miteshkumar Joshi, Shashank Priya, “PIEZO-BOW”—HIGH DISPLACEMENT AND HIGH BLOCKING FORCE ACTUATOR, *Integrated Ferroelectrics*, Volume 82, Issue 1 November 2006 , pages 25 - 43
- [67] Cook, R. D., Malkus, D. S., Plesha, M. E., and Witt, R. J., *Concepts and Applications of Finite Element Analysis*, 4th ed., Wiley, New York, 2001.
- [68] Bathe, K. J., *Finite Element Procedures*, Prentice–Hall, Upper Saddle River, NJ, 1996.
- [69] *Non-linear Finite Element Analysis of Solids and Structures, Volume 1: ADVANCED TOPICS*, John Wiley & Sons Ltd, 1997.
- [70] Y. I. Kim, G. J. Park, R. M. Kolonay, M. Blair, R. A. Canfield, non-linear Response Structural Optimization of a Joined Wing Using Equivalent Loads, *AIAA JOURNAL* Vol. 46, No. 11, November 2008.
- [71] A. Srikantha Phani, Richard Butler, Stephen Habgood and Christopher R. Bowen, *Analysis of Wing Morphing via Frame Buckling*, University of Bath, Bath, BA2 7AY, UK.
- [72] Livesly, R.K. and Chandler, D.B, *Stability functions for structural frameworks*, Manchester University Press, 1956.
- [73] Deepak S. Ramrakahyani, George A. Lesieutre, Mary Frecker†, and Smita Bharti, Aircraft Structural Morphing using Tendon Actuated Compliant Cellular Trusses, 45th AIAA/ASME/ASCE/AHS/ASC Structures, Structural Dynamics & Materials Conference 19 - 22 April 2004, Palm Springs, California..
- [74] Ted Belytschko, *LAGRANGIAN AND EULERIAN FINITE ELEMENTS IN ONE DIMENSION*, Northwestern University, 1997.
- [75] Jae-Sung Bae, T. Michael Seigler, Daniel J. Inman, Aerodynamic and Static aero-elastic Characteristics of a Variable-Span Morphing Wing, *JOURNAL OF AIRCRAFT* Vol. 42, No. 2, March–April 2005.
- [76] Prof. G. Dimitriadis, *Introduction to aero-elasticity, Equations of motion aero-elasticity*, Université de Liege, 2009
- [77] <http://encyclopedia.thefreedictionary.com>, 18.03.2010
- [78] Zafer Gürdal, Aerospace Structures Chair, Structural Design for Morphing Wings, Lisboa, Portugal, 17-20 November 2008.
- [79] <http://en.wikipedia.org>, 10.03.2010
- [80] <http://galileoandeinstein.physics.virginia.edu/tns.htm>, 10.03.2010
- [81] Frank H. Gern, Daniel J. Inman, and Rakesh K. Kapania, Computation of Actuation Power Requirements for Smart Wings with Morphing Airfoils, *AIAA JOURNAL* Vol. 43, No. 12, December 2005
- [82] <http://defense-update.com/products/p/predatorB.htm>, 10.03.2010

- [83] Roelof Vos, Roeland De Breuker, Ron Barrett, and Paolo Tiso, Morphing Wing Flight Control Via post buckled Precompressed Piezo-electric Actuators, JOURNAL OF AIRCRAFT Vol. 44, No. 4, July-August 2007.
- [84] Alan Baker, Stuart Dutton, Donald Kelly, Composite Materials for Aircraft Structures, Second Edition, 2004, American Institute of Aeronautics and Astronautics, Inc. 1801 Alexander Bell Drive, Reston, VA 20191-4344.
- [85] Raymond Parnes, Solid mechanics in engineering, 2001, John Wiley
- [86] Jan R. Wright, and Jonathan E, Introduction to Aircraft aero-elasticity and Loads, John Wiley & Sons Ltd, 2007.
- [87] Anderson, J., Fundamentals of Aerodynamics, 4th ed., McGraw-Hill, New York, 2007
- [88] Michael I Friswell, Active Winglets, Bi-stable Structures and Compliant Mechanisms, 18 November 2008.
- [89] Bob Canfield and James Westfall, Distributed actuation system for flexible in-plane morphing wing, Lisboa, 20 November 2008.
- [90] Blondeau, J., Richeson, J., and Pines, D. J., Design, Development and Testing of a Morphing Aspect Ratio Wing Using an Inflatable Telescopic Spar, 44th AIAA/ASME/ASCE/AHS/ASC Structures, Structural Dynamics, and Materials Conference, Vol. 4, AIAA, Reston, VA, 2003, pp. 2881–2892.
- [91] Changho Nam, Aditi Chattopadhyay Arizona, and Youdan Kim, Application of shape memory alloy (SMA) spars for aircraft maneuver enhancement, Proc. SPIE, Vol. 4701, 226 (2002).
- [92] David Wagg, Ian Bond, and Paul Weaver, Adaptive structures: engineering applications, John Wiley, 2007
- [93] S.R. Turnock, A.J.Keane, N.W.Bressloff, R.F. Nicholls-Lee, S.W. Boyd, Morphing of ‘flying’ shapes for autonomous underwater and aerial vehicles, RTO-MP-AVT-168.
- [94] Locke, J. and Hidalgo, The Implementation of Braided Composite Materials in the Design of a Bend-Twist Coupled Blade, Sandia Report I.C., 2002, Sandia National Laboratories.
- [95] Zhong You, Jason Crabtree, and George Lederman, LARGE-SCALE SHAPE CHANGE IN AIRCRAFT WINGS, Department of Engineering Science, University of Oxford.
- [96] Weisshaar, T. A.. Morphing Aircraft Technology – New Shapes for Aircraft Design. Purdue University. Indiana. 2006.
- [97] Ying Shan, Charles E. Bakis, Static and Dynamic Characterization of a Flexible Matrix Composite Material, The Pennsylvania State University, University Park, PA.

- [98] L. Iannucci and A. Fontanazza, Design of Morphing Wing Structures, Imperial College London, 3rd SEAS DTC Technical Conference - Edinburgh 2008.
- [99] Frank Boria, Bret Stanford, Scott Bowman, and Peter Ifju, Evolutionary Optimization of a Morphing Wing with Wind-Tunnel Hardware in the Loop, AIAA JOURNAL Vol. 47, No. 2, February 2009, pp 399- 409.
- [100] Andras Sobester, Andy J. Keaney, Multidisciplinary Design Optimization of UAV Airframes, 47th AIAA/ASME/ASCE/AHS/ASC Structures, Structural Dynamics, and Materials Conference 1 - 4 May 2006, Newport, Rhode Island.
- [101] P. Gambo, J. Vale, and F. J. P. Lau, Optimization of a Morphing Wing Based on Coupled Aerodynamic and Structural Constraints, AIAA JOURNAL Vol. 47, No. 9, September 2009, pp 2087-2104.
- [102] S.Ricci, Adaptive Camber Mechanism for Morphing Experiences at DIA DIA-PoliMI, Instituto Superior Tecnico Lisboa, Portugal, 17-20 November 2008.
- [103] C. Thill, J. Etches, I. Bond, K. Potter and P. Weaver, Morphing skins, THE AERONAUTICAL JOURNAL, MARCH 2008
- [104] J. E. Cooper, Adaptive Stiffness Structures for Air Vehicle Drag Reduction, School of Mechanical, Aerospace and Civil Engineering University of Manchester, October 2006, RTO-MP-AVT-141.
- [105] R.G. Hutchinson, N. Wicks, A.G. Evans, N.A. Fleck, and J.W. Hutchinson, Kagome plate structures for actuation, International Journal of Solids and Structures 40, 2003, pp. 6969–6980 .
- [106] Jamie Martin, Jean-Jacques Heyder-Bruckner, Chrystel Remillat, Fabrizio Scarpa, Kevin Potter, and Massimo Ruzzene, The hexa-chiral prismatic wingbox concept, phys. stat. sol. (b) 245, No. 3, 570– 577 (2008) / DOI 10.1002/pssb.200777709.
- [107] D. Bornengo, F. Scarpa, and C Remillat, Evaluation of hexagonal chiral structure for morphing airfoil concept, Proc. IMechE Vol. 219 Part G: J. Aerospace Engineering, 2005.
- [108] Dario H. Baldelli, Dong-Hwan Lee, Ricardo S. Sánchez Peña, and Bryan Cannon, Modeling and Control of an aero-elastic Morphing Vehicle, JOURNAL OF GUIDANCE, CONTROL, AND DYNAMICS Vol. 31, No. 6, November–December 2008.
- [109] Aerospace consulting Dror Artzi, www.dror-aero.com/index.htm, 05.04.2010.
- [110] Sridhar Kota, Jinyong Joo, Zhe Li¹, Steven M. Rodgers, and Jeff Sniegowski, Design of Compliant Mechanisms: Applications to MEMS, ISSN 1573-1979, Springer Netherlands.
- [111] A.Y.N. Sofla, A.S. Meguid, K.T. Tan, and W.K. Yeo, Shape morphing of aircraft wing: Status and challenges, Elsevier, Materials and Design, 2009.

- [112] Julie Blondeau, Justin Richeson and Darryll J. Pines, Design, development and testing of a morphing aspect ratio wing using an inflatable telescopic spar, AIAA/ASME/ASCE/AHS Structures, Structural Dynamics, and Materials Confere 7-10 April 2003, Norfolk, Virginia
- [113] Jamey D. Jacob, Suzanne W. Smith, Dave Cadogan, and Steve Scarborough, Expanding the Small UAV Design Space with Inflatable Wings, 2007, Society of Automotive Engineers, Inc.
- [114] Andrew Simpson, Jamey Jacob, and Suzanne Smith, Inflatable and Warpable Wings for Meso-scale UAVs, Mechanical Engineering Dept. University of Kentucky, Lexington.
- [115] David Cadogan, Stephen Scarborough, Dan Gleeson, Anshu Dixit, Jamey Jacob, and Andrew Simpson, Recent Development and Test of Inflatable Wings, American Institute of Aeronautics and Astronautics.
- [116] Mujahid Ab dulrahim, Helen Garcia, Joe Dupuis, and Rick Lind, Flight characteristics of wing shaping for micro air vehicle with membrane wings, Department of Mechanical and Aeronautical Aerospace Engineering, University of Florida.
- [117] Fred Austin, Michael J. Rossi, William Van Nostrand, Gareth Knowles, and Antony Jameson, Static Shape Control for Adaptive Wings, Vol. 32, No. 9, September 1994, pp 1895-1901
- [118] Yu Dong, Zhang Boming, and Liang Jun, A changeable aerofoil actuated by shape memory alloy springs, Materials Science and Engineering, 2008, pp 243-250
- [119] Marc Robert Schultz, Use of Piezo-electric actuators to effect snap-through behavior of unsymmetric composite laminates, PhD dissertation, Virginia Polytechnic Institute and State University.
- [120] Marc R. Schultz, Michael W. Hyer, R. Brett Williams, W. Keats Wilkie , and Daniel J. Inman, Snap-through of unsymmetric laminates using piezocomposite actuators, Composites Science and Technology, 2006, 2442–2448
- [121] Dano ML, Hyer MW, Thermally-induced deformation behavior of unsymmetric laminates. *Int J Solids Struct* 1998;35:2101–20.
- [122] W. Hufenbach, M. Gude, and L. Kroll, Design of multistable composites for application in adaptive structures, *Composites Science and Technology* 2201–2207.
- [123] Chen, P.C., Sarhaddi, D., Jha, R., Liu, D.D., Griffin, K., Yurkovich, R., Variable stiffness spar approach for aircraft maneuver enhancement using ASTROS , 2000, *Journal of Aircraft*, v 37.
- [124] Lee C K 1987 Piezo-electric laminates for torsional and bending modal control: theory and experiment, PhD Dissertation, Cornell University.

- [125] Osama J Aldraihem and Robert C Wetherhold, Mechanics and control of coupled bending and twisting vibration of laminated beams, *Smart Mater. Struct.* 6 (1997) 123–133.
- [126] Yang S M and Bian J J, Vibration suppression experiments on composite laminated plates using an embedded Piezo-electric sensor and actuator, *Smart Mater. Struct.* 5 (1996) 501–7.
- [127] Bae, J. S., Seigler, T. M., Inman, D. J., and Lee, I. Aerodynamic and aeroelastic consideration of a variablespan morphing wing. *SDM Adaptive Structures Forum*, 2004.
- [128] Christopher Park, Curtis Walz, and Inderjit Chopra, Bending and torsion models of beams with induced-strain actuators, *Smart Mater. Struct.* 5 (1996) 98–113.
- [129] Prall, D. and Lakes, R. S. Properties of a chiral honeycomb with a Poisson's ratio -1 . *Int. J. Mech. Sci.*, 1996, 39, 305–314.
- [130] Alessandro Spadoni and Massimo Ruzzene, Static aeroelastic behaviour of a chiral core airfoil, School of Aerospace Engineering Georgia Institute of Technology, 16th International Conference on Adaptive Structures Technologies, France, October 2005.
- [131] N. Ameri, E. Livne, M. H. Lowenberg, and M.I. Friswell, Modelling Continuously Morphing Aircraft for Flight Control, *AIAA Guidance, Navigation and Control Conference and Exhibit 18 - 21 August 2008*, Honolulu, Hawaii.
- [132] Sofla AYN, Elzey DM, Wadley HNG. An antagonistic flexural unit cell for design of shape morphing structures. In: *Proceedings of the ASME aerospace division: adaptive materials and systems, aerospace materials and structures*, Anaheim, CA; 2004.
- [133] Elzey DM, Sofla AYN, Wadley HNG. A bio-inspired, high-authority actuator for shape morphing structures. In: *Smart structures and materials 2003: active materials: behavior and mechanics. Proceedings of SPIE 2003*.